Development of a Bioimpedance-Based Swallowing Biofeedback Device with Smart Device Integration

---

A thesis submitted in partial fulfilment of the requirements for the Degree of Masters of Engineering in Electronic and Electrical Engineering

By

Alexander J. P. Lippitt

University of Canterbury

December 2014

Abstract

Low resolution pharyngeal manometry is an invasive diagnostic method that has recently been used as a biofeedback device for swallowing rehabilitation. The University of Canterbury Rose Centre uses pharyngeal manometry to diagnose and rehabilitate subjects who suffer from pharyngeal mis-sequencing. Pharyngeal mis-sequencing occurs when pressure is applied simultaneously throughout the pharynx rather than sequentially. Rehabilitation can only be performed in clinic due to the need for specialized equipment and trained staff, and the invasiveness of the test limits the time that can be spent training.

As an alternative method to measure the pharyngeal pressure sequence, bioimpedance has been investigated by a previous University of Canterbury Master's student. A prototype was developed that measured bioimpedance in two locations as a proxy for pharyngeal pressure sequence. The prototype device named GULPS (Guided Utility for Latency in Pharyngeal Swallowing), measured a change in impedance during swallowing. However, the features of this waveform were inconsistent and were not present during every swallow.

The frequency of the current that passes through tissue affects its path through the tissue, therefore impacting the measured impedance. To improve the consistency of the impedance measurement, the effect of current injection frequency was investigated. A modular-hardware system was created from the original design to allow testing of different injection frequencies. The hardware was further developed by replacing the method of generating the constant amplitude current injection signal.

The improvement to the design resulted in a differently-shaped waveform to that of the previous prototype, including a new feature. This feature is a single peak that occurred in both channels and was reproduced in every swallow. Experimentation showed that the features were not obviously frequency dependent. The separation between the peaks of the two impedance channels was compared with the separation between the two pressure peaks recorded during simultaneous pharyngeal manometry but there was no significant correlation between the two measures of peak-peak separations.

Two alternative hardware/signal conditioning changes were trialled: electrical isolation of each channel and a subtraction method, which aims to remove the effect of the changing impedance between the two electrode channels. Electrical isolation of the two channels had no effect on the impedance waveforms. However, the subtraction method produced a different output and requires further investigation as the output was inconsistent.

Bluetooth communication was integrated into the GULPS hardware, and a corresponding Android Application (App) was written. The developed App was successful in displaying the impedance measurement output and adds greater user flexibility, allowing the user to interface with the bioimpedance measurement hardware from their tablet or phone.

With no measured significant correlation between GULPS and pharyngeal manometry, further research needs to be performed to better relate the features measured by GULPS to those seen during pharyngeal manometry. Until this can be achieved, the GULPS device cannot replace pharyngeal manometry for biofeedback-based rehabilitation of pharyngeal mis-sequencing.

Acknowledgements

I would like to thank my supervisors, Dr Paul Gaynor, Dr Richard Jones and Dr Maggie-Lee Huckabee for their help and guidance throughout this project. Thank you to the technical staff in the Electrical Engineering department and to students at Rose Centre for giving up their time to help me. Thank you to the subjects who participated in the testing of the device.

To my friends and family, you supported me when it was difficult and celebrated with me when it was good. You have made this an enjoyable journey, thank you.

Table of Contents

Chapter 1.0 Introduction

Biofeedback is used to provide people with greater awareness of their physiological functions by using instruments to provide feedback in a visual or auditory form. Subjects can then use this feedback to improve the physiological function in question. One clinical use of biofeedback is to relieve tension headaches using surface electromyography (sEMG) [1]. sEMG is used to show which muscles in the forehead, neck and shoulders are tensing, causing the headaches. Once the tense muscles have been identified, subjects can perform relaxation techniques and visibly see which techniques have an effect. sEMG is also been used to treat chronic lower back pain and strengthen the pelvic floor muscles for people with urinary incontinence.

To measure physiological events, transducers are used to detect the electrical signals produced by this event. Common electrical signals include electrocardiograph (ECG), electromyography (EMG) and electroencephalograph (ECG). However, often it is necessary to measure a physiological event for which there is no specialised transducer [2]. If the physiological event causes a change in the dimensions, dielectric properties or capacitance to the area then there is a change in the electrical bioimpedance of that area. Measuring the bioimpedance allows events to be measured without the need of a specialised transducer; using electrodes, the bioimpedance can be measured from the surface of the skin.

Dysphagia is the inability to swallow a food or liquid bolus. This is a growing problem for people who have suffered from stroke or other brain related trauma. One feature of dysphagia that is currently being investigated is pharyngeal mis-sequencing. Pharyngeal mis-sequencing occurs when the patient incorrectly applies pressure with their pharyngeal muscles, and disrupts the travel of the bolus along the throat. The gold standard for measuring pharyngeal mis-sequencing is pharyngeal manometry. Pharyngeal manometry is an invasive test that measures the pressure applied by the pharynx internally via force sensitive sensors on a catheter. The New Zealand Brain Research Institute (NZBRI), the Rose Centre, and the University of Canterbury have been collaborating on a non-invasive system of providing feedback on the sequencing of the pharyngeal muscles. This system measures the change in bioimpedance across the neck at two positions to provide visual feedback to the subject.

Smart devices are becoming the popular choice for phones and with the addition of tablets they are now beginning to replace the standard household PC or Mac computer. With such a readily available resource, integrating smart devices to the system to display the feedback information allows patients to use the system without being restricted to a desk, and to use devices they already own.

1.1 Thesis Goals and Overview

The aim of this thesis is to present continuing work on the development on the bioimpedance-based biofeedback tool: The Guided Utility for Latency in Pharyngeal Swallowing device (GULPS). There were two design goals for this project, the addition of smart devices to provide the visual feedback, and the continuation of the development of the hardware for the bioimpedance device, to improve the consistency of the output. The work carried out to achieve these goals is presented in the following chapters.

Chapter 1 – An introduction to the project.

Chapter 2 – Provides the reader with background information on the swallowing biomechanics, dysphagia and in particular pharyngeal mis-sequencing. Current methods of swallowing biofeedback and electrical bioimpedance measurement are also discussed.

Chapter 3 – Gives an outline of the previous work performed by a University of Canterbury Masters student. This covers the hardware prototype he developed, electrode position and the software used to present the biofeedback information.

Chapter 4 – Covers the new work performed on the smart device integration, this includes the hardware design, and the Android application software.

Chapter 5 – Detail of the design of the second (new) GULPS prototype and its functional testing.

Chapter 6 – The results of human subject trials using the new GULPS hardware.

Chapter 7 – Summary, discussion and concluding remarks of the trials and outline design changes and future work for the project.

Chapter 2.0 Background

Swallowing is a complicated process involving the co-ordination of different muscles groups and requires in-depth knowledge of the biomechanical process before the development of a biofeedback device can be started. This section presents a summary of swallowing biomechanics, followed by definitions and characteristics of dysphagia and pharyngeal mis-sequencing and the current methods of providing swallowing biofeedback. Finally, electrical bioimpedance will be discussed, the effect of injection frequency on the measurement and its current use in swallowing biofeedback.

2.1 Swallowing Biomechanics

Swallowing is a continuous process in which each phase has a mechanical dependency on the others. For this reason, a single phase may not be taken in isolation without considering the effect of other phases [3]. Despite this interdependency, swallowing is frequently categorized into four stages: pre-oral phase, oral phase, the pharyngeal phase and the oesophageal phase [3].

2.1.1 Pre-oral Phase

The pre-oral phase occurs before food has entered the mouth. The pre-oral stage takes into account pre-oral motor, cognitive, and psychosocial elements leading up to ingestion, all of which can affect eating behaviour and efficiency [3, 4].

The traditional model of swallowing does not include the pre-oral phase [3], only the movement of the bolus through the aerodigestive tract. Using this model, environmental and cognitive factors leading up to the intake of the food are ignored. Leopold and Kagel [4] state that whilst it is uncommon that the pre-oral stage is the cause of dysphagia, it may be a contributing factor, when superimposed on other ingestion stage pathologies. More importantly, rehabilitation attempts may rely heavily on pre-oral phase characteristics, in order to maximise premotor planning for swallowing.

2.1.2 Oral Phase

The oral phase begins when food has entered the mouth [3] and can be broken into two separate parts, preparation of the bolus and the transport of the bolus [5]. In the preparation of the bolus, the food is masticated and mixed with saliva to soften the food and to lubricate it. Chewing is continued until the food is the appropriate consistency for swallowing [6].

Mastication of food is performed by rotary movement of the mandible and with the aid of the tongue [7]. The upper and lower teeth come together, crushing the material. As the teeth pull apart, the food falls towards the tongue. The tongue will then push the material back towards the teeth and mix the material with saliva [7]. This cycle continues until the food is suitable for swallowing. For liquid or paste material, oral preparation will vary depending on the viscosity of the material. Some materials may require some manipulation before forming a cohesive bolus [7].

When preparing a bolus from a liquid, the soft palate and posterior of the tongue contact to seal the oral cavity and prevent the bolus from prematurely entering the oropharynx [8]. When chewing solid food, the tongue and the soft palate move cyclically in association with jaw movement (Figure 2.1) [8].

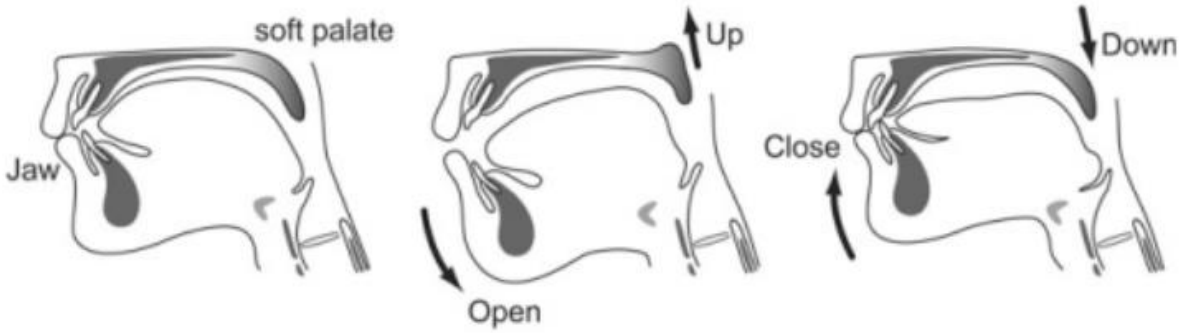

Figure 2.1. The movement of the soft palate during the mastication of solid food [6]

Once a portion of food has been prepared for swallowing, the tongue propels the food backwards to the oropharynx. The food is positioned in the middle of the tongue, then the anterior of the tongue pushes against the hard palate, squeezing the bolus backwards (Figure 2.2), until it reaches the anterior faucial arch [6]. The movements used for transporting food boli and liquid boli are nearly identical [9]. Although bolus preparation is quite variable in duration, depending on the size and type of bolus, the duration of the transfer of the bolus is less than one second.

Figure 2.2. The transport of the bolus once it has been prepared. The arrows indicate the direction of the tongue movement [6].

2.1.3 Pharyngeal Phase

The pharyngeal stage is an involuntary process that covers the transition of the bolus through the pharynx and into the oesophagus [5]. The coordination of respiration and swallowing is vital at this stage of swallowing, because they share a common passageway: the pharynx. During the pharyngeal stage of swallowing, respiration is paused [5].

At the start of the pharyngeal phase, the tongue propels the bolus backward into the oropharynx, and in doing so blocks the passage way to the mouth. As the tongue travels backward, the soft palate is lifted and retracted to allow the bolus to pass through the tonsillar pillars [5]. When the soft palate is fully elevated, it is in contact with the lateral and posterior pharyngeal walls, forming a seal over the nasal airway. This movement increases the pharyngeal pressure behind the bolus [3].

The bolus is compressed against the pharyngeal wall by the tongue; this creates the pressure needed to drive the bolus through the pharynx [9]. Transportation of the bolus down the pharynx is performed by the three pharyngeal constrictor muscles: superior, middle and inferior [3]. The superior constrictor contracts first, followed sequentially by the middle and inferior constrictors. The middle constrictor activates roughly 125 ms after the superior constrictor and the inferior constrictor activates around 300 ms after the superior [10]. The sequential pattern of the pharyngeal and other swallowing related muscles can be seen in an electromyograph performed by Doty and Bosma (Figure 2.3), however the timing is quite variable. The three muscles constrict superiorly to inferiorly to drive the bolus down the

pharynx. Very importantly, given muscle fibre orientation, contraction of these muscles also serve to shorten the pharynx, thus decreasing the distance the bolus must travel [3].

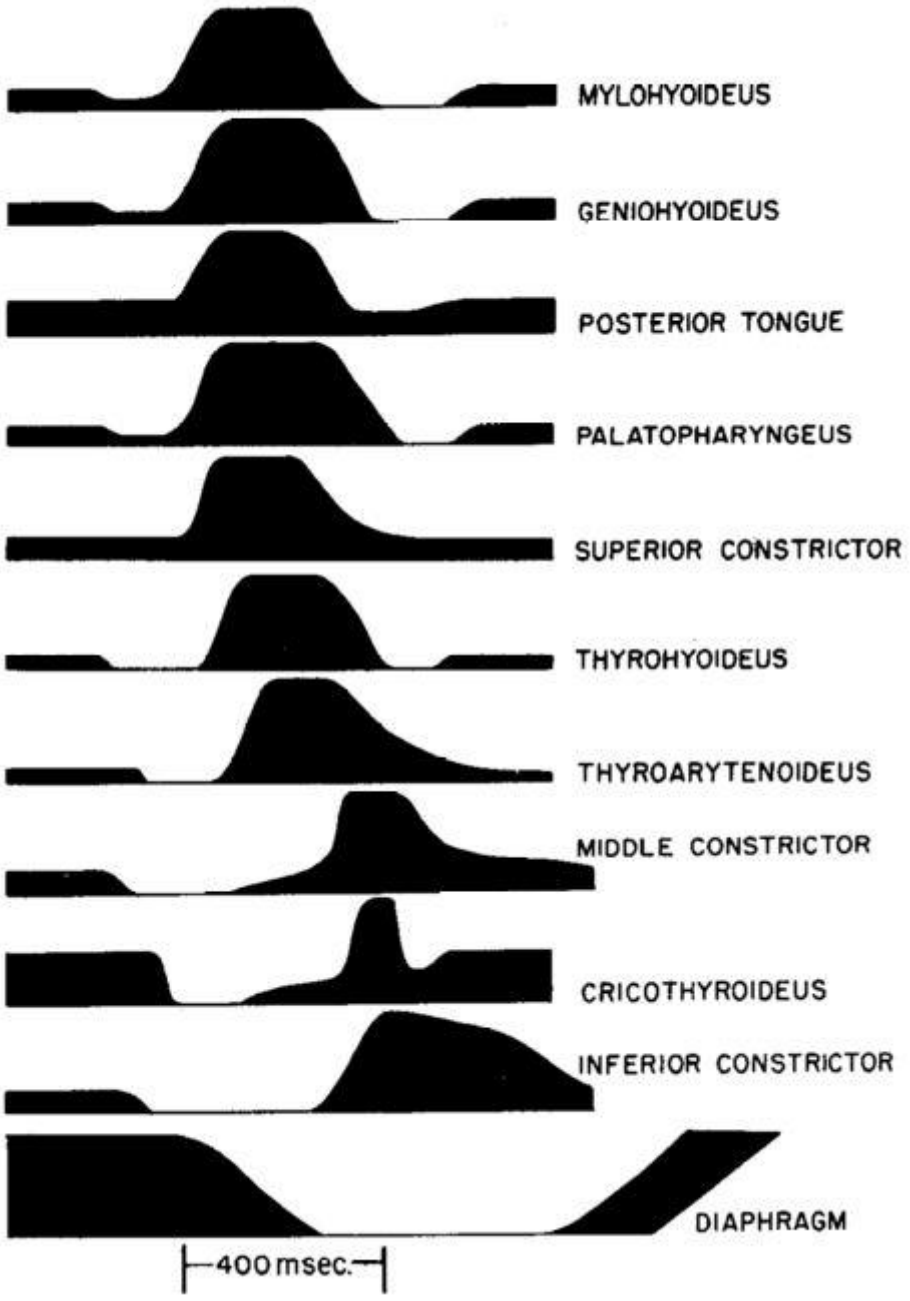

Figure 2.3. An electromyographic study of the temporal activation of the muscles of deglutition in a dog [11].

As the bolus moves down the pharynx (Figure 2.4), there are three events that are responsible for the closure and protection of the airways [6]:

1. The hyoid bone and larynx move upwards and forwards to rest under the base of the tongue. This movement is achieved by the contraction of the suprahyoid and throhyoid muscles. The hypopharyngeal chamber shortens and expands due to the movement of the larynx, causing a decrease in the pressure of the pharyngo-oesophageal (PE) segment, helping to pull the bolus down the pharynx [5, 6].

2. The true and false vocal folds seal the glottis, closing sequentially from bottom to top [5, 6].
3. As the hyoid and larynx are being pulled forwards, the epiglottis is folded over the laryngeal opening. The folding is achieved by the lifting of the hyoid bone and the contraction of the thyrohyoid muscles [5, 6].

For the bolus to pass from the pharynx to the oesophagus, it must pass through the upper oesophageal sphincter (UES). At rest, the UES is held closed by the contracted cricopharyngeous muscle. The opening of the UES occurs at the initiation of the pharyngeal phase [6]. To open the UES the following events must occur [3, 8]:

- The cricopharyngeous muscle relaxes.
- The forward movement of the larynx helps opens the sphincter
- The pressure of the descending bolus pushes on the UES, aiding its opening.

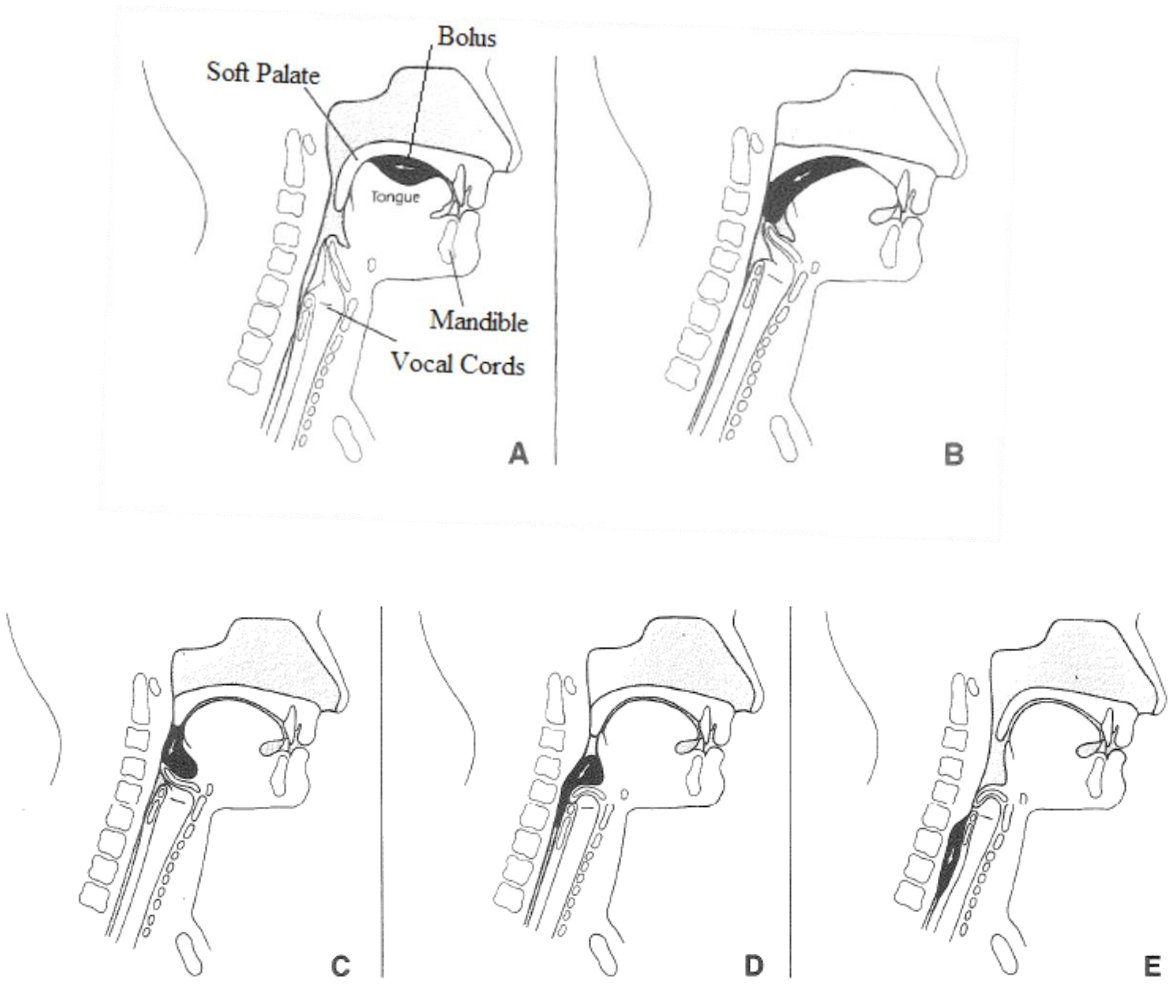

Figure 2.4. The passage of the bolus through the pharyngeal phase [7].

2.1.4 Oesophageal Phase

The oesophageal phase begins with the passing of the bolus through the UES. The UES closes to prevent the bolus from travelling back towards the pharynx. The bolus is pushed down the oesophagus into the stomach by the rhythmic contraction (peristalsis) of the smooth and striated muscles of the oesophagus [3]. The time taken for the bolus to travel the oesophagus varies from 8 to 20 s [3].

2.2 Dysphagia

Dysphagia is the interruption of the swallowing process and can occur during the three phases following the pre-oral phase of swallowing. People who suffer from dysphagia have difficulty swallowing food and liquids. The level of difficulty varies from occasionally struggling to swallow, to being completely unable to swallow food and liquid. For these people it is a struggle to maintain nourishment, and patients often require an external feeding device which bypasses the aerodigestive tract and goes directly to their stomach.

Dysphagia is generally classified based on region of abnormality: oropharyngeal or oesophageal [12]. The cause for both types of dysphagia can be due to a neuromuscular or neurogenic disorder, or biomechanical failure due to an obstructive lesion.

Neurogenic and neuromuscular dysphagia results from central or peripheral sensory and muscular impairment of the oral and pharyngeal phases of swallowing due to a neurologic disorder [13]. The causes of neurogenic and neuromuscular dysphagia include stroke, head trauma, tumour, multiple sclerosis, motor neuron disease and Parkinson's disease [13].

Obstructive lesions are abnormalities which are located within or adjacent to the mouth, pharynx and oesophagus. The lesions interfere with the swallowing biomechanics and prevent a normal swallow occurring. The lesions can be caused by tumours or abscess [12].

2.2.1 Pharyngeal Mis-sequencing

Recent research has identified the phenomenon of pharyngeal mis-sequencing [3]. Pharyngeal mis-sequencing occurs when pharyngeal pressure is generated throughout the pharynx at the same time rather than constricting sequentially (Figure 2.5). This can disrupt the flow of the bolus down the pharynx, and can cause some of the bolus to be directed upwards towards the nasal cavity [3].

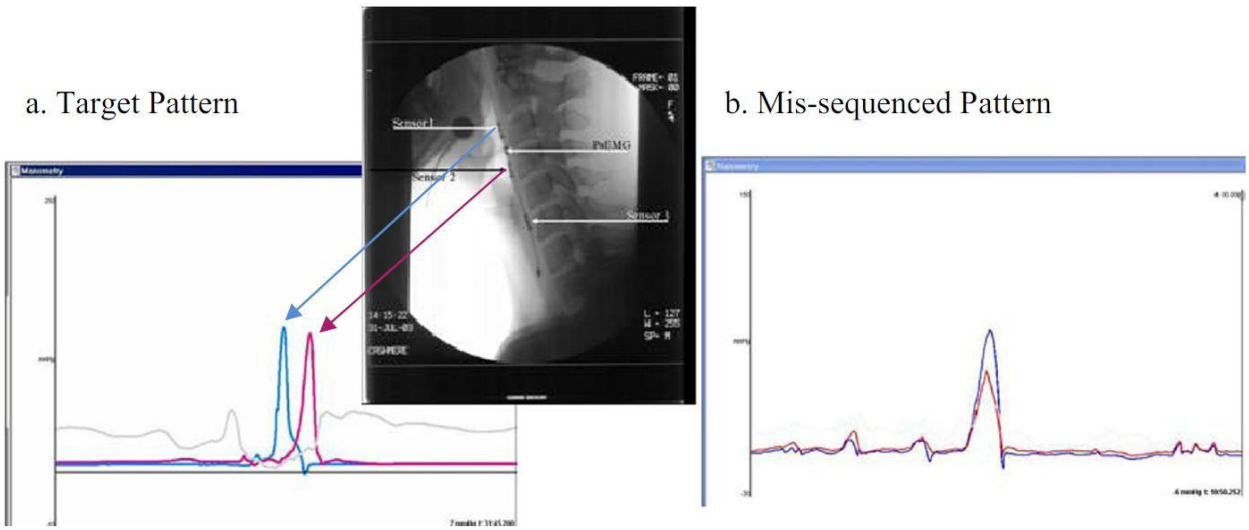

Figure 2.5. Pharyngeal manometry (see Section 2.3.1.1) output for a) a "correctly" sequenced swallow and b) a "mis-sequenced" swallow. A videoflouroscopy image is used here to show nominal sensor position. Sensor 1, the blue line, is placed at the bottom of the tongue, and sensor 2, the red line, is placed below the laryngeal additus [14].

This phenomenon has been identified with pharyngeal manometry evaluation, but with videofluoroscopy as the more commonly used dysphagia diagnostic tool, little is known about pharyngeal mis-sequencing [3]. Huckabee *et al*. [14] demonstrated that patients provided with visual biofeedback via pharyngeal manometry are able to train themselves to sequence pharyngeal pressure

correctly, so that the first sensor peaks before the second. In the study performed by Huckabee *et al.* [14], 16 patients were diagnosed with pharyngeal miss-sequencing, and 11 were successfully rehabilitated. Four of the five patients who were unsuccessful could not attend the follow-up rehabilitation sessions after the initial treatment due to geographical reasons.

2.3 Biofeedback

Biofeedback is the use of instrumentation to make a physiological process visible to the user. This is achieved by providing auditory and/or visual representations of that process [15]. Biofeedback gives the person being tested real-time recordings of their physical system, quantifying the level at which the physical system is performing. This allows the patients to see the changes in the system when they vary the system's behaviour. It can help patients recognize when a system is not functioning as intended, and what it should look like. Examples of biofeedback include electrocardiogram (ECG), electromyography (EMG), and electroencephalography (EEG).

2.3.1 Current Methods of Swallowing Feedback

To evaluate a patients' swallow, clinicians have several tools available to them. The tools each have their own merits and weaknesses; however, their suitability for evaluating and providing feedback for pharyngeal mis-sequencing is limited. Below are several popular methods for evaluating swallowing behaviour.

2.3.1.1 Pharyngeal Manometry

Pharyngeal manometry is an invasive method of evaluating swallowing behaviour. Low-resolution pharyngeal manometry measures the pressure applied by the pharyngeal muscles in the pharynx and the pressure applied by the upper oesophagus sphincter (UES). Pharyngeal manometry uses three sensors (Figure 2.6), which are unidirectional and orientated posteriorly [16]. The top two sensors (sensors 1 and 2), are separated by 20 mm, and the spacing between the second and the third sensor is 30 mm [16]. Sensors one and two are used to measure the pressure applied by the pharynx. Sensor 1 is located in the upper pharynx, and this is approximately even with the base of the tongue. Sensor 2 is placed in the hypopharynx, approximately even with the laryngeal additus [16]. Sensor 3 is used to measure the pressure applied by the UES and is located at the top of the cricopharyngeal muscle [16] (Figure 2.7).

Pharyngeal manometry has several disadvantages which make it an unsuitable tool for extended patient rehabilitation. Firstly, the invasive nature of the test can be uncomfortable for patients, and requires a trained specialist to correctly place the manometry catheter. The equipment is expensive and difficult to relocate, forcing all testing to be done at a clinic.

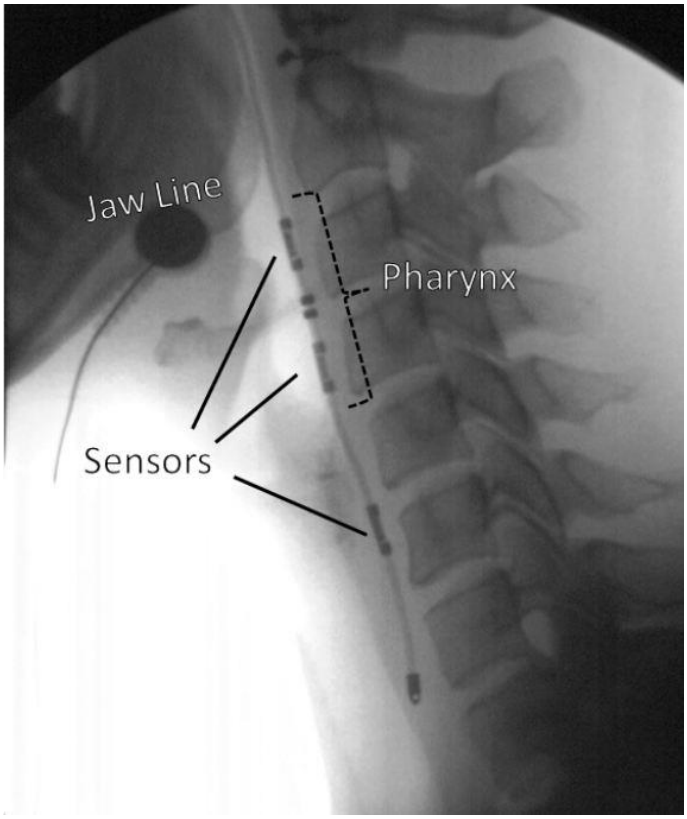

Figure 2.6 - Using videofluoroscopy the positioning of the low-resolution pharyngeal manometry sensors can be seen [3].

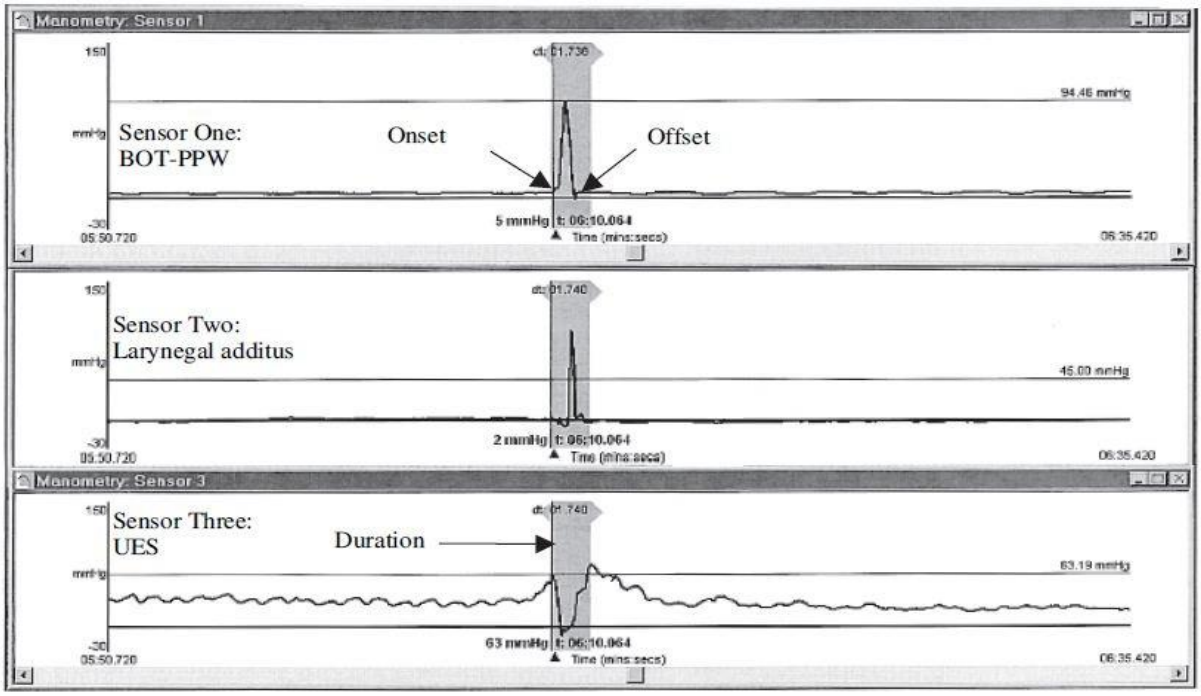

Figure 2.7 - Pharyngeal manometry waveform during a swallow. Sensor one is placed at the base of the tongue (BOT), sensor two at the Larynegal additus and sensor three at the upper oesophagus sphincter (UES).

2.3.1.2 Videofluoroscopy

Videofluoroscopy is a radiological investigation which records fluoroscopic images of the patient swallowing a radio-opaque bolus [17]. This gives the examiner a visual view of the oral, pharyngeal, and oesophagus stages of the swallow, and allows the examiner to study the flow of the bolus [3]. Radiation during the examination limits the time and the number of repetitions the exam can be performed, and prevents it from being used for swallowing rehabilitation. Another limiting factor, which rules out videofluoroscopy for pharyngeal mis-sequencing rehabilitation, is videofluoroscopy's inability to observe the pressure applied by the pharyngeal constrictors to the bolus [18].

2.3.1.3 Electromyography

Electromyography (EMG) uses electrodes to measure the electrical activity generated by muscles. EMG has been successfully used to monitor the muscles used in swallowing in animals (Figure 2.3) [11], however this method used copper wire which was sown into the surgically-exposed muscle. Perlman et al. [19] used needle EMG electrodes to successfully measure the muscle activity in the superior pharyngeal constrictor. A non-invasive approach uses surface-mount electrodes (sEMG) and is used in swallowing rehabilitation, when the focus of the training is muscle strengthening on aspects of the swallow[20]. The biggest obstacle in using sEMG for monitoring the pharyngeal stage of swallowing is the correct placement of the electrodes to measure the pharyngeal muscle activation.[7].

2.4 Electrical Bioimpedance

Electrical bioimpedance is a non-invasive method of measuring the electrical resistance and reactance of tissue. To electrically model tissue, it can be broken down into two parts (Figure 2.8), cells and extracellular space [21]. The intracellular and extracellular spaces both contain ions, which are conductive. The cell membrane is an insulator that separates the two conductive spaces.

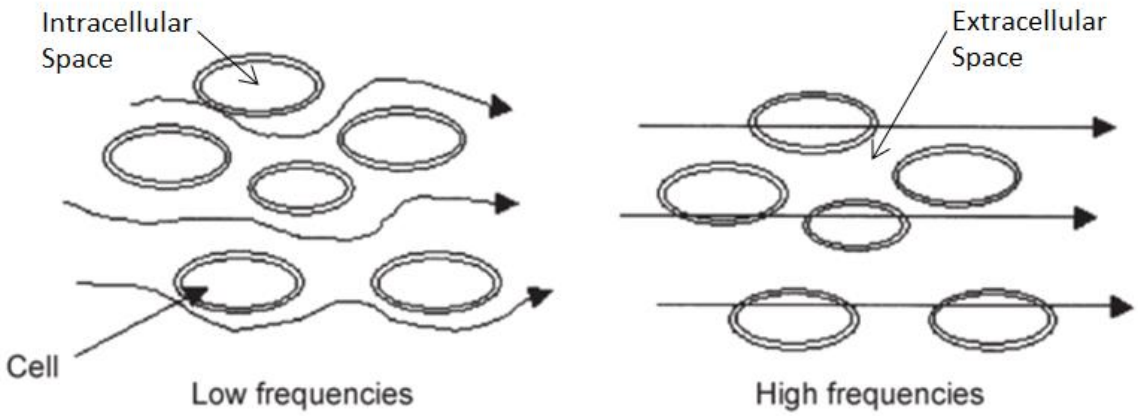

Figure 2.8. The current path through tissue at high and low frequencies [21]

A simple, but commonly used electrical model for tissue is a resistor-capacitor circuit (Figure 2.9) [21, 22]. The intracellular and extracellular spaces are both modelled as resistors and the cell membrane is modelled as a capacitor, placed in series with the intracellular resistance [21]. At low frequencies the cell membrane prevents the current from entering the cell, and the impedance is related to the extracellular resistance. At high frequencies the reactance of the membrane is small and current can pass through the membrane (Figure 2.8).

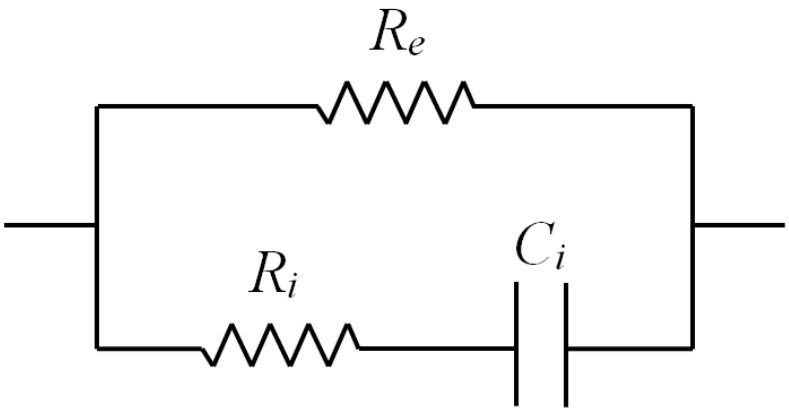

Figure 2.9. The tissue electrical circuit equivalent. R_e is the resistance of the extracellular space around the cells, R_i, is the resistance of the intracellular space, and C_m is the capacitance representing the cell membrane [21].

Ivorra *et al.* [22] states that this model does not accurately describe the impedance over a large frequency spectrum, but rather a small region. This statement is supported by Schwan [23], who first stated that the relationship between impedance and frequency is broken down into three different regions, called dispersion regions. Each dispersion region is defined by the observed electrical properties which are related to the dielectric properties of the tissue and the losses caused by the relaxation of electric dipoles. The average relaxation time characterizes each dispersion zone [24].

2.4.1 Dispersion Regions

There are three dispersion regions: alpha, beta and gamma. Alpha dispersion occurs at frequencies lower than 10 kHz, beta dispersion between 10 kHz to 100 MHz, and gamma dispersion is greater than 100 MHz (Figure 2.10) [24, 25].

The beta dispersion region is based upon the Maxwell-Wagner polarization effects [25, 26]. This dispersion zone is considered to be caused by the dielectric properties of the cell membranes and their interactions with the extra- and intra-cellular electrolytes [22]. This region is qualitatively defined by the electrical model seen in Figure 2.9 [22].

In the alpha dispersion region, the extra-cellular space resistance is the largest component of the impedance [21]. The physical cause of the alpha dispersion zone is unknown [22, 26]. Grimnes and Martinsen [27] investigated alpha dispersion in living tissue and came to the conclusion that it is generated by a different mechanism to beta dispersion. However, alpha dispersion is related to the cell membranes of living tissue [27].

In the gamma dispersion region, the dielectric properties of the tissue are determined by their aqueous content [25]. Schwan [26] found that the dielectric property of the aqueous content of tissue has the same dielectric properties as water.

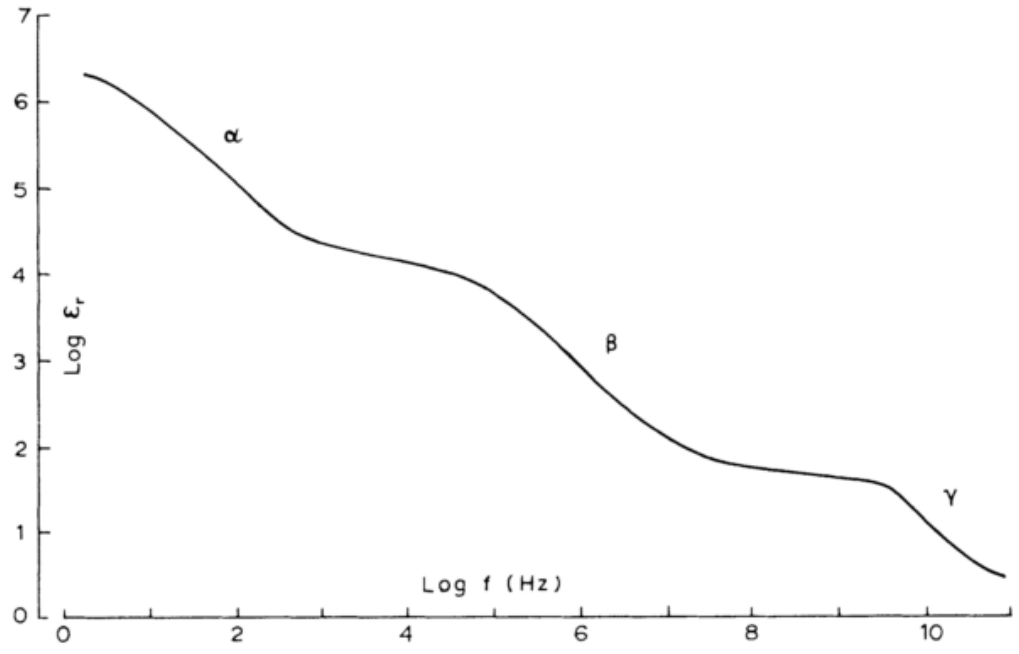

Figure 2.10. The variation of relative permittivity with frequency for a typical biological tissue [24].

2.4.2 Applications of Bioimpedance

Bioimpedance differs from other electrical biosignals because it does not passively measure signals produced by the body, such as the ECG. Instead a constant amplitude signal (current or voltage) is injected into the patient and the change of its pair (voltage or current respectively) is measured. Bioimpedance is then calculated using Ohm's law. With bioimpedance, biological events or objects which do not produce electrical biosignals can be observed.

2.4.2.1 Body Composition

Measuring the body composition of a subject with bioimpedance uses the principle that different tissues have different electrical properties. Fat-free tissue is a good conductor due to its high water and conducting electrolyte content, whereas fat tissue is a poor conductor [28]. Conventional systems for human body composition measurements use four electrodes, placed on the arms and legs of the subject and require the subject to lie supine. However, newer systems use four electrodes which the subject stands on [29]. This technique is used in meat processing factories where the quality of meat (the ratio of fat to muscle) is assessed using body composition measurement [30].

2.4.2.2 Electrical Impedance Tomography

Electrical Impedance Tomography (EIT) is an imaging technique which produces a two-dimensional image of the distribution of the body's impedance by taking measurements from the body's surface [31]. EIT systems use multiple electrodes which are placed in a single plane around the body's surface. Multiple frequency systems are becoming common due to the difference in impedance of organs at different frequencies [31]. EIT has been applied to a range of clinical applications with varying success, including breast tumour imaging, brain imaging and gastrointestinal function [32].

EIT systems use reconstruction algorithms to generate the impedance image. Part of the reconstruction algorithm (also known as the forward problem) is to predict the voltage at the electrodes for a given current and conductivity distribution. The most common method for implementing the forward problem is the finite element method [32]. When voltages are measured the reconstruction algorithm then

estimates the impedance distribution by comparing it to the predicted voltages produced by the forward problem [33].

The biggest problem facing EIT is that the injected current is not confined to a single plane; rather, the current takes the path of least resistance [33]. To build an accurate impedance image, the reconstruction algorithm used must try to account for the impedance changes outside the desired plane.

2.4.2.3 Swallowing Bioimpedance

The use of bioimpedance to assess elements of swallowing function was evaluated by Kusuhara *et al*. [34]. Kusuhara *et al*. built a single-channel impedance meter which used four electrodes and injected a 0.5 mA RMS constant amplitude sinusoidal waveform at 50 kHz. To relate the change of impedance with swallowing behaviour a microphone was placed on the front of the neck corresponding to the pharynx, to measure the sound of the bolus passing through the pharynx (Figure 2.11).

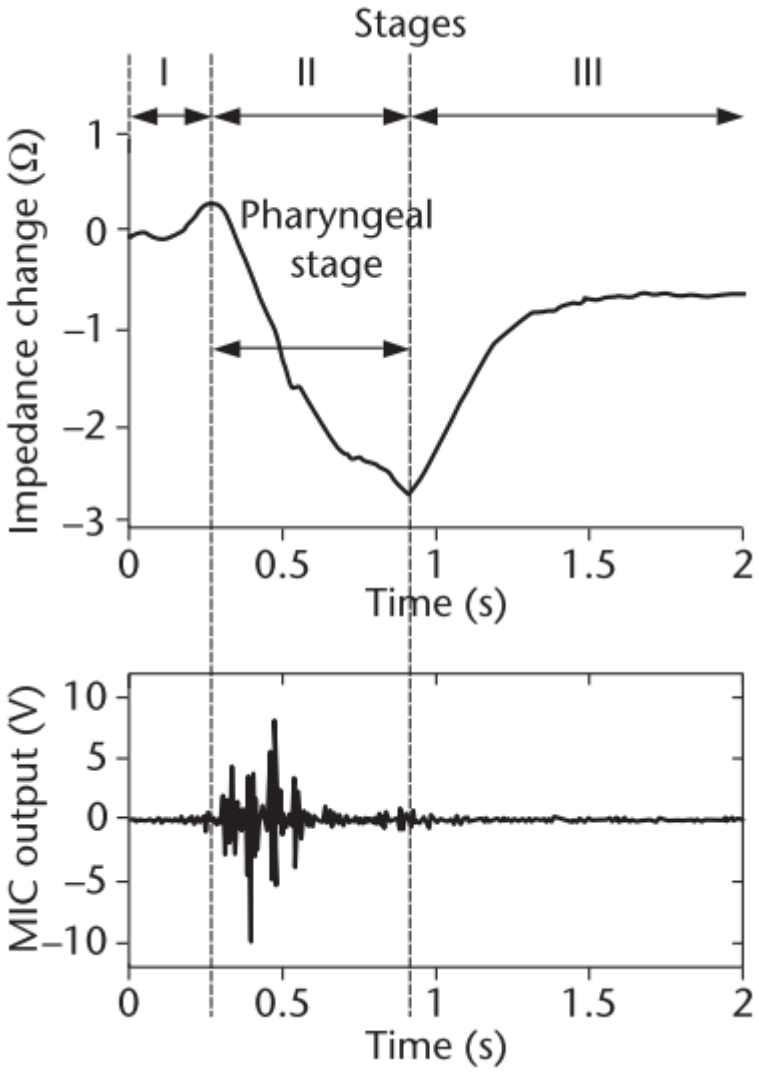

Figure 2.11. Comparing the impedance pharyngography waveform with the microphone output [34].

Kusuhara *et al*. concluded that using bioimpedance, the level of activity and the normality of the movements of the organs during the pharyngeal stage could be shown in the changes in the impedance.

The duration of the pharyngeal stage and the number of swallowing reflexes that appeared during a session can also be determined by bioimpedance.

Hughes *et al*. [35] conducted a study comparing EIT with videofluoroscopy to find the relationship between the change in impedance and the swallowing phase. The arrival of the bolus in the pharynx did not decrease the impedance. Hughes *et al.* thought this was due to the bolus having a similar conductivity as air. The decrease in impedance occurred when the muscles contracted, squeezing the air out of the pharynx and larynx, and pushing the bolus down the pharynx. When the muscles relax, and the pharynx refills with air, the impedance increases.

2.5 Chapter Summary

The current methods used for swallowing rehabilitation have limiting factors that prevent them being used for pharyngeal mis-sequencing rehabilitation. The current methods are invasive, require supervision of trained staff at a clinic and cannot be used for an extend duration. An alternative method, which is non-invasive, inexpensive and portable, is needed. This system needs to be able to be used by the subject outside of the hospital, with minimal application guidance from a specialist. Its purpose is to provide visual feedback to the subject on the sequence of their pharyngeal lumen closure to aid in pharyngeal mis-sequencing rehabilitation. Bioimpedance has already been evaluated for use in swallowing diagnosis and could successfully detect the pharyngeal stage of swallowing. Research has shown the impedance measured is related to injection frequency, and the path it takes through the tissue.

Chapter 3.0 Previous Work

This chapter covers the previous work carried out on GULPS, a device designed to provide patients with feedback on their pharyngeal lumen closure. GULPS uses bioimpedance to measure the sequence of the closure of the pharyngeal lumen, with measurement taken from the surface of the neck. The initial prototype of GULPS was developed in 2012/2013 by a previous Master's student at the University of Canterbury, Chris Chester [36]. Chester developed a hardware prototype which used two channels to measure the spatio-temporal differences in the swallowing sequence and a computer program that interfaced between a computer and the device. This chapter covers the design of Chester's hardware prototype, the software program, electrode positioning, and the results of the testing of GULPS carried out by Chester.

3.1 Hardware

The developed GULPS hardware underwent several iterations before coming to the design identified by Figure 3.1. Outlined below is the final hardware design completed by Chester, which is split into two parts: the constant current generation and the voltage measurement. Circuit schematics of the GULPS prototype can be seen in Appendix A.

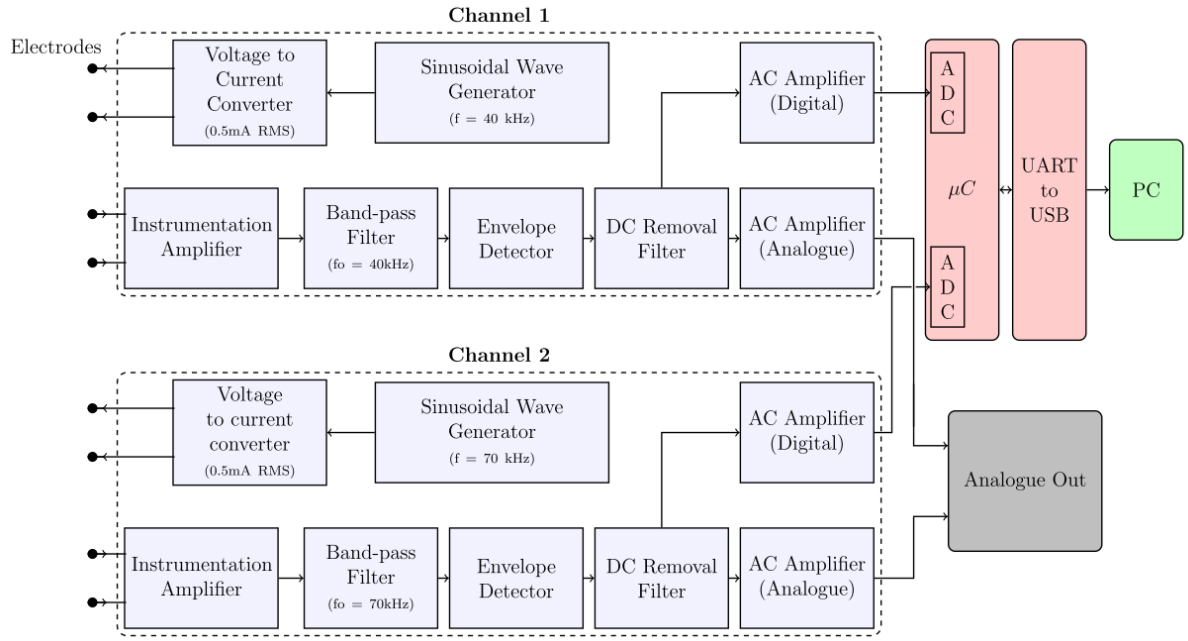

Figure 3.1. Block diagram of the final GULPS system prototype from [36].

3.1.1 Constant Current Generation

The constant current waveform was to be sinusoidal and have a constant Root Mean Squared (RMS) value of 0.5 mA. To generate the constant current waveform, first a sinusoidal voltage at the channel frequency was generated, and then the voltage waveform is converted into a current waveform.

Injection frequencies of 40 kHz and 70 kHz were chosen as they are not integer multiples of each, reducing harmonic interference. They are also the same order of magnitude as the injection frequency Kusuhara *et al.* [34] used in their bioimpedance meter.

3.1.1.1 Sinusoidal Wave Generators

A quasi-sinusoidal voltage waveform at the operating frequency was generated by a square-wave oscillator, LTC6900 [37], and passed through a low-pass filter to remove the harmonic frequencies above the fundamental frequency. It was also passed through a high-pass filter to remove the dc offset and centre the wave at zero volts. The band-pass filter was implemented using a single-order resistor-capacitor (RC) filter.

3.1.1.2 Voltage to Current Converter (Transconductance amplifier)

The constant current was generated using a voltage to current converting opamp circuit, shown in Figure 3.2. The current through the load is determined by applying Kirchhoff's current law at node 1. An opamp has zero voltage difference between its two inputs, and draws zero current. Therefore the currents going into node 1 are I_{Set} and I_L and by Kirchhoff's current law must be the inverse of each other. The current through R_{Set} and hence the inverse current through R_L is calculated using equation 1.

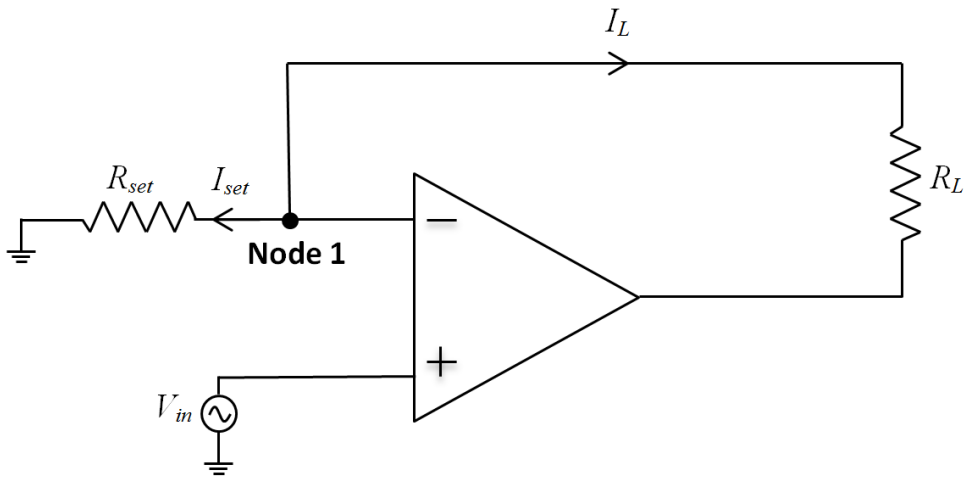

Figure 3.2. The voltage to current converter using an opamp.

$$I_{Set}(\text{RMS}) = \frac{V_{in}(RMS)}{R_{Set}} = -I_L \qquad 1$$

3.1.2 Voltage Measurement Stage

This stage covers measurement of the voltages at the neck through to the analog-to-digital conversion (ADC) and sending them to the computer. For each channel, two voltages, one on either side of the neck, were measured. The measured signals were passed through several signal conditioning modules (Figure 3.1) to isolate the signal, remove noise, and amplify the signal ready for ADC conversion.

3.1.2.1 Instrumentation Amplifier

The instrumentation amplifier was used to amplify the difference between the two signals whilst rejecting the common-mode signals. An example of a signal that is common to both inputs is 50 Hz mains interference. The instrumentation amplifier chosen was the AD620 by Analog Devices [38] and the gain was set at 42.1 V/V. A high-pass filter was placed at each input to the amplifier with a cut-off frequency of 16 Hz to remove any dc offset.

3.1.2.2 Bandpass Filters

A bandpass filter was used for each channel to isolate the frequency of interest. The IC used was the UAF42AU [39] and was configured into a second-order bandpass filter. Two were cascaded together to form a fourth-order filter. The bandpass filter characteristics for both channels are in Table 1.

Table 1. The bandpass filter characteristics used in Chester's final design [36].

Channel	Gain	Centre frequency f_0	Q factor	Low cut-off frequency f_1	High cut-off frequency f_2
1	0.5	39.8 kHz	2.83	33.4 kHz	47.4 kHz
2	0.5	70.2 kHz	5.94	64.5 kHz	76.4 kHz

3.1.2.3 Demodulator

A change in the impedance will be seen as a change in the amplitude of the carrier frequency. An envelope detector is used to bring the carrier frequency down to base band. A half-wave rectifier and a low-pass filter form the envelope detector. A Schottky diode was used for the half wave rectifier and for the low pass filter an opamp [40] in a second-order Sallen-key configuration with a cut-off frequency of 21 Hz was used.

3.1.2.4 High pass Filter

A high-pass filter was used to remove the dc component of the impedance measurement. The cut-off frequency for the high-pass filter is 0.05 Hz, which is approximately 10 times smaller than the smallest frequency a change in impedance occurred at. The LM258 [41] opamp was used in a second-order Sallen-Key configuration.

3.1.2.5 Amplifier

The signal was amplified to provide ample dynamic range for the microcontroller to sample it. The amplifier also added a dc offset to bring the voltage into the microcontrollers sampling range of 0V – Vcc. An inverting amplifier configuration was used with the gain set to 56V/V. To perform the amplification a TLE2022 [42] opamp was used. The inverting operation results in a positive slope change when the impedance is decreasing. This was intentional so that the impedance change waveform somewhat mirrored that of pharyngeal manometry (an increase in pressure corresponding to a drop in impedance).

3.1.2.6 Anti-Aliasing Filter

Before the signal was read by the ADC of the microcontroller, the signal was passed through a low-pass anti-aliasing filter. The filter was a third-order resistor-capacitor (RC) filter with a cut-off frequency of 20 Hz.

3.1.2.7 Microcontroller and Computer Interface

Analog-to-digital conversion was conducted using a dsPIC30F3013 microcontroller [43]. Two 12-Bit ADCs were used, one for each channel, with sampling frequency of 50 Hz. UART (Universal Asynchronous Receive/Transmit) was used to output the data from the microcontroller to a UART to USB converter [44]. The GULPS device could then be connected to the computer via a USB cable.

A custom-data protocol was created (Figure 3.3) to send the ADC values to the computer because UART only transmits 8 data bits in each packet. Each ADC value was split into two bytes, the least 8 significant bits into one, and the four remaining bits were placed in the second. A synchronizing byte was sent first so the software could determine the start of the data protocol.

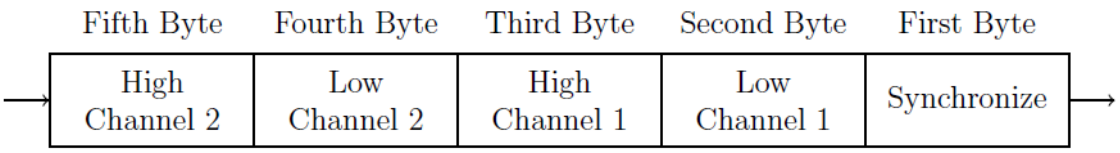

Figure 3.3. The custom data protocol used to send data to the computer [36].

3.2 Electrodes and Position

The position of the electrodes on the patient was crucial for successfully measuring the impedance change in the pharynx [36]. Another factor to the quality of the signal was the type of electrode that was used.

3.2.1 Tetrapolar Configuration

The electrodes for each channel were placed in a tetrapolar configuration. This configuration uses four electrodes: two for current injection and two for the voltage measurement. Using this formation, the measurement takes place at a different location to the current injection. When an ac current is applied to tissue, the boundary tissue will be polarized and a potential which is out of phase with the current will be induced [45]. With the tetrapolar configuration measuring the voltage at a different location to the current injection, the evoked potential does not influence the measured voltage.

By using different electrodes for carrying the current, zero current will travel through the voltage-measuring electrodes, provided the input impedance is significantly larger than the load impedance. With zero current traveling through the measurement electrodes then there will be no loss of signal due to skin-electrode resistance [2]. The skin-electrode resistance is not constant and can be affected when there is movement between the electrodes and skin, so removing this variability is important for an accurate voltage measurement.

3.2.2 Electrodes

Several different electrodes were trialled, and the final electrodes chosen were Triode electrodes by Thought Technology Ltd [46]. The Triode electrodes were chosen because they are dry electrodes and could be reapplied multiple times. To maintain a constant separation between the electrodes an adhesive wafer by ConvaTec [47] was used as a frame. One was used for each side of the neck and housed four electrodes.

Figure 3.4. The electrode pad used for the prototype GULPS device [36]

Individual wet-gel electrodes were also trialled; the Norotrode electrodes [48] by Myotronics, and Blue sensor N [49] and Blue sensor NF [49] electrodes by Ambu. It was found that often the wet gel would bridge the gap between the sensing and injection electrodes and it was difficult to maintain constant electrode positioning when placing individual electrodes. They also had limited reusability as the adhesive would dry out.

3.2.3 Electrode Position

To find the optimum electrode placement, Chester used a 3 x 4 electrode grid separated in either direction by 20 mm. Using this electrode grid it was found that a 40 mm separation in the vertical direction gave the best results by providing two waveforms with clearly defined features, and that have a temporal separation. A 20 mm separation between the current and voltage electrodes on the horizontal plane was chosen because the separation prevented the voltage electrode from measuring the boundary issue, yet it was within the recommended separation distance of 40 mm, outlined by Kusuhara *et al.* [34].

The position of the electrodes on the throat was also determined using the electrode grid, and it was found that the best position had the top channel almost directly below the ear with the second channel placed 40 mm below. The final electrode position can be seen in Figure 3.5.

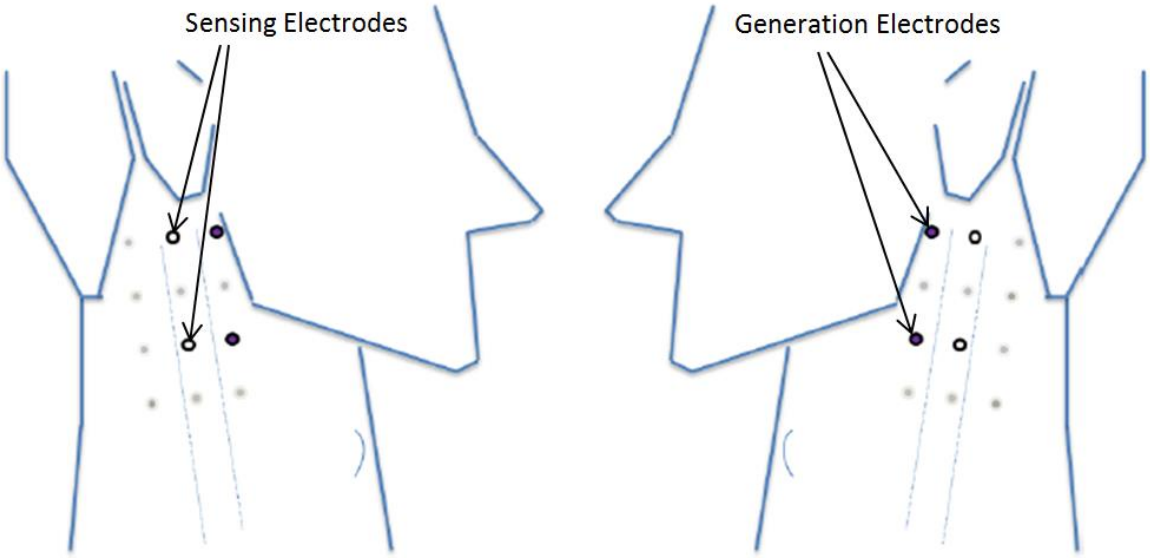

Figure 3.5 - The electrode positions used by Chester for his testing. The white-centred electrodes are signal detection electrodes and the black electrodes are for current generation [36].

3.3 Software

To provide the feedback to the patient, a software program was developed to read the data sent from the GULPS device. The GULPS software was written in the Python programming language and is distributed as an executable (.EXE) format. The GULPS software automatically establishes a connection between the software and the GULPS hardware over USB and reads the data sent by the hardware. These data are then displayed on a real-time plot, showing the two channels. The user creates a patient profile and can save the plotted data to their file, which can be reloaded and reviewed at a later time.

3.4 Results

Chester tested three healthy subjects with the GULPS system, two males and one female. The testing identified that bioimpedance could be used to detect pharyngeal sequence and the GULPS system could produce waveforms that had desired features. Examples of the waveforms measured by Chester can be seen in Figure 3.6. The features presented in the waveforms are two peaks and one trough, which differ from the waveforms produced by manometry. Due to this, the GULPS system was then tested alongside pharyngeal manometry to help characterize the waveforms produced by GULPS (Figure 3.7 and Figure 3.8).

Whilst testing GULPS and manometry simultaneously it was found the GULPS output varied substantially from when GULPS was tested alone. The cause of the variance was identified to being the invasive nature of the manometry test, causing discomfort to the subject and disrupting their swallowing sequence.

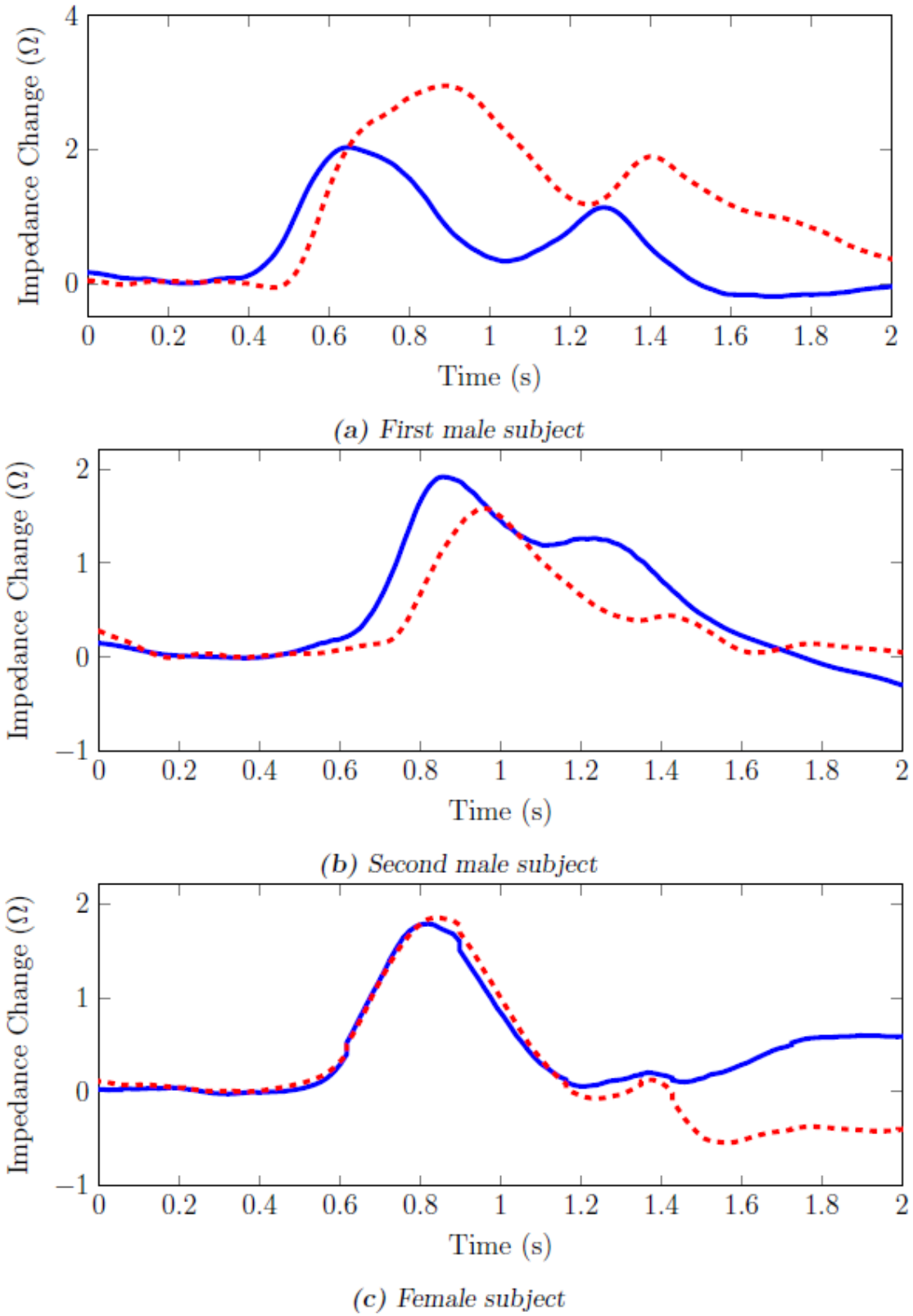

Figure 3.6 - The features produced by the GULPS system on "healthy" patients during a swallowing event were two peaks and a trough. The solid waveform corresponds to the top channel and the dashed line is the bottom channel [36].

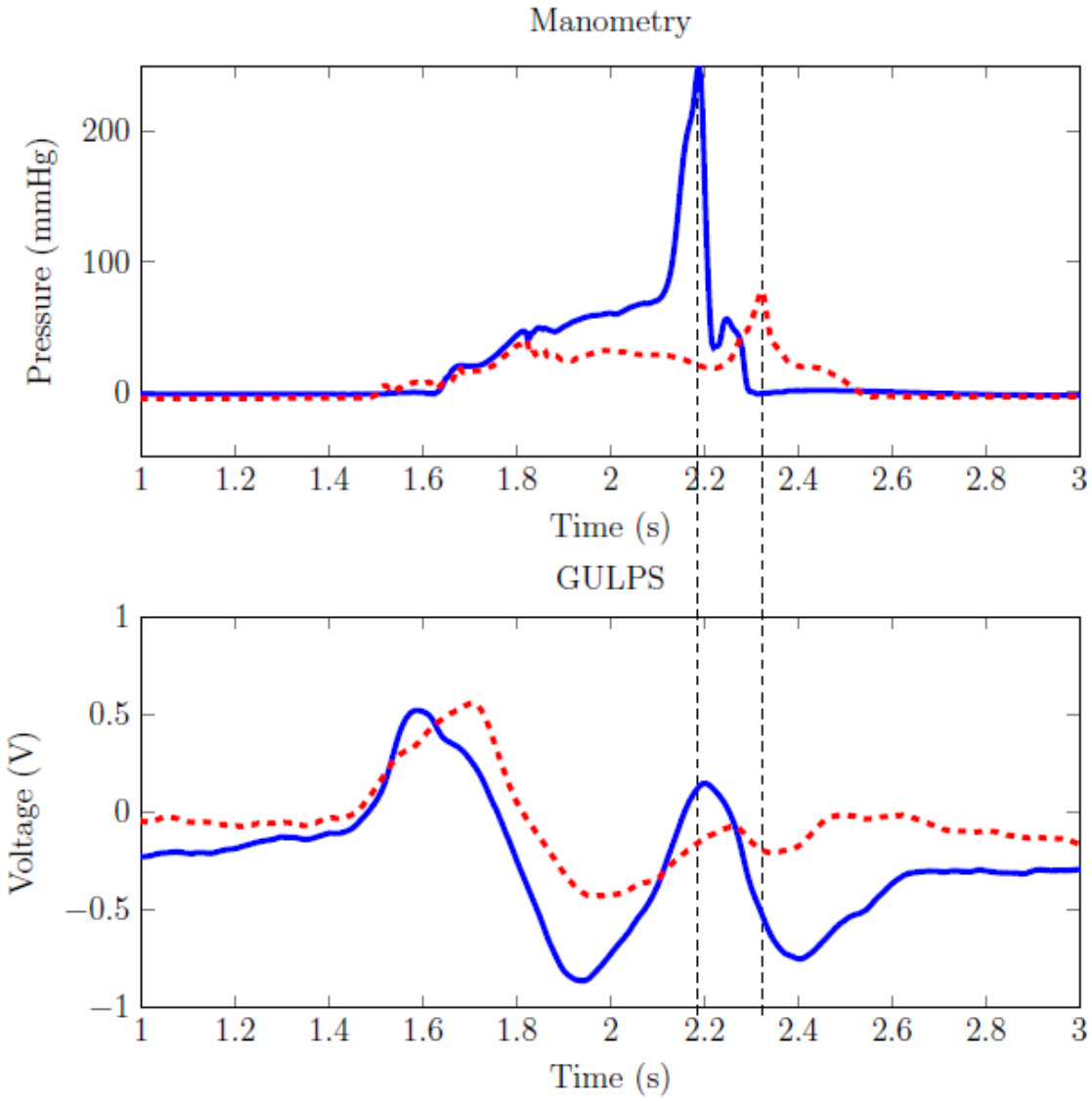

Figure 3.7 - Manometry and GULPS used alongside each other. The dashed line is the lower channel for both measurements and the solid line is the upper channel for both [36].

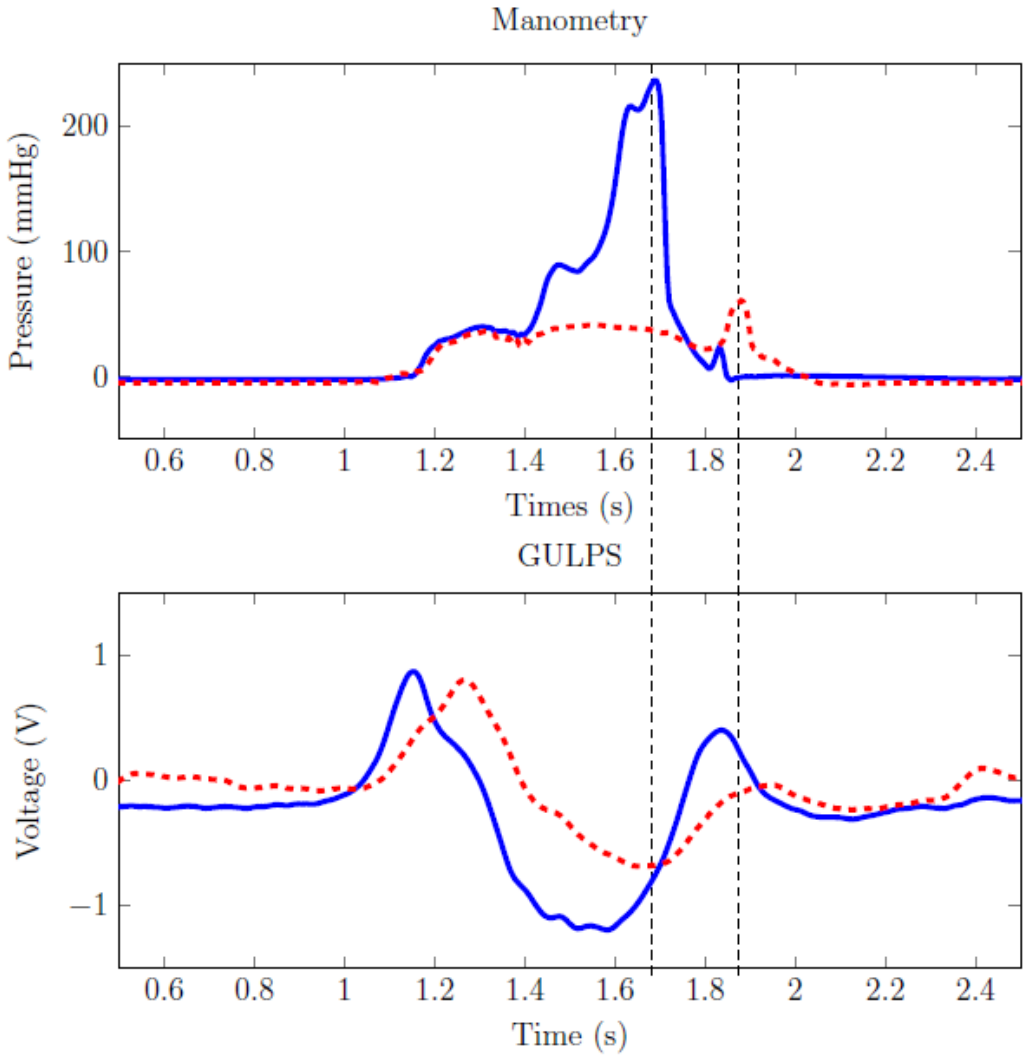

Figure 3.8 - A second example of manometry alongside GULPS, the solid line represents the top channel and the dashed line represents the bottom channel [36].

The primary problem of Chester's prototype was the inconsistency of the waveforms produced by GULPS. The features present in Figure 3.6 were often undetectable. It was found that the loss of detail occurred when the electrodes were adjusted or reapplied and would require several attempts at repositioning the electrodes before being able to reproduce the desired waveforms again. The type of swallow was also determined to have a large effect on the result. Chester used three conditions of swallowing during the testing, an effortful swallow with a water bolus, a normal swallow with a water bolus and a dry swallow. Overall Chester found that using an effortful swallow, GULPS was able to produce an output with the features 64% of the time, 22% with a normal effort, water bolus swallow and 16% with a dry swallow.

When using GULPS alongside manometry it was found that only 23% of the swallows produced an output with the three features using an effortful swallow. Chester analysed the swallows that did produce the distinguishable features and found that the first peak of the GULPS occurred substantially before the peaks produced by manometry, and that the troughs and second peaks from GULPS were

more identifiable with manometry. However, the GULPS waveform did not produce a constant temporal relationship with manometry.

3.5 Future Development Recommendations

Chester outlined two potential hardware design changes that could improve the system's ability to detect pharyngeal sequencing - changing the frequency of the injection wave and quadrature modulation. Chester also mentioned developing the software further to provide peak detection. While this would be a useful component to have, development of this feature should be delayed until the hardware can produce repeatable peaks.

Chapter 4.0 Smart Device Development

Smart devices were desired to be added to the GULPS project because they provide advantages such as being portable and therefore do not restrict the testing to a fixed work station, the testing can be performed in an environment of the patient's choice, and patients can use their own devices. Using wireless communication removes the cable connecting the GULPS device to the computer and gives range and flexibility to the location of the smart device relative to the GULPS platform. Wireless communication hardware was prototyped and a smart device application (App) was written to determine if smart devices could be integrated with the GULPS system.

4.1 Smart Device Operating System

There are two popular Operating Systems (OSs) for smart devices currently on the market; iOS (Apple) and Android (Google) [50]. For this project, Android was the OS used as the target development platform. The Android platform was selected because of its widespread use among end users (Figure 4.1), availability of hardware, utilisation of the Java programming language, open source licencing, and large online support community. The Android open-source licence allows hardware and software to be freely developed, whereas iOS requires separate hardware and software development licences. For these reasons the Android OS was selected on the basis of cost, availability and support offered by an active online developer community.

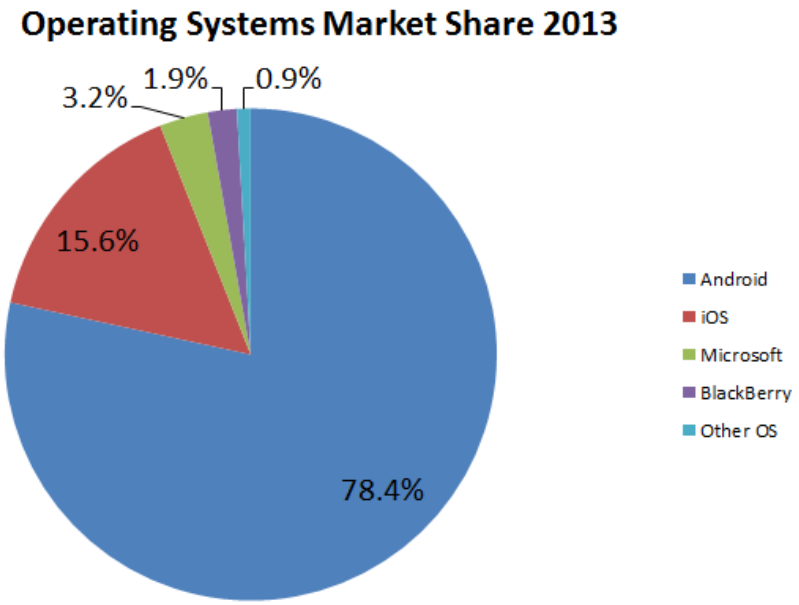

Figure 4.1. The market share for the largest operating systems for smart devices at the end of 2013 [50]

4.2 Bluetooth

Bluetooth was chosen as the method of communication for this project due to the decrease in development time its use would achieve. Bluetooth hardware modules are available to implement the communication protocols, removing the need to develop the hardware and embedded software to carry out the communication. Bluetooth is available in the majority of smart devices, and Android has developed API's (Application Programming Interface) to handle the connection and the sending and receiving of data over the Bluetooth link.

Bluetooth was originally designed as a wireless alternative to RS-232 cables [51]. Bluetooth exchanges data over short distances using radio transmissions at 2.4 GHz [52] and is found in many products including phones, computers and cars. It allows the user to share voice, music and other data wirelessly between paired devices [51]. Classic Bluetooth devices are classified into three classes. Class 2 is the most commonly used class for mobile devices [53].

Table 2. The power and range of the three classic Bluetooth classes [53]

Class	Maximum Permitted Power		Typical Range (m)
1	100 mW	20 dBm	100
2	2.5 mW	4 dBm	10
3	1 mW	0 dBm	1

A new addition to Bluetooth named Bluetooth Low Energy (LE), also marketed as Bluetooth Smart, was introduced in 2011. Bluetooth LE consumes between ½ to $^{1}/_{100}$ of the power of classic Bluetooth. However, the trade-off is a slower data rate [52], hence why it was not considered for this application.

4.2.1 Hardware

For the Bluetooth communication, the Roving Networks RN42 module [54] was used. This Bluetooth module is a class 2 Bluetooth radio and uses Bluetooth 2.1 + EDR (Enhanced Data Rate). It contains an on-board embedded Bluetooth stack, removing the need for a host microprocessor, and has a PCB (Printed Circuit Board) trace antenna resulting in a completely self-contained communications unit. It uses UART (Universal Asynchronous Receiver/Transmitter) to communicate to the microcontroller on the GULPS device and can provide a data rate of up to 3 Mbps (Megabits per second) up to a distance of 20 m [55].

A deciding factor in choosing this Bluetooth module was the availability of a second version that supported the iAP (iPod Accessory Protocols), which would enable development of an iOS version. This version is footprint compatible with the basic RN-42 module [56], however it requires an Apple Hardware developer's license to be purchased.

4.2.1.1 GULPS Simulator

To test the Bluetooth module's functionality, a hardware prototype was designed based upon the Stellaris LM4F120 Launch Pad Evaluation board [57]. This prototype was designed to sit on top of the Stellaris (Figure 4.2). The board has two LED's, one green, to symbolise when the module is connected and one blue, to indicate when in discovery mode. A switch was connected to the reset pin of the Bluetooth module to reset the module if needed. As previously stated, the two boards communicated using the UART method. This test kit was used later in the project to develop the Bluetooth software for the Android tablet.

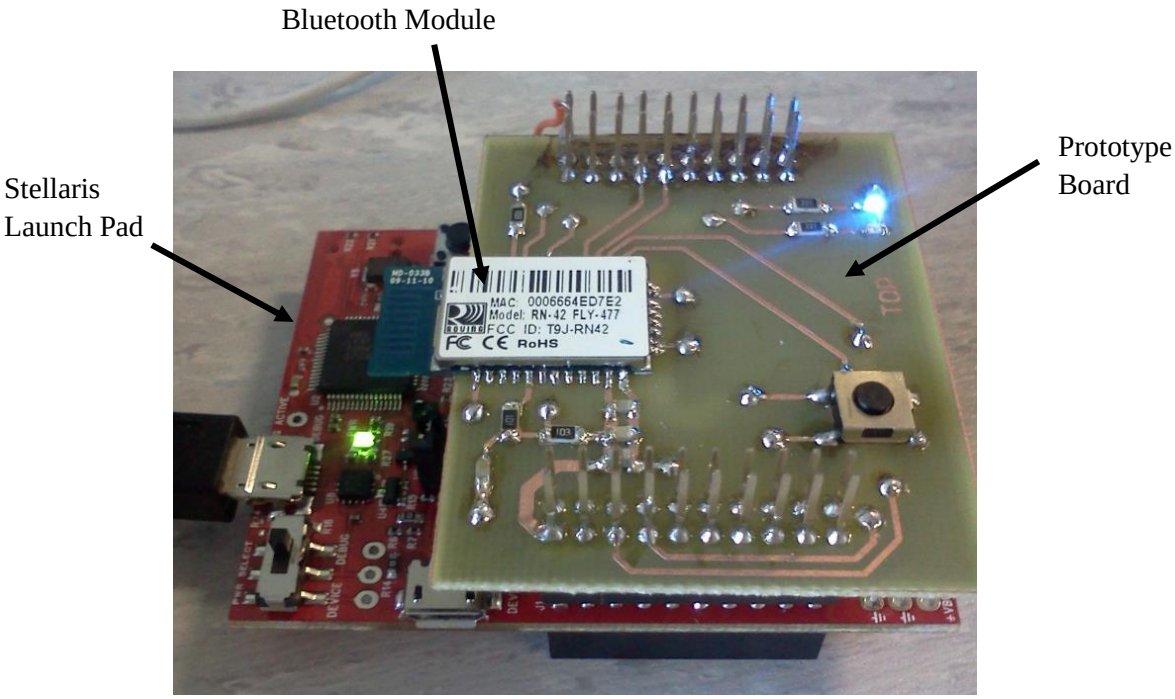

Figure 4.2. Complete Bluetooth board sitting upon the LM4F120 development board.

The firmware implemented on the evaluation board was designed to replicate the GULPS device by sending a signal at the same frequency and format. The GULPS device sends out the impedance measurements for both channels every 20 ms (50 Hz) in the format seen in Figure 4.3 [36].

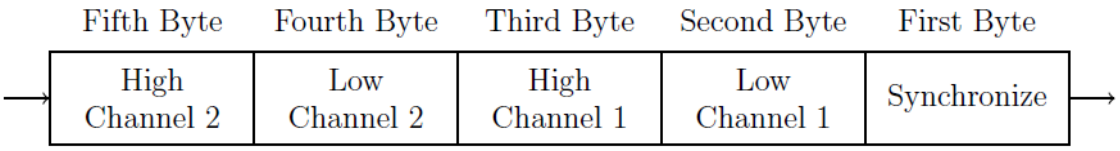

Figure 4.3. The data packet sent by the GULPS device [36].

To imitate the impedance measurement signals, the embedded software on the LM4F120 iterates through the following discretised amplitude arrays to produce two triangle waves, with the second lagging by 180 deg:

Channel 1 signal:

0 1 2 3 4 5 6 7 8 9 10 9 8 7 6 5 4 3 2 1

Channel 2 signal

10 9 8 7 6 5 4 3 2 1 0 1 2 3 4 5 6 7 8 9

4.3 Android App Components

This section provides background knowledge on some of the low-level classes used in Java programming for Android devices. The classes covered in this section have been built by Android (Activity, Fragment, Service, Bluetooth) or are provided by third party developers (Dropbox and AChartEngine). The classes in this section form the foundation of the developed App.

4.3.1 Activity

An Activity is a component that consists of a Graphical User Interface (GUI) and the background code to perform the Activity's functions [58]. An Android App is made up of one or more Activities. One Activity can start another Activity in order to perform different functions in the App. When moving to a new Activity the previous Activity is stopped, but its state is preserved and is added to the Apps stack. This allows the user to navigate back to the previous Activity by pressing the back button.

Activities follow a life cycle state machine (Figure 4.4), which the Activity can enter and leave at any point. The Activity life cycle has five states. In three states the Activity can spend an extended period of time [58], and the other two are transition states. The three main states are:

- Resumed
  - This is the running state, where the Activity is in the foreground and the user can see the GUI and interact with it.
- Paused
  - An Activity enters this state when it is partially hidden from view by another Activity. The activity will not receive input from the user and does not execute any code.
- Stopped
  - In this state, the Activity is in the background, completely removed from view. Information such as member variables will be retained; however the Activity cannot execute any code.

When passing through the other two states (Created and Started), the activity will call their methods then move onto the next state. The final method called in the Activity's lifecycle is `onDestroy()`. This method is called by the system when the Activity is about to be completely removed from the system memory.

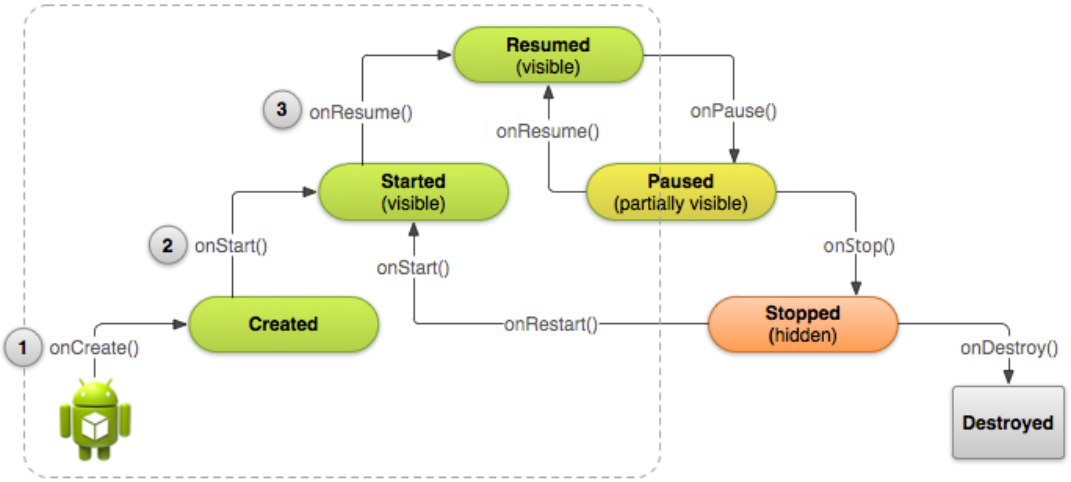

Figure 4.4 - Lifecycle of an Activity [58]

4.3.2 Fragments

Fragments are used to break down an application into reusable modules. Fragments may or may not have a user interface (UI) and have their own lifecycle (Figure 4.5); however, a fragment must be attached to an Activity. The state of the host Activity impacts on the state the fragment is in. For example, if the host Activity is paused, then the fragment is also paused. Multiple fragments can be attached to an Activity at once, creating a multi-plane UI.

The lifecycle of a fragment is very similar to the life cycle of an Activity. A fragment can exist in three states: resumed, paused, and stopped [59].

- Resumed
  - The fragment is visible and is attached to the running Activity.
- Paused
  - The fragments' host activity has been paused but not stopped.
- Stopped
  - The fragment is not visible. The Activity has been stopped or the fragment has been removed from the Activity. A stopped fragment is still alive, maintaining all state variables, but is no longer visible and will be destroyed if the Activity is destroyed.

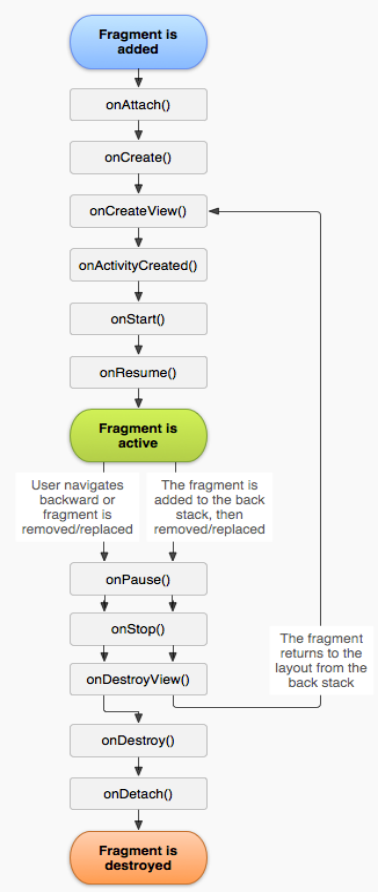

Figure 4.5 - Fragment Lifecycle [59]

4.3.3 Services

A service is a component which is used to perform long running tasks in the background, and does not have a user interface. An application can start a service, and the service can continue to run even if the starting application is destroyed. Applications can also bind to an existing service to interact with it. By default the service runs in the main thread of the hosting process. However, a new thread should be created within the service if CPU intensive operations are going to be performed.

4.3.4 Bluetooth Package

Android has developed a number of classes to implement Bluetooth communications. The Bluetooth module created for the project uses three classes to locate devices, connect to a device and read and

write data to connected devices. The classes can be used at Android API level 5 and higher, and are compatible with platform version Android 2.0 (Eclair) onwards [60].

The classes used are:

- BluetoothAdapter
    - This class represents the device's Bluetooth radio. Through this class, tasks such as device discovery and creating Bluetooth sockets can be performed. [61]
- BluetoothDevice
    - Represents a discovered Bluetooth radio. Using this class, a connection to the represented device can be established and queries for device information can be sent. [62]
- BluetoothSocket
    - Used to create an outgoing connection and manage the connection. Uses an interface similar to a TCP (Transmission Control Protocol) socket (java.net.Socket). The BluetoothSocket supports the most commonly found socket type, RFCOMM (Radio Frequency Communication), also known as SPP (Serial Port Profile) [63].

4.3.5 Third-Party Android Packages

An advantage of using the Android platform is the amount of 'free to use' software. For this App, two third-party Android Packages were used and are covered below.

4.3.5.1 Dropbox Package

Dropbox is a file hosting service provided by Dropbox Inc. [64]. Dropbox allows users to upload files and view them from anywhere over an internet connection. Dropbox also allows users to share files and folders with other users. Dropbox Inc. has developed a series of API's for Dropbox integration to an App. There are four different Dropbox API's, each giving the App different Dropbox functions. For this project the Sync API was chosen because it presents the developer with a file system similar to java.io.File class, used for saving to the SD card. It handles caching, network unreliability, and folder synchronizing. Every App that requires Dropbox permission must first be registered with Dropbox.com. When registering the App, the read/write permission for the App is selected. For this project, the permission type chosen was App Folder [65]. The App Folder permission will create a folder named after the App in the user's Dropbox. The App is given read/write access to this folder, but is restricted to items contained in this folder. The classes used in this App are:

- DbxAccountManager
    - This is the starting point when using the Sync API. This class is used to link to the user's Dropbox account [66]. From this a reference to the Dropbox file system (DbxFileSystem) can be obtained.
- DbxFileSystem
    - Allows the App access to the Dropbox files and folders. It presents the Dropbox directory as if it was a local directory, allowing the App the same functions as a file browser. Through the DbxFileSystem the App can create, delete, open, and modify folders and files [65].
- DbxFile
    - Represents a file in the Dropbox, it can be used to read and write to and from the file. It can also make a call to update the file if modified [65].

4.3.5.2 AChartEngine Package

AChartEngine is an open source graphing software package published by 4ViewSoft [67]. AChartEngine provides API's for various graphs including line, scatter, pie and bar graphs. There are also tutorials on YouTube that outline the basic graphing tools, which make learning to use this software very easy. This package was chosen because it is the most common free to use graphing package in the Android market. It is used in over 3000 Apps which is more than twice than that of its nearest competitor, androidPlot [68, 69].To produce a line graph the following three classes from the AChartEngine library were used:

- XYValueSeries
  - This class is used to hold x, y points for one set of data in the chart. Points can be added, removed, or read from the series.
- XYSeriesRenderer
  - This class is used to configure the display settings for the matching XYValueSeries.
- GraphicalView
  - This class creates a view that contains the chart. This uses the settings set in the XYSeriesRenderer to display the XYValueSeries. The global graph settings of the chart, for example, axis labels can be modified through this class.

4.4 The App Design

The App uses fragments to implement every GUI and module, and uses one Activity as a container, holding all the fragments and passing data between each fragment. The advantage to this structure is that each module is decoupled. Background tasks, such as the Bluetooth connection and the data decoding thread, were easier to maintain in a single Activity design. In a multiple Activity design, the background tasks would need to be passed between Activities, slowing the transition down.

4.4.1 Graphical User Interface

The UI for the App was designed to be simple, with large text and buttons for ease of use. To accommodate the variety of different screen sizes and orientations, Android developers can create different layout designs for each property. This was utilized to enable the App to function on any Android device. To design for different pixel density screens, all dimensions were defined in density-independent pixels (dp), which are scaled by the system at runtime based on the device's screen.

A flow diagram of the App can be seen in Figure 4.6. This shows the possible displays presented to the user. To move forward in the App buttons are provided to the user, allowing the user to move into the next stage. To navigate backwards the user presses the back button on the tablet.

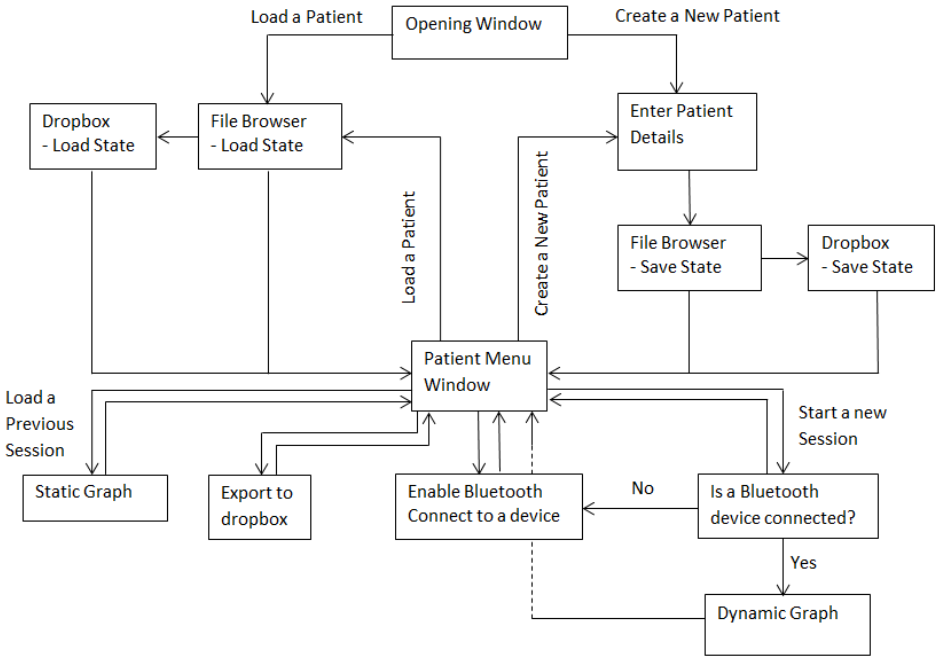

Figure 4.6 - Flow diagram of the App's GUI

The App, named GULPS2GO, has two menu fragments and a fragment where the user can enter their personal details. The first menu fragment is presented to the user when the App is first opened (Figure 4.7), from this window the user can create a new profile or load a previous profile.

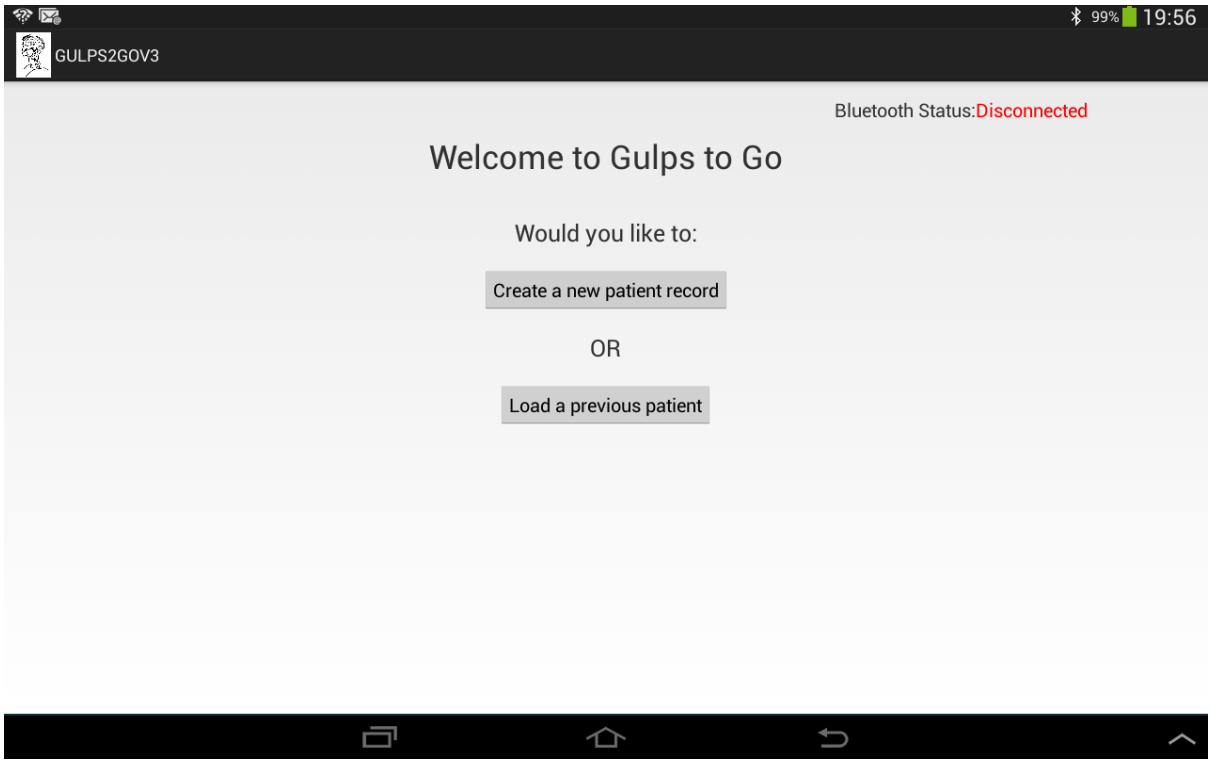

Figure 4.7. The opening screen of the GULPS2GO App.

If the user selects to create a new patient profile, then the user is present with the screen as shown in Figure 4.8. The patient can enter in information by selecting the desired field to open the keypad.

To select the user's date of birth, a pop-up window with three swipe fields is presented (Figure 4.9). To select the gender a drop-down box is used when the gender field is pressed. The user cannot continue past this screen unless the patients ID, patient name, date of birth and gender fields are complete. These fields are mandatory because they are required to create and save the patient profile. An extra field was added to allow the user to enter additional notes if needed, however, completing this field is not mandatory.

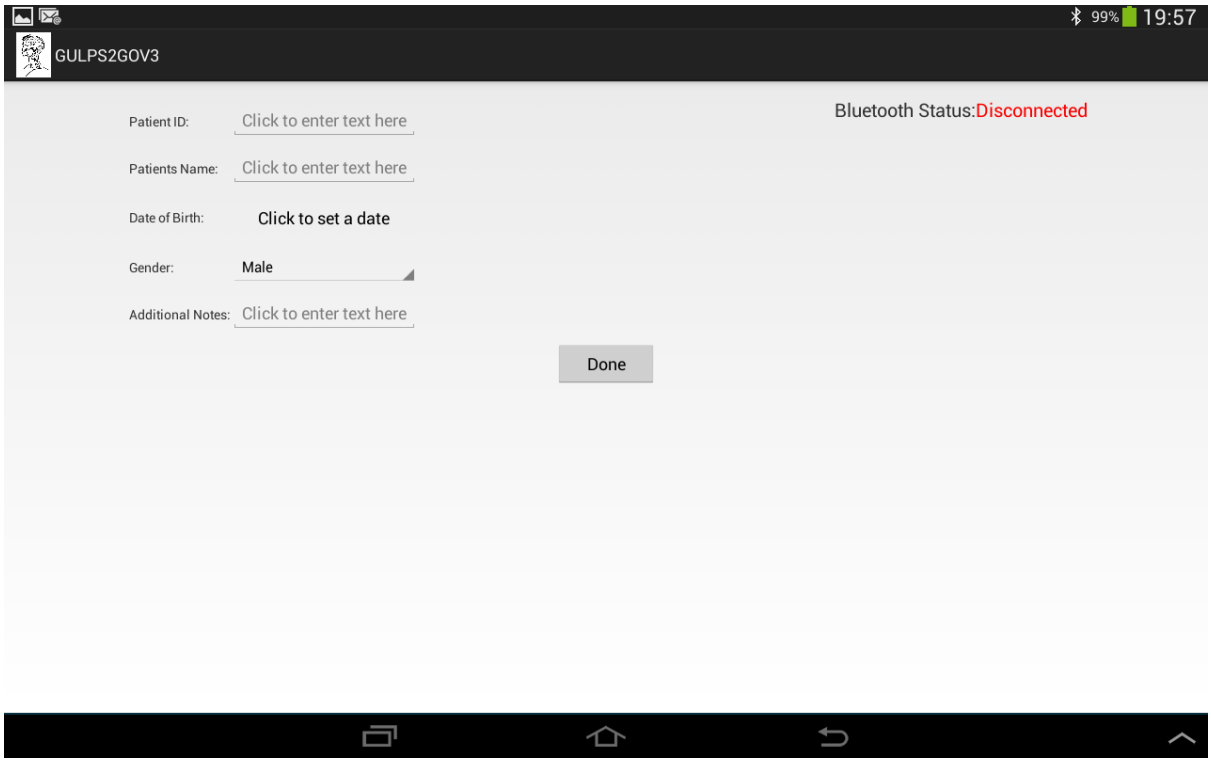

Figure 4.8. The UI of the fragment that records patient details

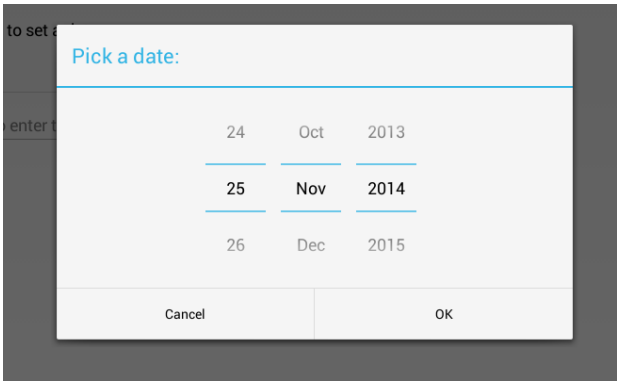

Figure 4.9. The pop-up window with three swipe entry fields for the user to select their date of birth.

Once a patient profile has been created or loaded, the user is then presented with the main user menu (Figure 4.10). From this menu the patient can start a new recording session, load a previous session connect or disconnect Bluetooth and export the patient file to Dropbox. The disconnect button is not visible until Bluetooth connection has been established (Figure 4.11). When connect has been established the status indicator changes from Disconnect to Connected. A new session cannot be started without a Bluetooth connection and if the user attempts to start a session without a connection, Bluetooth will automatically start a search sequence.

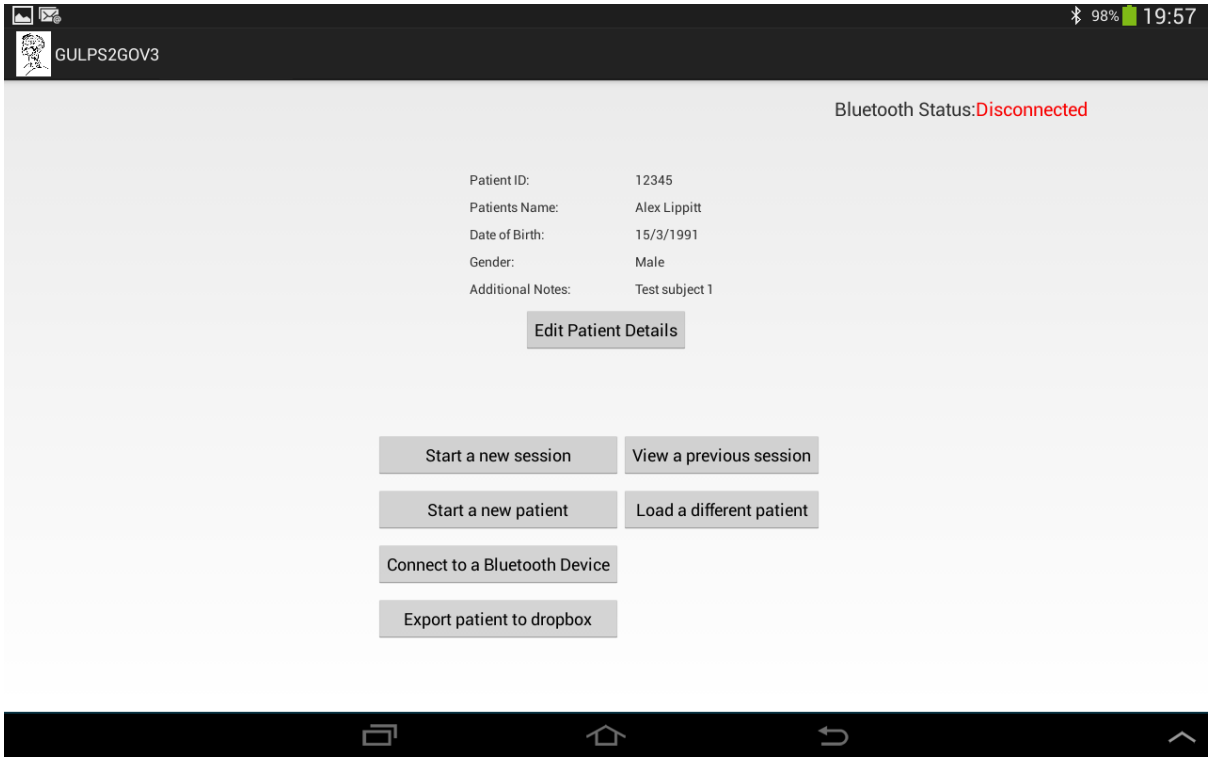

Figure 4.10. The main patient menu window UI without a Bluetooth device connected.

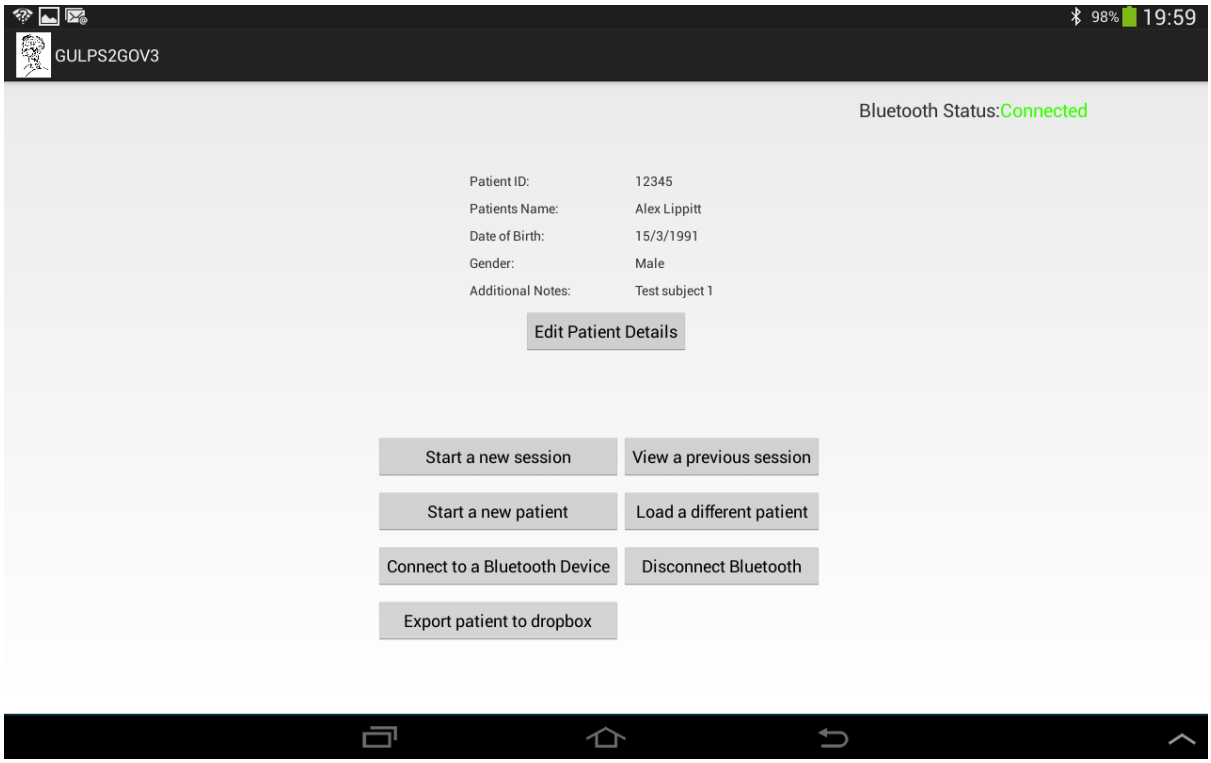

Figure 4.11. The main patient menu UI with a Bluetooth device connected.

4.4.2 Bluetooth Module

This section covers the design of the Bluetooth module. This module was created to implement the following functions:

- Search for available Bluetooth devices and list the discovered devices.
- Allow the user to choose which device they would like to connect to.
- Initiate connection and provide feedback on whether connection was successful.
- Establish communication with the device once connected.
- Provide a method to handle the incoming and outgoing data.
- Allow the connection to be closed.

At the top level, a fragment without a GUI is used, allowing it to operate constantly in the background of the App. Through this Fragment the functions listed above can be performed by the host Activity. A Fragment must be used because the Bluetooth module creates several dialog box Fragments and displays Toasts (a pop-up message) during the connection operations, and this can only be performed by either a Fragment or Activity.

4.4.2.1 Searching for devices

To begin the discovery process (Figure 4.12), the module first checks if Bluetooth is enabled. If it is not, the user is prompted to turn it on because the Android OS requires the user to be prompted by the App to turn on Bluetooth. Discovery is then started and two broadcast receivers are registered. Broadcast receivers asynchronously respond to messages broadcasted by other applications or by the application itself and pass information in an object called Intent. In this case the receivers react when a device is found (Flag: BluetoothDevice.ACTION_FOUND) and when the discovery is finished (Flag: BluetoothDevice.ACTION_DISCOVERY_FINISHED).

```
private void findDevices() {

  // Disable discovery
  if (btAdapter.isDiscovering())
    btAdapter.cancelDiscovery();

  clearArrays();

  if (mDevice == null) { // If not connected to device
    toastText = "Starting discovery for remote devices....:";
    Toast.makeText(appContext, toastText, Toast.LENGTH_SHORT).show();
    // Start discovery
    if (btAdapter.startDiscovery()) {
      hasDiscovered = false;
      toastText = "Discovery thread started...Scanning for devices";
      Toast.makeText(appContext, toastText, Toast.LENGTH_SHORT).show();
      appContext.registerReceiver(discoveryResult,
                      new IntentFilter(BluetoothDevice.ACTION_FOUND));
      appContext.registerReceiver(discoveryResult,
        new IntentFilter(BluetoothAdapter.ACTION_DISCOVERY_FINISHED));
    }
  }
}
```

Figure 4.12. The code to initiate the search for Bluetooth devices. This code is part of the BluetoothFragment.java class.

In the case of device found, the name and the class BluetoothDevice.java are pulled from the passed Intent and stored in arrays. When discovery is finished, the user is alerted with a Toast which displays a new dialog fragment showing the discovered devices (Figure 4.13). This dialog fragment allows the user to select a device to connect to, rediscover or cancel.

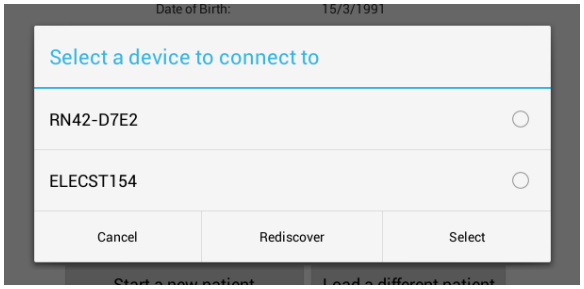

Figure 4.13 - Dialog fragment displaying the discovered devices after a search

4.4.2.2 Connecting to a device

Connecting to a Bluetooth device is handled in the custom class called ConnectToBluetooth.java. This class implements Runnable.java. The class constructor requires a specification of the desired device to connect to, the Bluetooth adapter, and a message passer handler. A socket is initialized to connect to the device using a common SPP UUID (Serial Port Profile Universally Unique Identifier).

In the `run()` method (Figure 4.14), a call to cancel discovery is first made. This is due to the discovery process being a resource heavy procedure and will significantly slow down the connection attempt [63]. An attempt is then made to connect to the device through the socket. If the connection is successful then a message is passed to the Bluetooth fragment to begin communicating with the device through the SendReceiveBytes.java class. If the connection is unsuccessful, another message is passed to the Bluetooth fragment to display a Toast pop up message. The attempt to connect is a blocking method, and is placed in a separate thread to prevent the Apps UI becoming unresponsive during the connection process.

```
public synchronized void run() {

  android.os.Process.setThreadPriority(
      android.os.Process.THREAD_PRIORITY_BACKGROUND);
  // Cancel discovery on Bluetooth Adapter to prevent slow connection
  btAdapter.cancelDiscovery();

  try {
    mySocket.connect();
    isConnected = true;
    mHandler.obtainMessage(CONNECTED).sendToTarget();
  } catch (IOException connectException) {
    try {
      isConnected = false;
      mHandler.obtainMessage(FAIL_CONNECT).sendToTarget();
      mySocket.close();
    } catch (IOException closeException) {
      Log.e(EXCP_LOG, "exception", closeException);
    }
    return;
  }
}
```

Figure 4.14. The `run()` method for the connectToBluetooth.java class.

4.4.2.3 Sending and Receiving

A class called SendReceiveBytes.java is responsible for reading data from the Bluetooth radio and also sending data. In this application, checking for newly received data needs to happen as often as possible and this is best achieved in a separate thread; this class implements the Runnable.java class to achieve this. To initialise the class, the Bluetooth socket (created when connecting to a device) and a message

handler are passed in. To read from the smart device's Bluetooth radio, an Input Stream (java.io.InputStream) is retrieved from the Bluetooth socket. To write data to the radio, an Output Stream (java.io.OutputStream) is opened to the socket.

Reading from the Bluetooth radio is performed in the `run()` method of the class (Figure 4.15). The `run ()` method will loop through the following sequence, until it is cancelled by the App:

- Read from the Input Stream.
- Store the data read in an array and store the number of bytes read.
- Loop through the array, storing each element in a blocking queue (java.util.concurrent.BlockingQueue).

A blocking queue is used because it is thread safe, with the concurrency methods handled internally. To read from this buffer, a method is passed up to the Bluetooth Fragment to be called by an external Activity or Fragment. To send data, an array of bytes is passed to the opened Output Stream (Figure 4.16).

```
public synchronized void run() {
  android.os.Process.setThreadPriority(
      android.os.Process.THREAD_PRIORITY_BACKGROUND);
  byte[] buffer = new byte[1024]; // buffer store for the stream
  int bytes; // bytes returned from read()

  // Keep listening to the InputStream until an exception occurs
  while (!Thread.currentThread().isInterrupted()) {
    try {
      // Read from the InputStream
      bytes = btInputStream.read(buffer);
      //Write to the queue
      for (int i = 0; i < bytes; i++) {
        queue.offer((int)buffer[i]);
      }
    } catch (IOException e) {
      mHandler.obtainMessage(LOST_CONNECTION).sendToTarget();
      Log.e(EXCP_LOG, "exception", closeException);
      break;
    }
  }
}
```

Figure 4.15. The `run()` method for reading from the Bluetooth radio in the SendReceiveBytes.java class.

```
public void write(byte[] bytes) {
    try {
      btOutputStream.write(bytes);
    } catch (IOException e) {
      mHandler.obtainMessage(LOST_CONNECTION).sendToTarget();
      Log.e(EXCP_LOG, "exception", e);
    }
}
```

Figure 4.16. The method used to write data to the Bluetooth radio in the SendReceiveBytes.java class.

4.4.2.4 Bluetooth Service

The largest problem the Bluetooth module showed was losing connection when the App was recreated. An App can be recreated for many reasons - the two most common were screen rotation and displaying the keyboard [70]. The problem was that the BluetoothSocket variable could not be stored in a Bundle

to be retained upon restart. The solution to this problem was found by using a Service. An Android Service is not affected by the Apps life cycle and is not stopped or paused during a configuration change [60]. In the Service, instances of the BluetoothAdapter, BluetoothDevice and BluetoothSocket are held. The connecting thread and the reading and writing thread are also performed in the service. Using a Service, Bluetooth connection can now be maintained during recreation of the App.

4.4.2.5 Reading from the Bluetooth Module

To read from the Bluetooth module, a thread in the main activity is used. This thread loops continuously, reading from the Bluetooth Buffer. The read value is bitwise AND-ed with 0xFF (255) to reduce the number size from 32-bit to 8-bit, the same bit size sent by the GULPS device. If the user is not recording a session or the session is being saved, paused, or stopped, the data will be discarded. When a session is being recorded the thread follows the state machine shown in Figure 4.17. Each impedance value sent by the GULPS device consists of a high and a low byte (outlined in Section 4.2.1.1). The high byte is left shifted by 8 bits and added to the low byte Figure 4.18. This value is then stored in the dynamic graph's blocking queue.

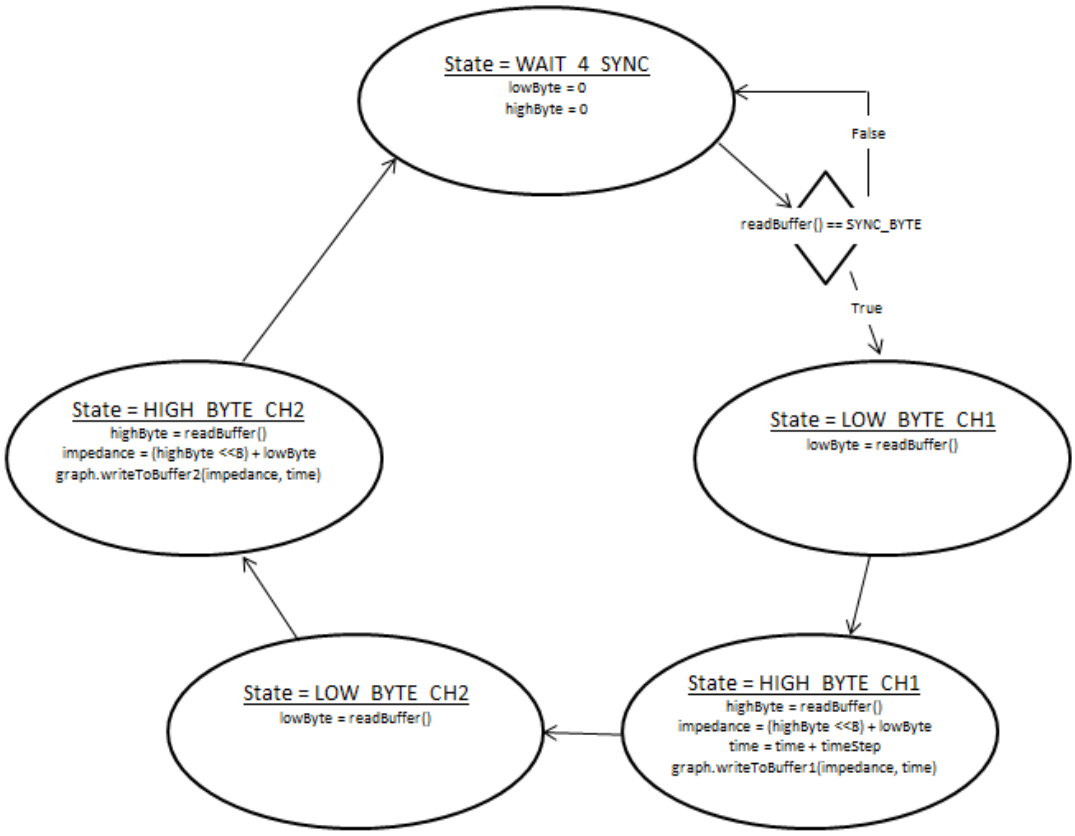

Figure 4.17 - State machine for decoding the data received by the Bluetooth module

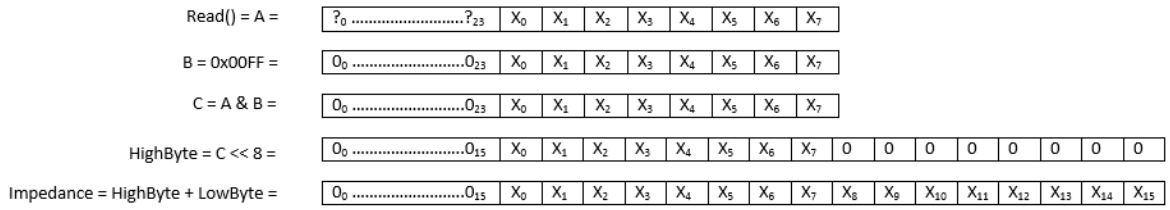

Figure 4.18. Bit operations that occur in the high byte states

4.4.3 Graphing Module

A line graph is used to display the data received by the Bluetooth module. The data is displayed in a dynamic graph updating in real time. This data can be saved and re-displayed later in a static line graph. Both types of graphing use the same base classes, only differing in the method the data is added. Some additional features of the graph include zooming, displaying a value at a selected point and graph rotation.

4.4.3.1 Dynamic Graphing

The dynamic graph module was designed as a fragment that could be placed inside a host activity or another fragment. To prevent slowing down the response time of the main Activity thread, the reading of data and redrawing of the graph was carried out in a separate thread (Figure 4.19). A read from the first channel's buffer is performed, and the returned value is checked to see if it is within 5% of the current maximum/minimum displayed values. If it is within the 5% threshold, the y axis will be increased/decreased in the appropriate direction. The data point is added to the channel one data set then the same process is carried out to read from the second channel. A flag is then set, to indicate that the graph needs to be redrawn and the latest x value plotted is compared with the x-axis. If the current value is greater than the x-axis, the graph window will be shifted over by the range currently being displayed.

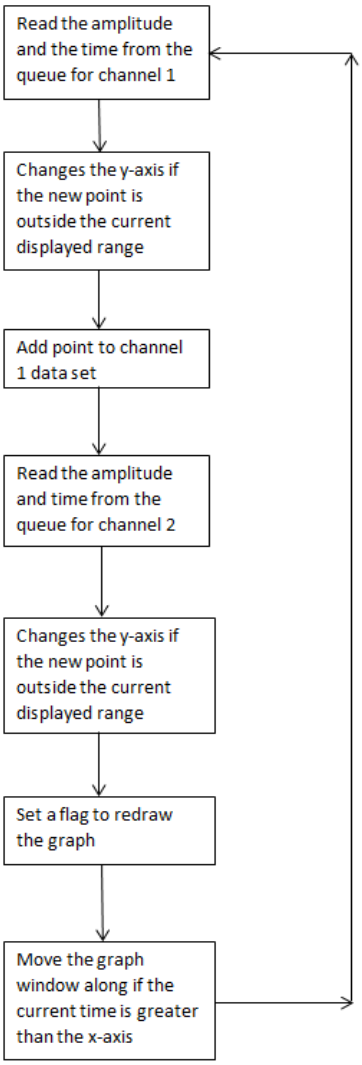

Figure 4.19 - Operations performed in the Dynamic Graphing Thread.

Before entering the dynamic graphing fragment, the user is presented with a text box (Figure 4.20) in which they can enter in information about the session they are about to undertake. This will then be presented to the patient later when they review recorded sessions.

The user interface for the dynamic graph fragment was kept simple (Figure 4.21), with the plot taking up the majority of the screen. Buttons were added to perform the functions: pause, stop, restart, save and rotate graph (Figure 4.22). In-built into the AChartEngine API were the three zoom buttons; two buttons will allow the user to zoom in or out, at a constant rate, and the last button will zoom the plot to a 1:1 scale.

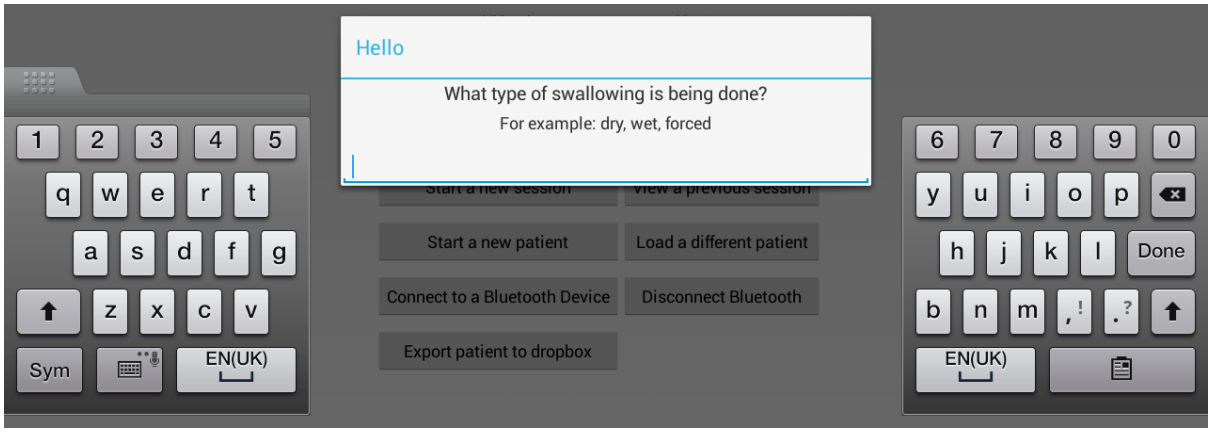

Figure 4.20. The text box presented when starting a new session.

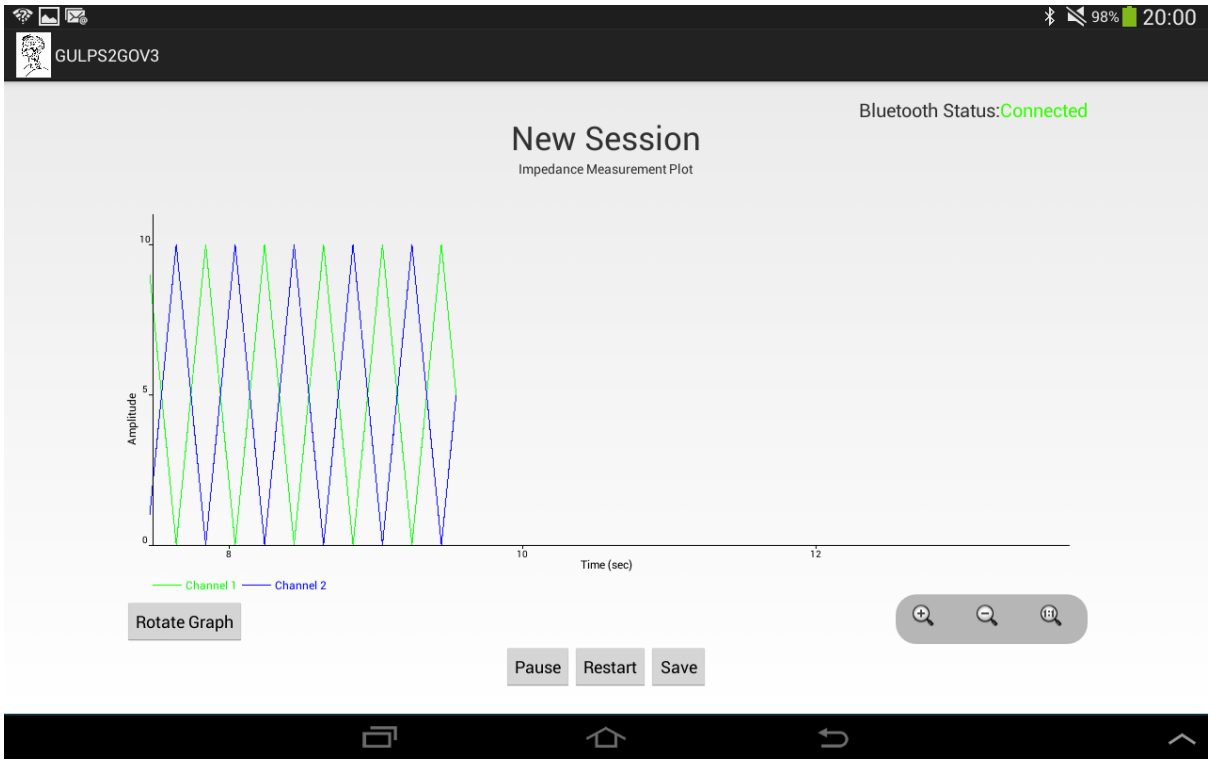

Figure 4.21. Screen shot of the dynamic graph fragment plotting data sent via Bluetooth from the GULPS simulator.

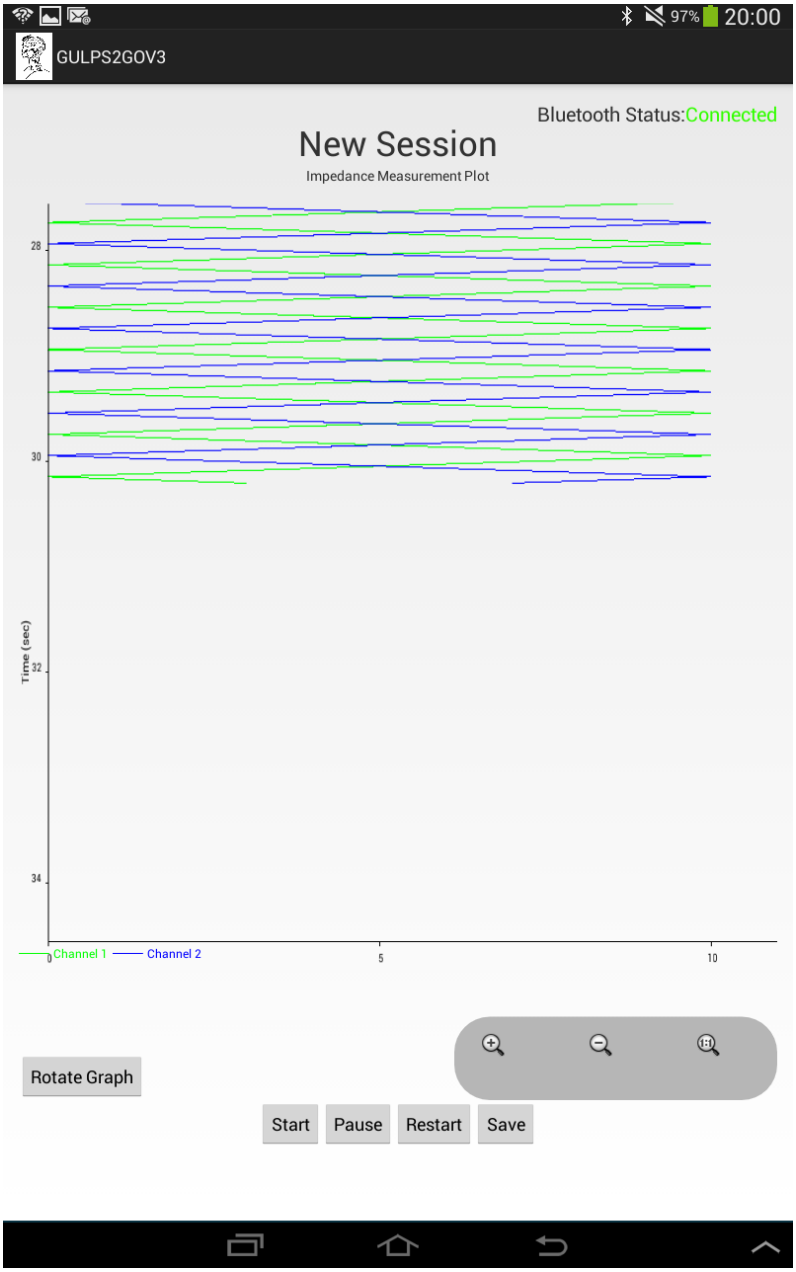

Figure 4.22. A screen shot of the dynamic graph fragment when the plot has been rotated.

4.4.3.2 Timer Class

Originally a class was created to keep track of the time while the session is being recorded. This class used the Timer class (java.util.Timer) to increment a counter at a fixed interval, every millisecond. The counter was then read by the decoding thread and divided by 1000 to give the time in seconds. Using this method it was found that the points were not plotted at a constant time step. Based on the performance of the timer class, it was found that this method of keeping time was not accurate to 1ms and the time could be influenced by other tasks scheduled by the Android OS. Traceview [71] was used to generate a profile of the Timer thread and the main thread during a recording session (Figure 4.23). The yellow boxes indicate the time spent in the run method of the Timer, which increments the counter. It can be seen that the Timer is not restricted to incrementing every millisecond. Using Traceview affects the overall timing of the App but can be used to view timing of events relative to each other.

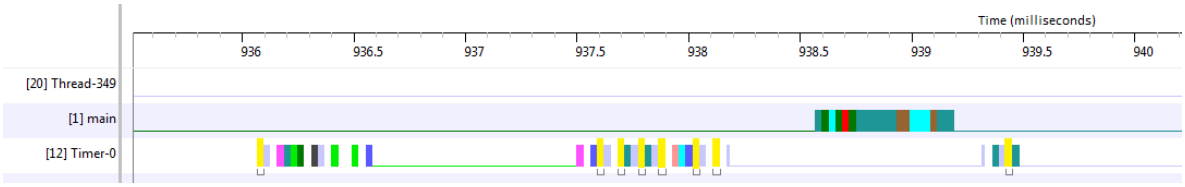

Figure 4.23. Traceview of the Timer thread (Timer-0) and the main thread for the App. The yellow boxes represent time spent in the run method of the Timer, the other boxes represent the time spent in other methods of the main and Timer threads.

Instead, a counter was used that incremented by 20 ms every step and was incremented every time a new data point for both channels was added (Figure 4.17). Chester [36] noted that the embedded software developed for the GULPS project did not use a constant transmission frequency, and this would need to be adjusted to ensure the data was sent out at 20 ms intervals to match the counter used in the App. With this solution, the assumption is made that no data is missed by the App and that the data is sent every 20 ms. A possible improvement would be to send the time stamp from the microcontroller with the measured impedance, and use the time stamp to plot the data.

4.4.3.3 Performance

When using the dynamic graph to display data from the GULPS simulator, the graph lagged as more data points were added. This was due to the increasing amount of points being drawn every time the graph was being redrawn. To reduce the number of points to be plotted, two datasets for each channel were created. One held all the data written to the series, whereas the second only held the currently displayed data. The second dataset was used for real-time plotting, and would be cleared every time the x-axis window was shifted. The first dataset was used for saving and displaying the data when the graph was paused. A significant visual increase in the performance was noticed, although the graph could still lag. Due to the infrequent and small amount of lag occurring, no further work was carried out on improving the module's performance.

4.4.3.4 Static Graphing

A static graph is used to display sessions which have already been recorded. This is done in a fragment which is to be embedded inside an Activity or another Fragment. To create a graph, arrays containing the historic x and y co-ordinates are passed to the Fragment. A `For` loop is used to iterate through the arrays adding the data points to the datasets. Once this is complete the graph is drawn.

When a user selects to view a previous session, they are presented with a list of all previously recorded sessions (Figure 4.24). The list contains the session number and the information entered for that session. From this list the user can select the session they are to view. The UI of the static graphing fragment (Figure 4.25) is similar to the dynamic graphing UI, with the addition of the session information being displayed at the top of the screen.

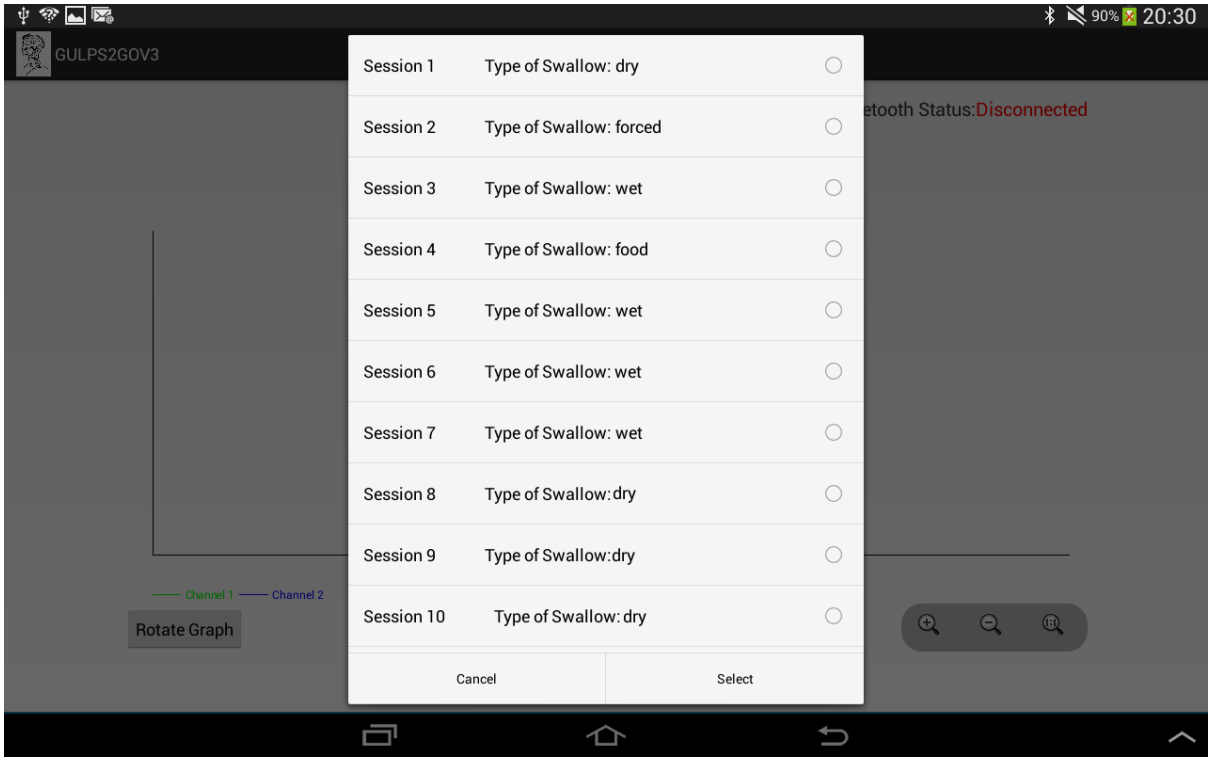

Figure 4.24. An example of the list presented when a user is selecting to view a previous session

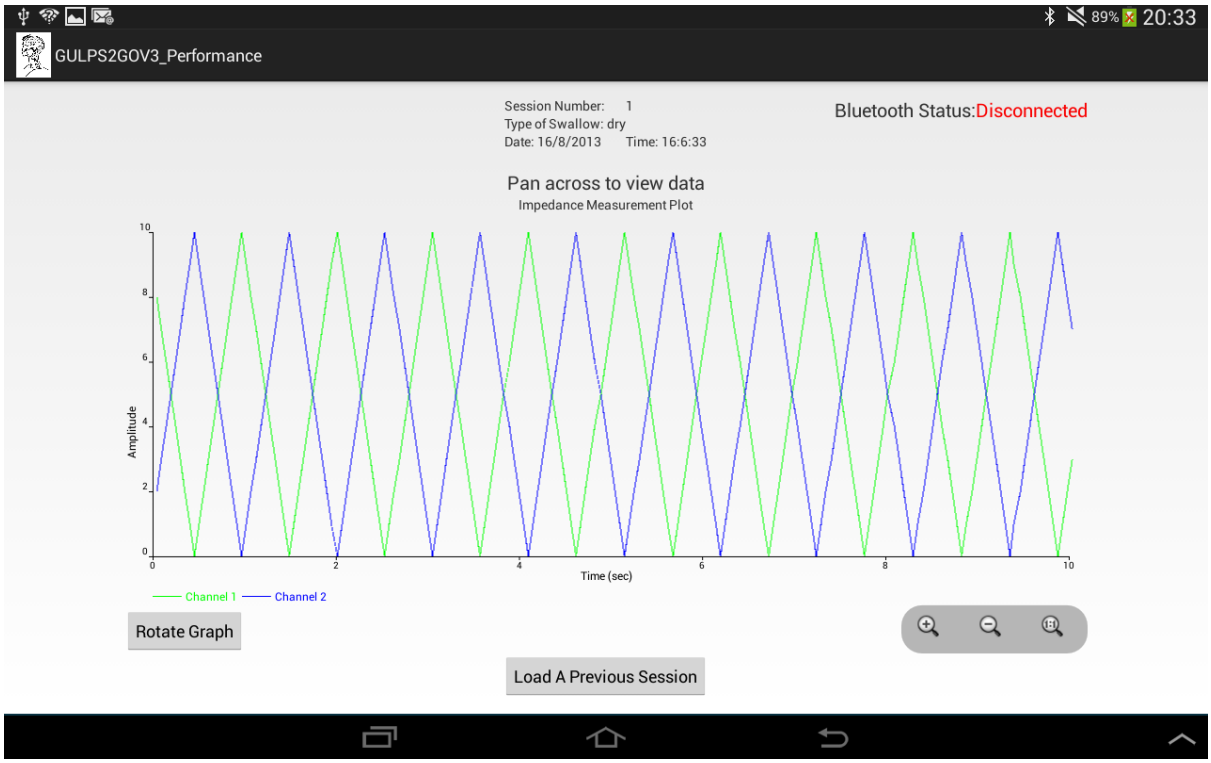

Figure 4.25. The UI for the static graph fragment.

4.4.4 File Saving and Loading Module

There are two methods of file storage being used in this App: the local SD card and to Dropbox. Both methods of data storage use the same Java methods to write and read from a file, but differ in the method of gaining access to the file. A base class (FileOperationsClass.java) was implemented which carried

out the writing and reading functions. For each method of file storage, a class was created to set up access to the files, and then feed the files into the base class. Another class wraps the two top level classes into a single interface. This reduced the code complexity in the host activity, using the same function calls for both methods of storage, and therefore removing the need for the host Activity to know which method of storage was currently being used (Figure 4.26).

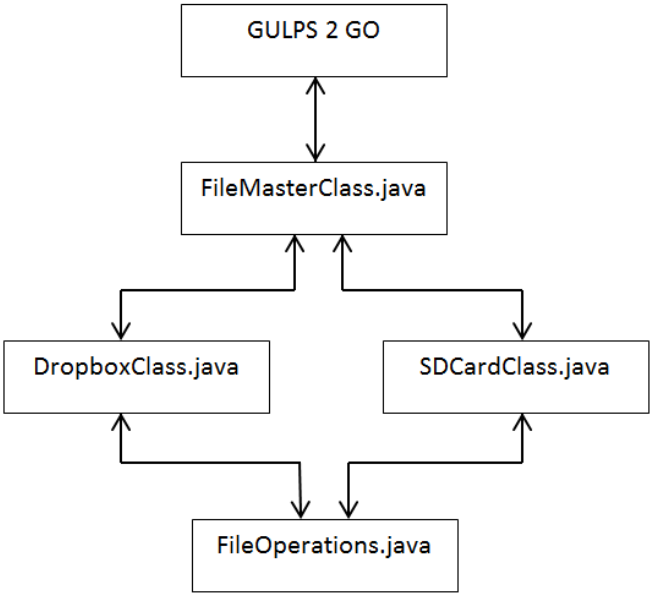

Figure 4.26. Hierarchy of the file saving and loading module.

To access files on the SD Card, the File.java libraries [72] were used. Using the File.java constructors, the App only requires the pathname to the file to open or create a new file. To read from a file the FileReader.java [73] class is used, and to write to a file the FileOutputStream.java [73] class is used.

For an App to have access to Dropbox, it must first obtain an instance of the Dropbox account manager (DbxAccountManager.java). This will establish a connection to Dropbox, asking the user to log-in to Dropbox if this is the user's first time using the App. Once this has been done, the Dropbox file system (DbxFileSystem.java) is obtained. Through the file system, files can be created, opened and written to. With the DbxFileSystem.java the process of reading and writing files is the same process used with the SD Card.

Each patient dataset created has a text file containing the patient information, labelled after their name. In the patient information file is the patient's name, date of birth, gender, ID number, additional patient notes, number of sessions and the file path to the session data. A folder was created in the same location. This folder contained all the data on recorded sessions.

For each session saved, two files are created; a session information file (.txt) and a session data file (.csv). In the session information file, the date and time of saving is recorded and the type of swallow being performed. The session data file stores the data in the csv format with the columns: time channel 1, amplitude channel 1, time channel 2, and amplitude channel 2.

A file browser (Figure 4.27) was created which would allow the user to graphically select the location they would like to save at or the file they would like to load. This file browser is the same for both SD Card and Dropbox, with a button at the bottom of the screen for the user to switch between the two.

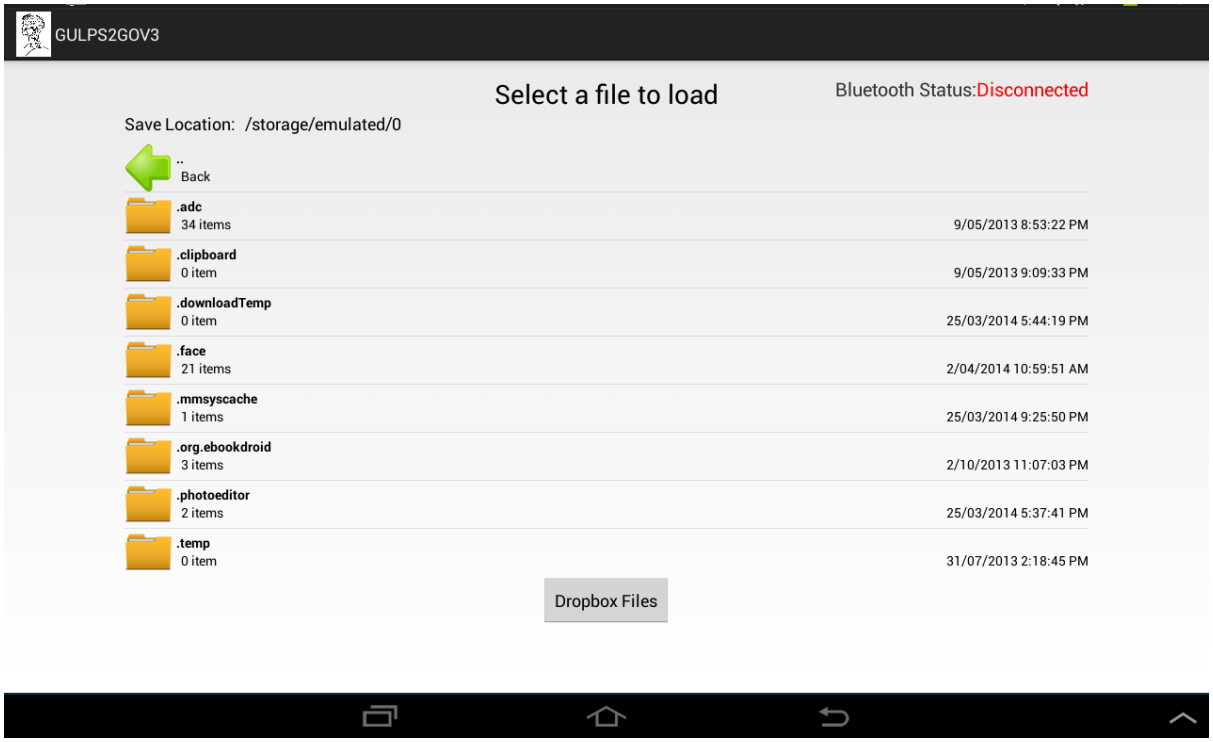

Figure 4.27 - The file browser developed for the GULPS 2 GO project

4.5 Summary

An Android App was successfully created that could communicate with the designed Bluetooth module, which sends data every 20 ms, the same speed as the GULPS device. This data was then plotted on a real time graph which infrequently suffered from visible lag. The data could be recorded and saved on the devices' SD card or in the user's Dropbox. The Bluetooth module is ready for integration with the GULPS prototype.

The developed App software code has been stored in a repository at this location: https://github.com/ALippitt1/GULPS2GO.git

Chapter 5.0 Hardware Development

To improve the consistency of the GULPS output waveform, the effect of the injection frequency of the constant current signal was investigated. The hardware design was kept the same as the previous prototype where possible, so only the effect of the injection frequency would be apparent. In Chester's [74] GULPS prototype, there are two sections that are frequency dependent, the sinusoidal wave generator and the bandpass filter. A modular hardware design approach was utilised, allowing easy switching of the frequency dependent boards for this investigation and also allowing the design to be flexible and easy to make changes in future development.

The original frequency pair was 40 kHz and 70 kHz which was placed at the beginning of the beta dispersion zone. A frequency pair one decade lower will be in the alpha dispersion zone. The middle of the dispersion zone is one decade higher at 400 kHz and 700 kHz and the top of beta dispersion zone is 4 MHz and 7 MHz. Picking frequencies moving in both directions of the frequency spectrum will give an indication of what the effect frequency has on the output waveform of GULPS and if new identifying features are present (Table 5.1).

Table 5.1. The frequency pairs used to test the effect of the injection frequency. 40 kHz and 70 kHz was the original frequency pair used by Chester.

f_1 (kHz)	f_2 (kHz)
4	7
40	70
400	700
4000	7000

5.1 Hardware Design

The original GULPS hardware was broken down into modules that separated each section of the design (Figure 5.1). The design of each module duplicated the original design, except when changes were required due to the increase in operation frequency. The modules are:

1. Sinusoidal wave generator
2. Constant Current Generator
3. Instrumentation Amplifier
4. Bandpass filter
5. Signal processing
    a. Demodulator
    b. High-pass filter
    c. Anti-aliasing filter
6. Microcontroller
7. Power

To reduce development time the power module was not designed and a dual output lab power supply was used to provide the ±5 V rails. The interface between each module can be seen in Figure 5.1.

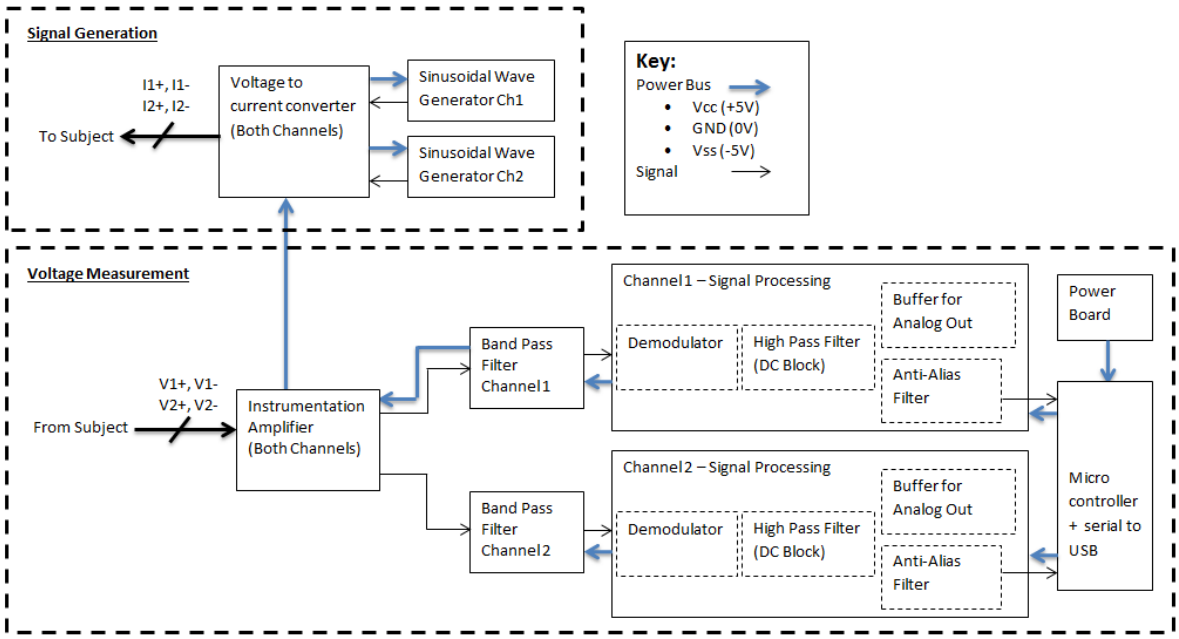

Figure 5.1. Module block diagram, showing the interface between each board.

5.2 Frequency-Dependent Design Changes

It was desired to keep everything as close to the original design as possible, however, due to the increased bandwidth of test frequencies, several components required changing. The two frequency dependent modules, the sinusoidal wave generator and the bandpass filter, were redesigned and an individual board was made for each frequency, based on a common design.

5.2.1 Sinusoid Wave Generator

The original generator chip, LTC6900 [37], was used because it has a frequency range of 1 kHz to 20 MHz with a 0-5V, rail-to-rail, 50% duty cycle square wave output. The output frequency of the chip is set by two resistors. To calculate the resistor value Equation 2 from the datasheet was used (Table 5.2). Two different settings were used for N, due to its limiting impact on the output frequency (Figure 5.2). An N value of 100 was used for frequencies less than 100 kHz and for frequencies greater than 100 kHz, an N of 1 was used.

$$f_{OSC} = 10MHz \cdot \left(\frac{20k}{N \cdot R_{SET}} \right) \quad 2$$

Table 5.2. Resistor and Capacitor values for the sinusoidal waveform generator for the different injection frequencies. R_{SET} = R1 + R2

Resistors to set oscillator frequency			Low Pass Filter			High Pass Filter		
Frequency (kHz)	R1 (kΩ)	R2 (Ω)	R_{lp} (Ω)	C_{lp} (nF)	F_C (kHz)	R_{hp} (kΩ)	C_{hp} (nF)	F_C (kHz)
4	470	30000	27 000	1	5.89	160	1	1
7	270	15000	18 000	1	8.84	160	1	1
40	47	3300	2 700	1	58.9	16	1	9.95
70	27	1500	1 800	1	88.4	16	1	9.95
400	4.7	300	270	1	589	1.6	1	99.5
700	2.7	150	180	1	884	1.6	1	99.5
4000	0.47	33	27	1	5840	0.16	1	995
7000	0.27	15	18	1	8840	0.16	1	995

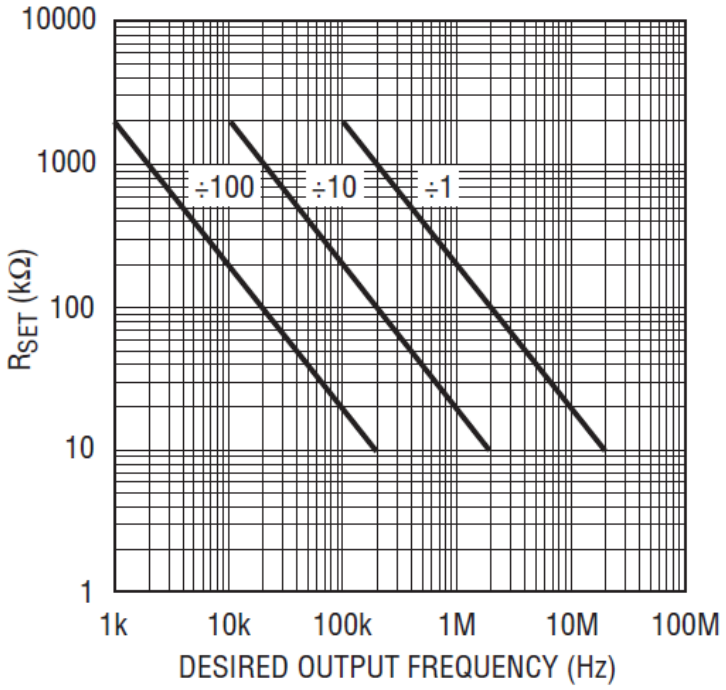

Figure 5.2. R_{SET} versus the desired output frequency for the LTC6900 [37].

To remove the third harmonic of the square wave and the 2.5 V dc offset a passive RC bandpass filter was used (Figure 5.3). For each frequency the resistors were changed to shift the cut-off frequency depending on the centre frequency (Table 5.2).

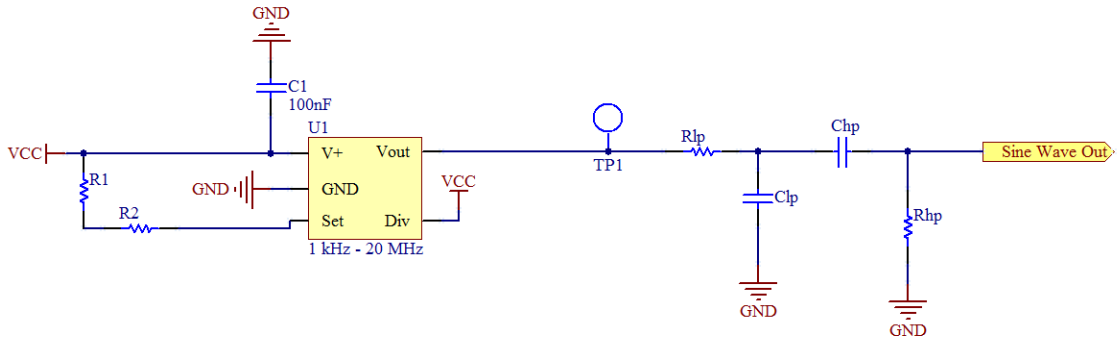

Figure 5.3. The circuit diagram of the sinusoidal wave generator.

An imperfection of the previous GULPS design which has been carried over to this design is the presence of odd harmonics in the sinusoidal wave (Figure 5.4). With none of the paired frequencies being integer multiples of each other, the odd harmonics will not affect the measured impedance, provided the pass band of the bandpass filter stage does not include the odd harmonic frequencies. A future area of investigation could involve measuring the impact these harmonics have on the measured impedance.

A) **B)**

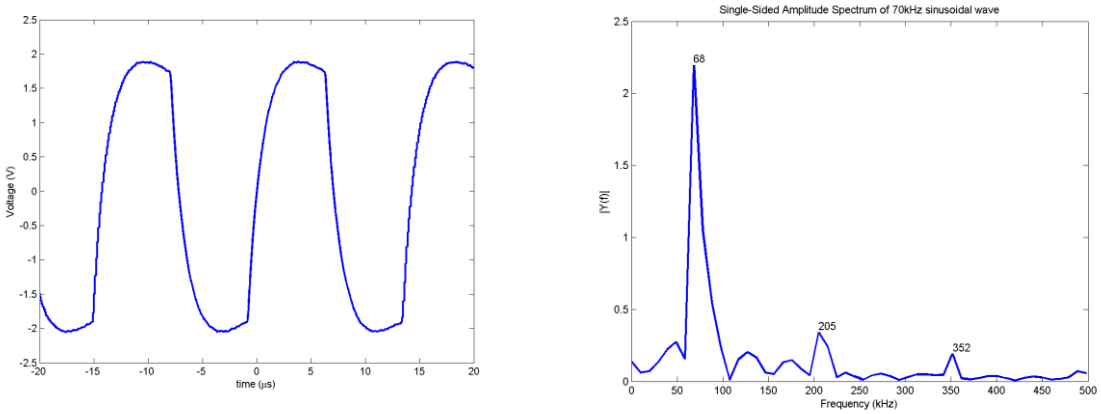

Figure 5.4. A) The output of the 70 kHz sinusoid wave generator B) the Fast Fourier Transform (FFT) showing the presence of third and fifth harmonics in the output

At the higher frequencies the oscillator could not produce a rail-to-rail square wave, and after it had passed the bandpass filter, the output had more of a triangular shape and had a peak-to-peak voltage of 3V (Figure 5.5). Because the lower frequencies are not sinusoidal the difference in shape was not adjusted and with the focus of detecting a temporal difference in the output features, the difference in amplitude was not corrected.

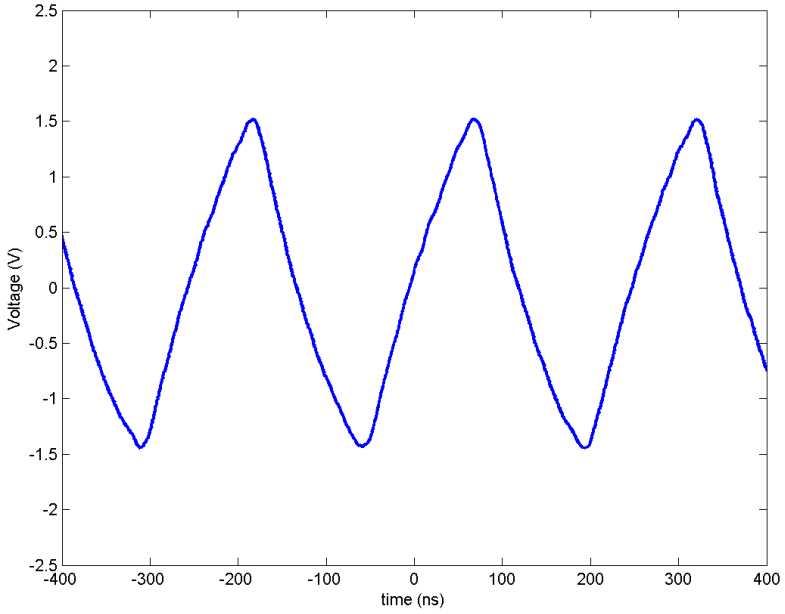

Figure 5.5. The output of the sinusoidal waveform generator, output frequency is 4 MHz.

5.2.2 Bandpass Filter

The bandpass filter IC used in the original design was the UAF42 produced by Texas Instruments [39]. The UAF42 is a universal active filter that can be configured as a bandpass filter and has a maximum frequency of 100 kHz. This bandwidth was not sufficient for this project's purposes, so alternative chips were investigated.

Other active filter IC's were investigated, but none that ranged from 1 kHz to 10 MHz were available. However, the LT1568 active filter chip produced by Linear Technologies [75] had a frequency range of 100 kHz to 10 MHz. It was decided that two different filter designs would be used; The UAF42 for frequencies lower than 100 kHz, and the LT1568 for the frequencies greater than 100 kHz.

5.2.2.1 Low-frequency bandpass filters

The characteristics of the 40 kHz and 70 kHz filters were kept the same from the first GULPS prototype [74], and for the 4 kHz and 7 kHz filters the same gain and quality factor was used. This would scale the bandwidth for each (Equation 3), whilst keeping the filter characteristics constant over the different filter frequencies (Table 5.3). The required resistors were calculated using the equations provided in the datasheet [39].

$$Bandwidth = \frac{f_c}{Q} \quad 3$$

Table 5.3. Filter characteristics for the bandpass filters using the UAF42 active filter chip

Centre Frequency	Pass band Gain	3dB Bandwidth	Q Factor
4 kHz	0.5 V/V	1.4 kHz	2.86
7 kHz	0.5 V/V	1.15 kHz	6.09
40 kHz	0.5 V/V	14 kHz	2.84
70 kHz	0.5 V/V	11.5 kHz	6.07

The final design of the module paired two UAF42 IC's in series to produce a fourth-order bandpass filter. The final circuit diagram of the low frequency bandpass filter can be seen in Figure 5.6. The resistor values to determine the centre frequency shown in Appendix C. Table C.1.

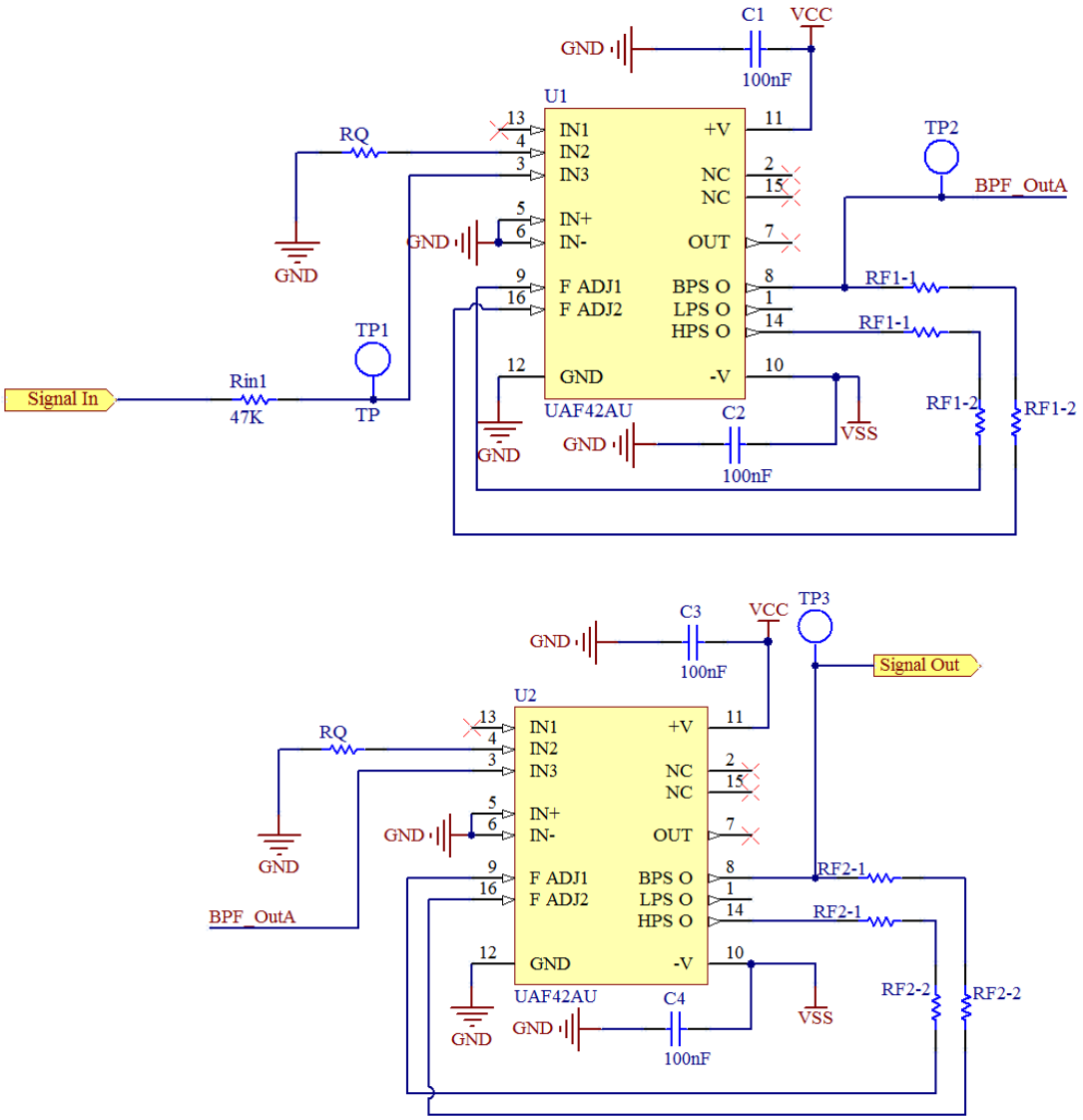

Figure 5.6. Bandpass filter circuit diagram using the UAF42. The resistor values can be found in Table A.2

5.2.2.2 High-frequency bandpass filters

To aid in the designing of the filters, the design guide [75] provided by Linear Technologies was used. With this guide the desired filter characteristics were entered and the resistor and capacitors were calculated. The pass band gain was chosen to be 1 V/V which would compensate for the lower signal amplitude generated by the sinusoidal wave generators. The 3 dB bandwidth for each filter was chosen to be as small as possible to isolate the channel of interest (Table 5.4).

Table 5.4. The filter characteristics for the injection frequencies over 100 kHz, using the LT1568 active filter chip

Centre Frequency	Pass band Gain	3dB Bandwidth	Q Factor
400 kHz	1 V/V	80 kHz	5
700 kHz	1 V/V	80 kHz	8.8
4 MHz	1 V/V	500 kHz	8
7 MHz	1 V/V	1050 kHz	6.7

As with the low frequency bandpass filter, this module paired two IC's in series to produce a fourth order bandpass filter. The final schematic for the high frequency bandpass filter can be seen in Figure 5.7, with the resistor and capacitor values that determine the centre frequency found in Appendix C. , Table C.2.

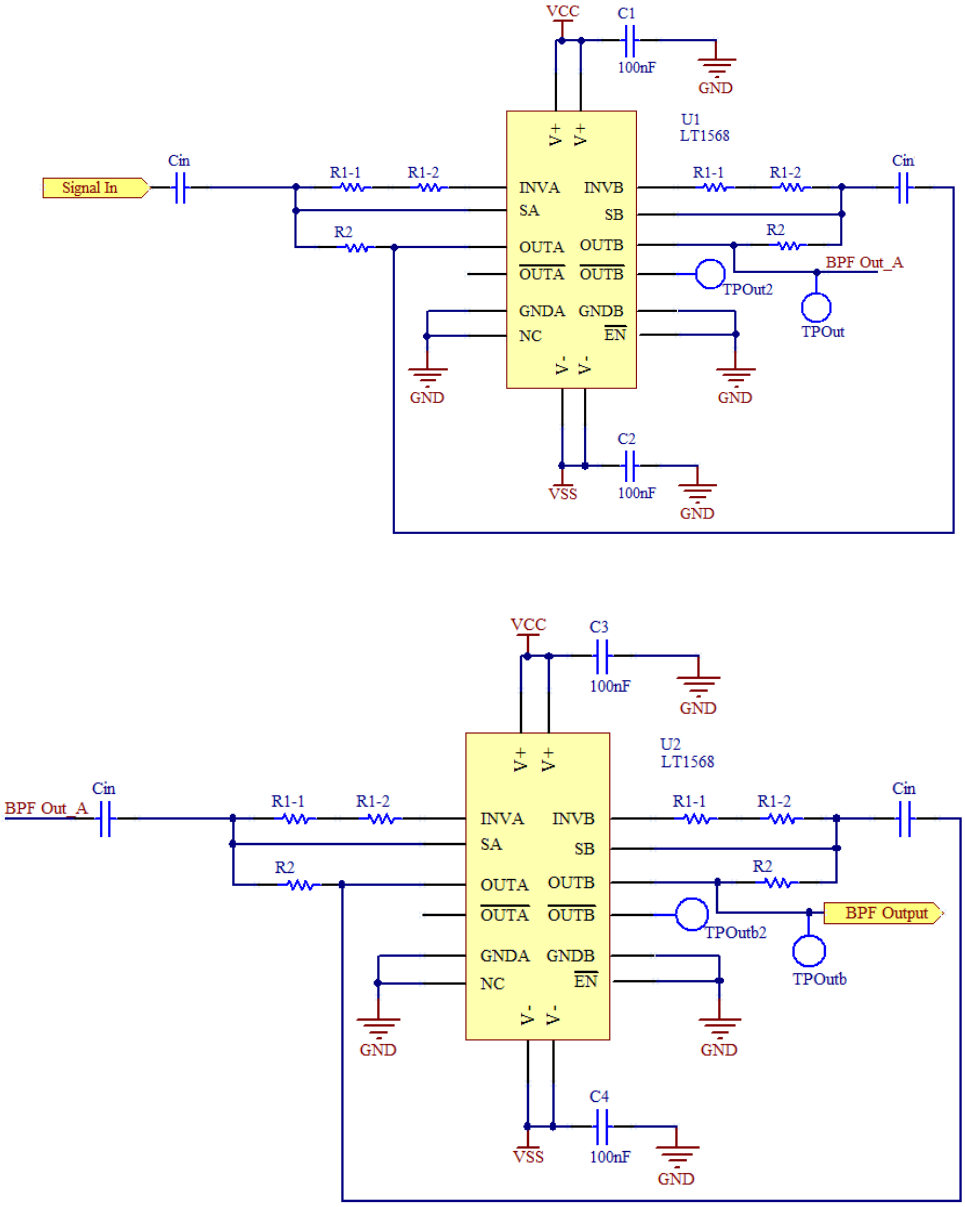

Figure 5.7. Circuit diagram of the high frequency bandpass filter using the LT1568. Values for the resistors can be found in Table A.3

5.2.2.3 Bandpass Filter Performance

It was important that each of the bandpass filters could significantly remove its paired frequency from the input signal, to isolate the impedance change for that channel. Each filter was tested using two different sinusoidal wave inputs, one at its centre frequency and the second at its corresponding paired frequency. The bandpass filters using the UAF42 IC passed the signal with a measured gain close to the calculated gain. The LT1568 band pass filters had a smaller measured gain that was close to 0.5 V/V. Every bandpass filter provided a minimum of 65 dB of attenuation to its paired frequency, reducing the output voltage to less than 4% of its original amplitude (Table 5.5).

Table 5.5. Testing the bandpass filters with two sinusoidal waves, at the filters' centre frequency and at the paired frequency

Filter Centre Frequency (kHz)	Input Wave Frequency (kHz)	Gain (V/V)	Input Wave Frequency (kHz)	Gain (V/V)
4	4	0.5195	7	0.0388
7	7	0.5305	4	0.0394
40	40	0.6150	70	0.0395
70	70	0.7510	40	0.0408
400	400	0.4795	700	0.0068
700	700	0.5059	400	0.0022
4000	4000	0.4840	7000	0.0147
7000	7000	0.6250	4000	0.0159

5.2.3 Other Components

All components were required to have a minimum bandwidth of 10 MHz, the span of the test frequencies. The opamp, MCP6H01, used in the constant current module and the demodulator module, and the instrumentation amplifier, AD620, had bandwidths below this. The OPA140 [76] was chosen to replace the MCP6H01. The OPA140 has a bandwidth of 11 MHz and like its predecessor it uses dual supply voltages and operates rail-to-rail. The replacement instrumentation amplifier was the AD8421 and has a bandwidth of 10 MHz. Circuit diagrams for both, the adjusted constant current module and demodulator are shown in Figure 5.8 and Figure 5.9 respectively.

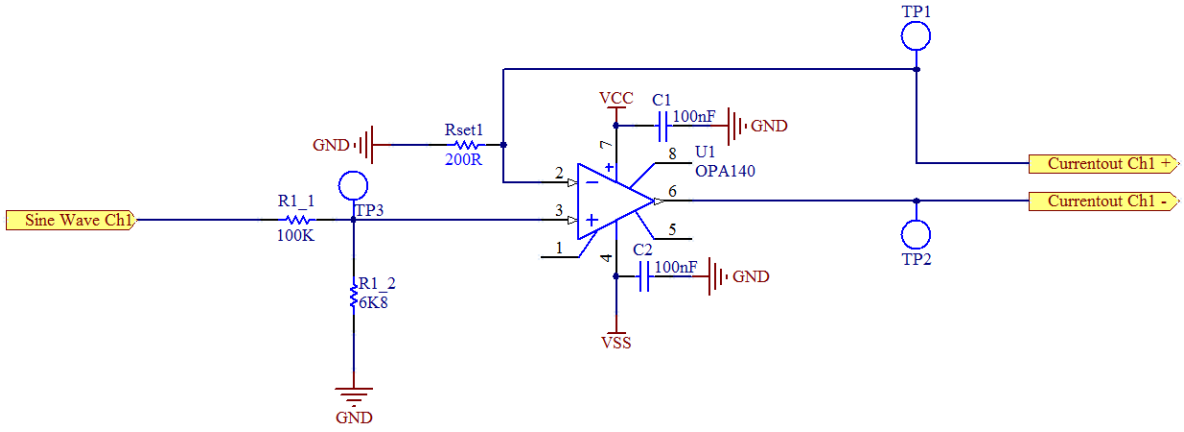

Figure 5.8. The circuit diagram of the constant current module using the OPA140 opamp.

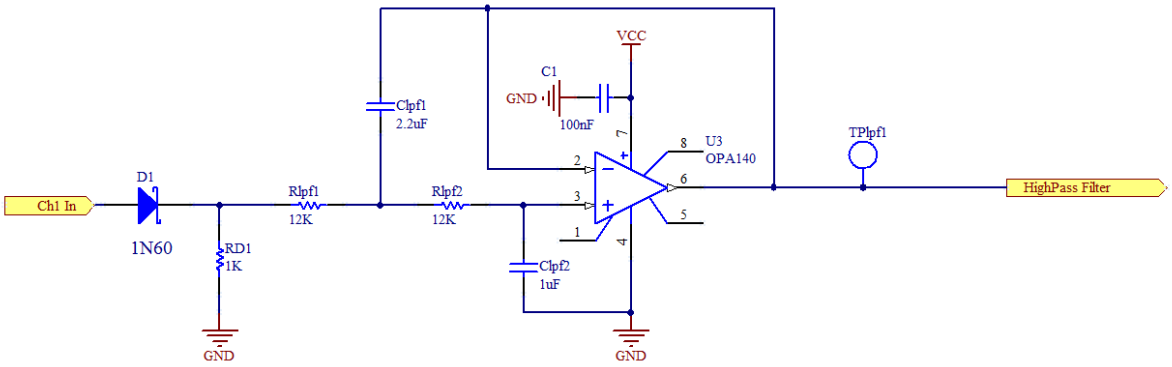

Figure 5.9. The demodulator circuit diagram used in the signal processing module. The opamp has been changed to the OPA140 due to its larger bandwidth.

To achieve a bandwidth of 10 MHz the maximum gain of the instrumentation amplifier was set at 10 V/V. This was lower than the original instrumentation amplifier, which was set at 42.1 V/V. Another modification made to the instrumentation amplifier was the removal of the resistors in parallel with the inputs of the instrumentation amplifier. The 100 kΩ resistors were reducing the input impedance, and these were removed to increase the input resistance to 30 GΩ [77]. The new circuit diagram for the instrumentation amplifier can be seen in Figure 5.10.

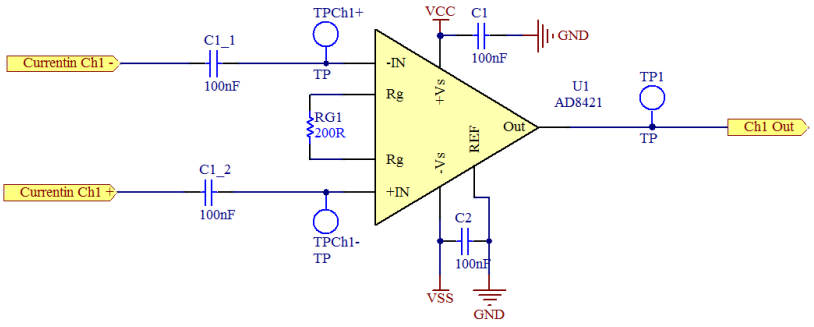

Figure 5.10. The circuit diagram for the instrumentation module, using the AD8421.

5.3 Constant Current Module

The constant current module, introduced in Section 3.1.1, Figure 3.2, was tested using a 50 Ω load. The output current was measured with an RMS of 609.8 µA (Figure 5.11). A second resistor was added to the circuit, coupling the two channels together (Figure 5.12). This resistance represented the tissue which exists in the throat between the two channels. With the addition of the coupling resistance, the voltage signal at the output of the opamp was modulated for both channels (Figure 5.13). The voltage measured at the inverting input and the current through R_{L1} matched the non-inverting input of the opamp (Figure 5.14). However, the output current of the opamp was much greater (Figure 5.13) and was unregulated, increasing as the total load resistance increased. To see if this affected the measurement of resistance, the voltage across the load was measured and divided by the current through the load. This did not produce a constant value approximating the resistance. The opamp regulates the current through R_{L1}, however, if there is a secondary path, the current through this secondary path will be unregulated and the output current exceeds the desired 0.5 mA RMS.

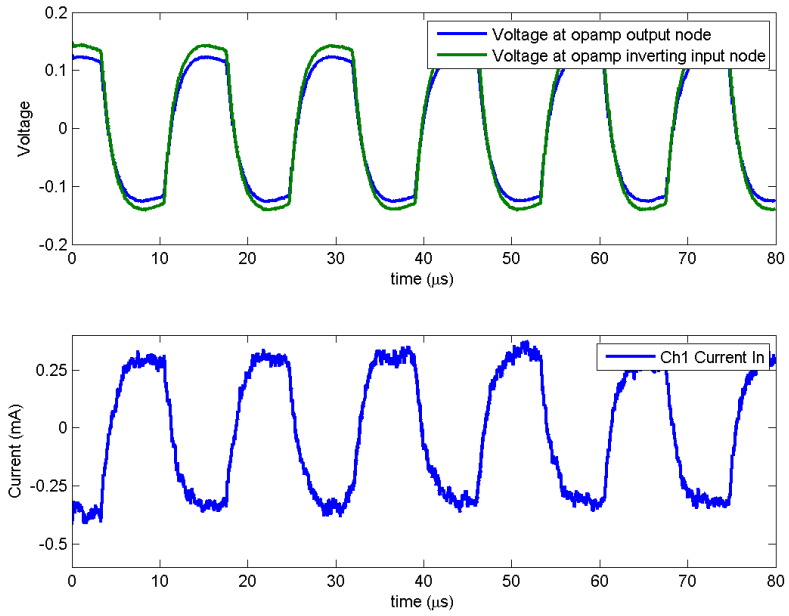

Figure 5.11. The current through a 50 Ω resistive load with no cross-channel coupling.

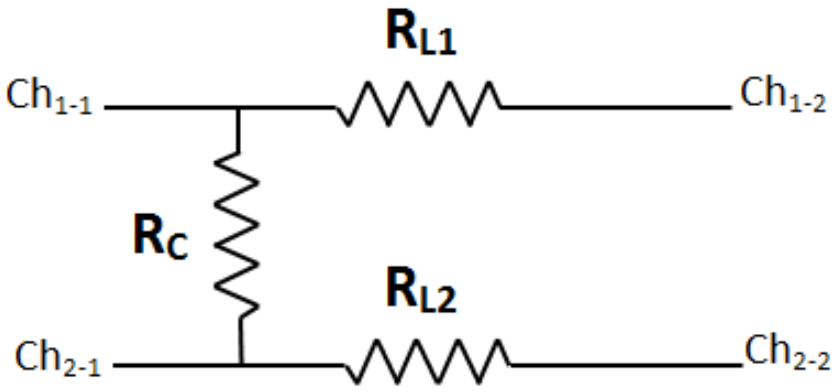

Figure 5.12. The resistor combination to test the constant current module.

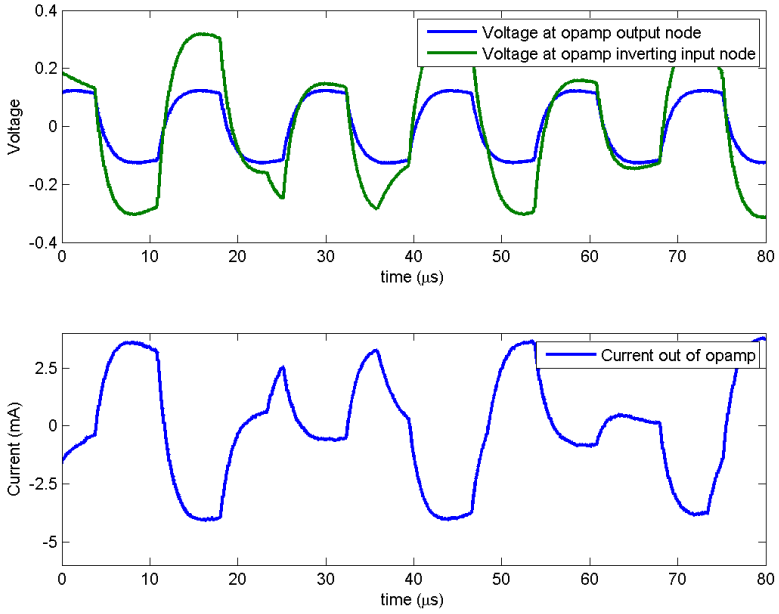

Figure 5.13. The output current of the opamp with a 50 Ω resistor and a 67 Ω cross-channel coupling resistor.

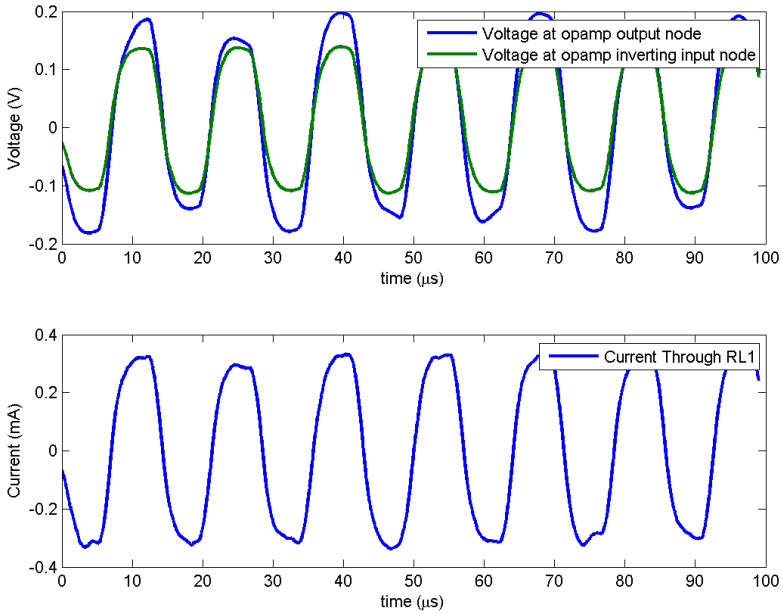

Figure 5.14. The current through the load resistor, R_{L1}.

Operational transconductance amplifiers (OTA) were investigated as a replacement constant current source using circuit simulation in TINA (Tool-kit for INteractive Analysis [78]). The OTA used was the OPA861 by Texas Instruments [79], chosen for its wide 80 MHz bandwidth. The OTA was configured into a common-emitter configuration (Figure 5.15) and the output current could be calculated by multiplying the input voltage with the transconductance of the OTA. The transconductance was specified by the datasheet, however, this used an emitter resistance of zero. To take into account the emitter resistance Equations 4 and 5 were used, supplied by the datasheet [79].

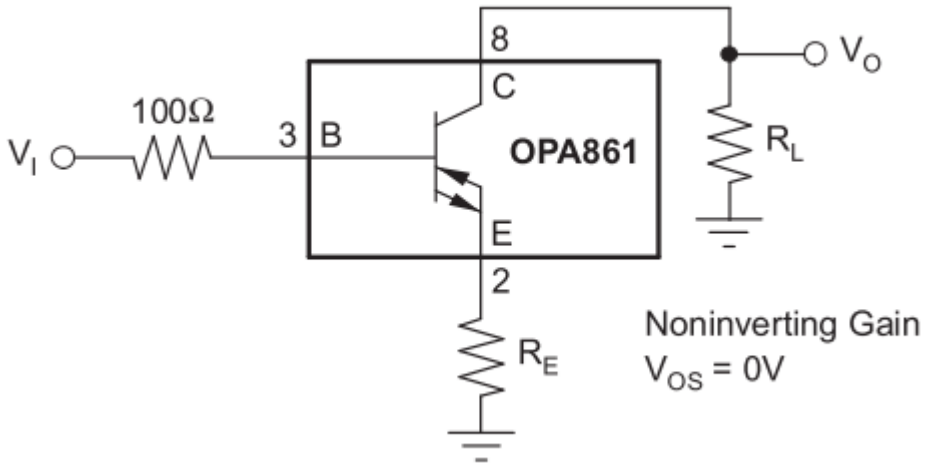

Figure 5.15. Common-Emitter configuration for the OPA861, taken from [79].

$$I_{L\_RMS} = V_{O\_RMS} * g_{m\_deg} \quad (4)$$

$$g_{m\_deg} = \frac{1}{\frac{1}{g_m} + R_E} \quad (5)$$

Where g_{m_deg} is the transconductance of the OTA in common-emitter configuration, g_m is the transconductance of the OTA and R_E is the emitter resistance.

The resistive load simulated was the same used for the experimental test, with a 50 Ω series resistance and a 67 Ω cross-channel coupling resistor (Figure 5.12). The collector was 529.5 µA RMS, however there was still modulation of the output voltage (Figure 5.16) and this modulation was present in the current through the load. The OTA differs from the opamp by not using feedback to regulate the current through R_L, and therefore the current through R_L reflects the modulation of the output voltage (Figure 5.16); this allows the resistance to be calculated when taking the voltage difference and current through R_L.

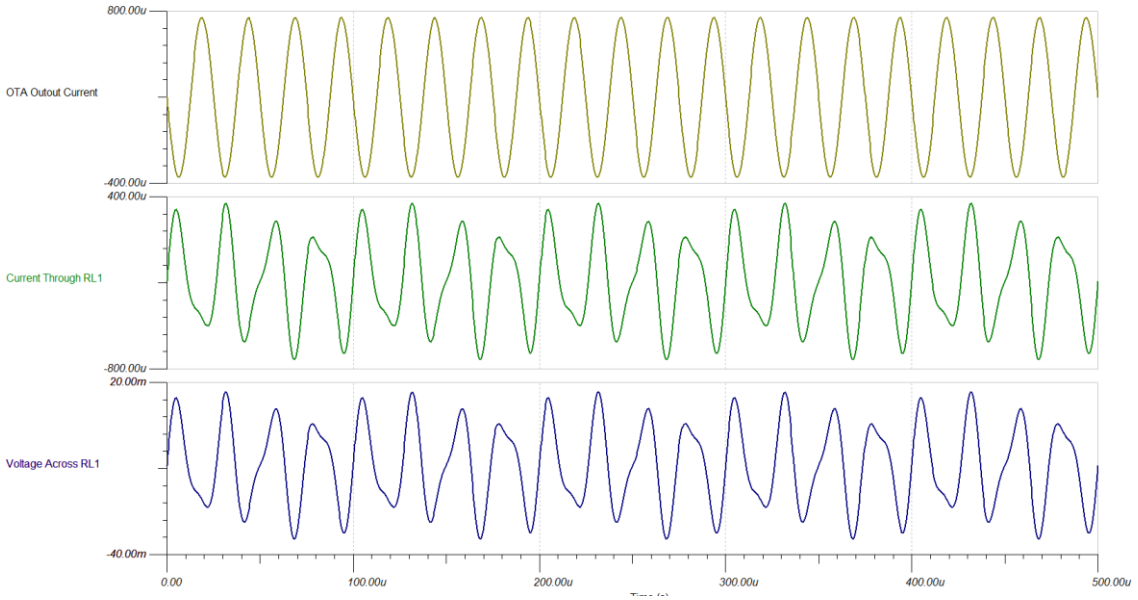

Figure 5.16. Simulated output current and voltage of the OTA using the load seen in Figure 5.12.

5.3.1 Implementation

A PCB for the new constant current method was made using the circuit simulated in TINA. This module contains both channels. The final circuit diagram for the OTA constant current module can be seen in Figure 5.17. Using the resistor test circuit in Figure 5.12, the current through R_{L1} was seen to follow the voltage across the load (Figure 5.18).

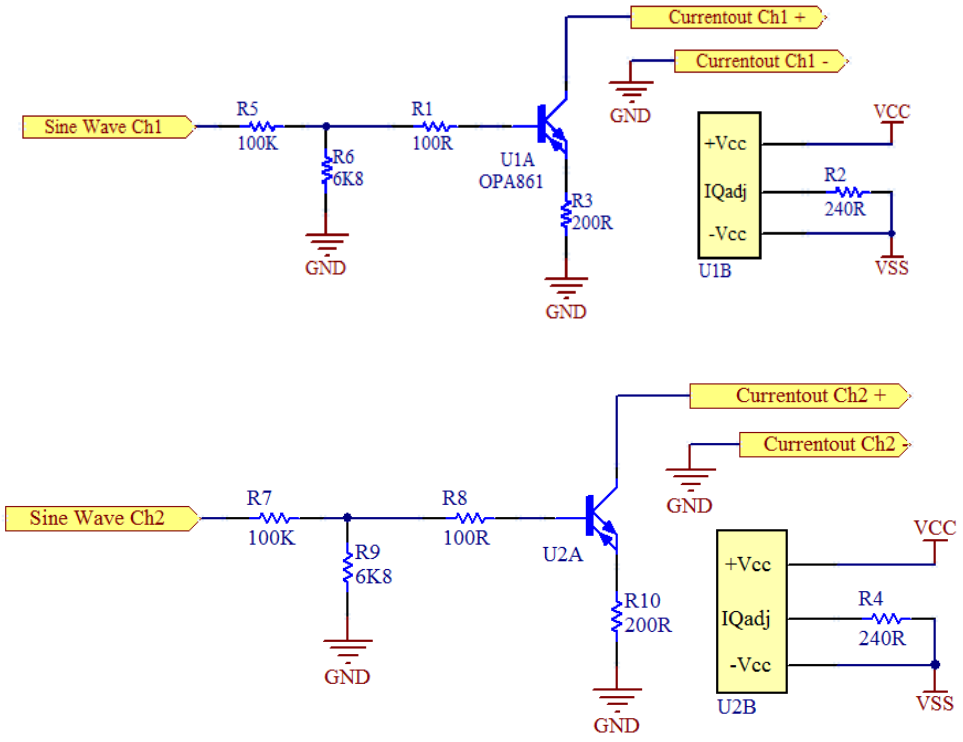

Figure 5.17. The circuit schematic of the constant current module using an OTA.

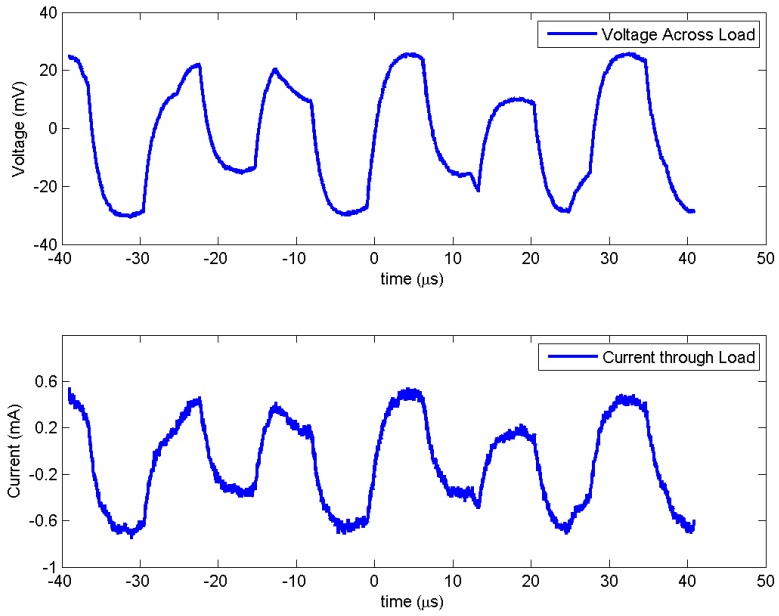

Figure 5.18. The current measured through the resistor R_{L1} using the OTA. F = 70 kHz.

The dynamic response of the new current module was tested using the circuit in Figure 5.19 to apply a step input. The voltage across the load can be seen in Figure 5.20. The constant current module took 0.1 ms to adjust to the step input, which is sufficient for measuring the swallowing response which occurs at 20 Hz (t = 50 ms) [74].

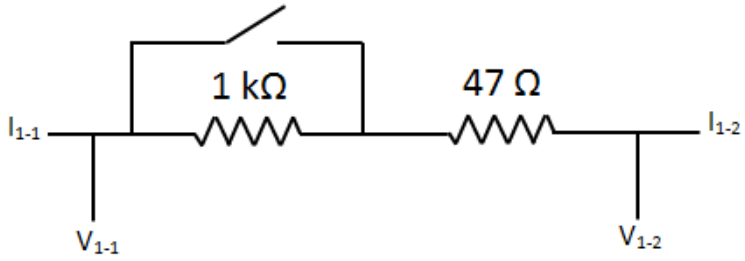

Figure 5.19. The resistive load used to test the dynamic response of the new constant current module

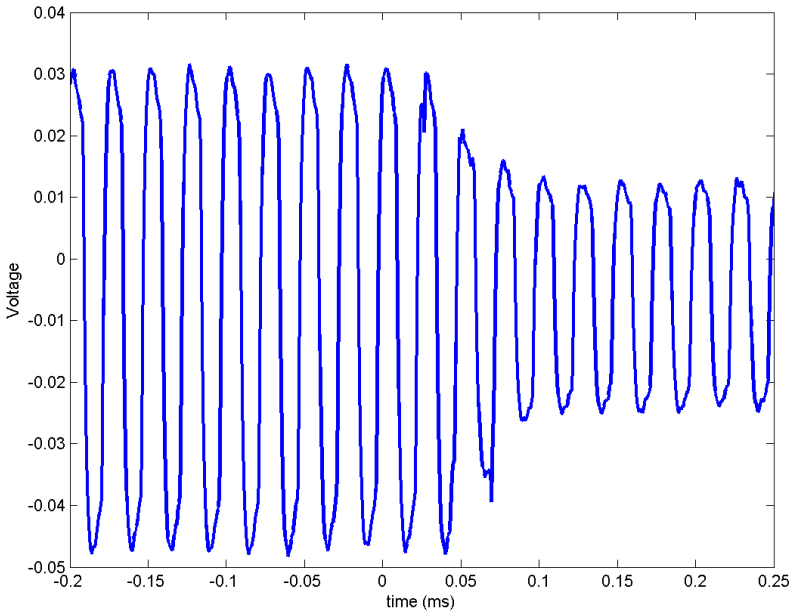

Figure 5.20. The voltage across the load used to test the dynamic response. It can be seen that the time it takes to settle is 0.1msec, which is much faster than the duration of a swallow. Frequency = 40 kHz.

5.4 System Testing on a Resistive Load

To test the combined GULPS system, a resistive network was designed to simulate throat impedance (Figure 5.21). To represent the base impedance across the throat, a 50 Ω resistor was used. A variable resistor was placed in series with the base impedance resistor to apply changes to the impedance, modelling the change in the cross-sectional area. A switch was placed in parallel to the variable resistor, to apply a step change in impedance. Four additional resistors were used to couple the two channels together. This coupling represents possible current paths between the two channels in the throat. To verify that the tetrapolar configuration eliminates the variable skin-to-electrode impedance, adjustable 50 Ω resistors were placed between the current input and the voltage measurement inputs.

The values for the base throat impedance and the resistor used to model the change of impedance during a swallow were taken from the impedance measured by Chester [74]. Chester measured the resistance of the neck to correspond to 60 Ω, with a 3 Ω change of resistance of during a swallow.

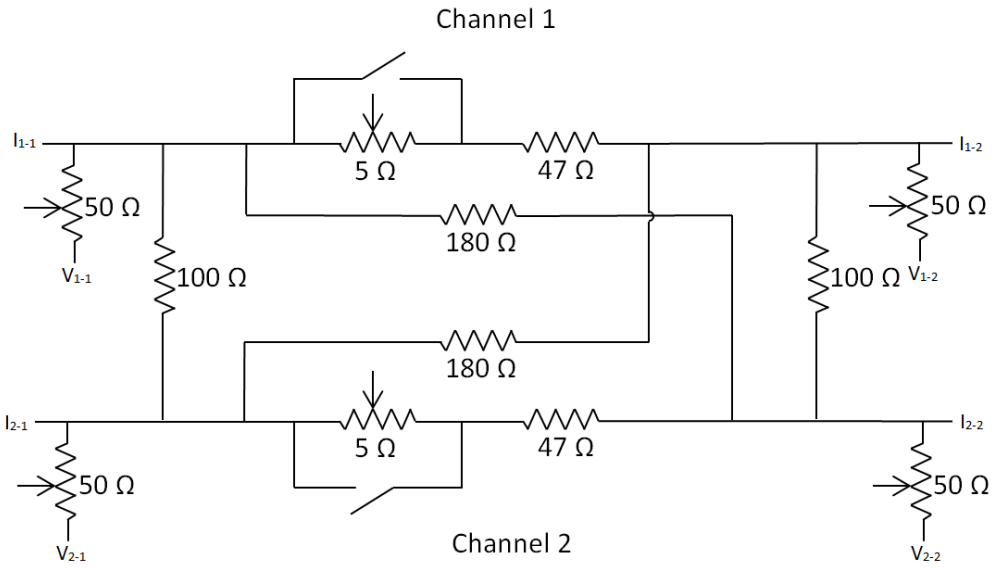

Figure 5.21. Resistive network used to test the dynamic response of the GULPS hardware

Using the resistive network, the output of the GULPS system was tested with each injection frequency to ensure that each channel could provide a wide signal range to be sampled by the microcontroller's ADC. It was found that the output voltage of the GULPS circuit was much lower for the 4 MHz frequency, and no change was measured for the 7 MHz frequency. This was due to the square wave not creating a rail-to-rail voltage, and the bandpass filters having a pass band gain of 0.5 V/V instead of the desired 1 V/V. To increase the signal range, the gain of the instrumentation amplifier was increased. The gain was increased to 50.6 V/V, however this reduced the bandwidth of the amplifier. When the gain for the higher frequencies was measured, it was found that the gain only dropped for 4 MHz and 7 MHz signals with a gain of 36.5 V/V and 20.2 V/V respectively.

The output of the 7 MHz bandpass filter was not greater than the 0.7 V forward voltage drop across the diode used in the following demodulation stage. The diode was replaced with a Germanium diode (1N60, produced by Taitron Components Incorporated). The Germanium diode has a lower forward voltage drop of 0.2 V compared to a silicon diode which has a forward voltage drop of 0.7 V. This resulted in a signal change when the resistance was changed, although the range of the signal was less than 0.5 V for a 5 Ω change in resistance.

The final step was to add a second amplifier stage after the bandpass filter module and before the signal conditioning module to amplify the signal (Figure 5.22). This was to increase the range of the output signal to be sampled by the microcontroller for the 4 MHz and 7 MHz frequencies. The opamp used was the LM6172 produced by Texas Instruments and was configured in an inverting configuration with a gain of 100, which resulted in 2.25 V amplitude for a 5 Ω change. This second amplifier stage was only used for the 4 MHz and 7 MHz frequency pair.

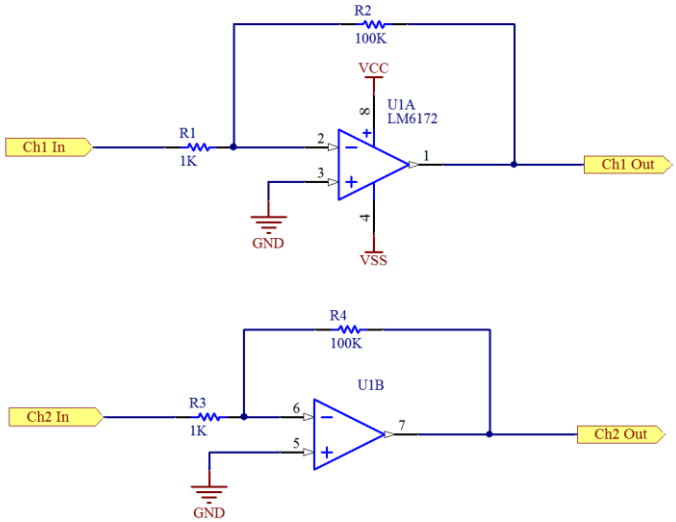

Figure 5.22. The schematic of the inverting opamp circuit used to provide extra gain for the 4 MHz and 7 MHz frequency pairs.

Using the adjustable resistors between the voltage measurement and the current input, there was no change in impedance output when the resistance was dynamically changed. This indicates the variable resistance between the skin and the electrodes should not greatly affect the measured bioimpedance.

The output when applying a step response to both channels can be seen in Figure 5.23. This showed that all modules were functioning correctly and by applying a pulse input of -5 Ω, the output of GULPS registered that change. It was noticed that a 5 Ω step change in impedance could be measured on the second channel. A 9% impedance change was measured on the second channel. This is an unwanted cross-over noise effect.

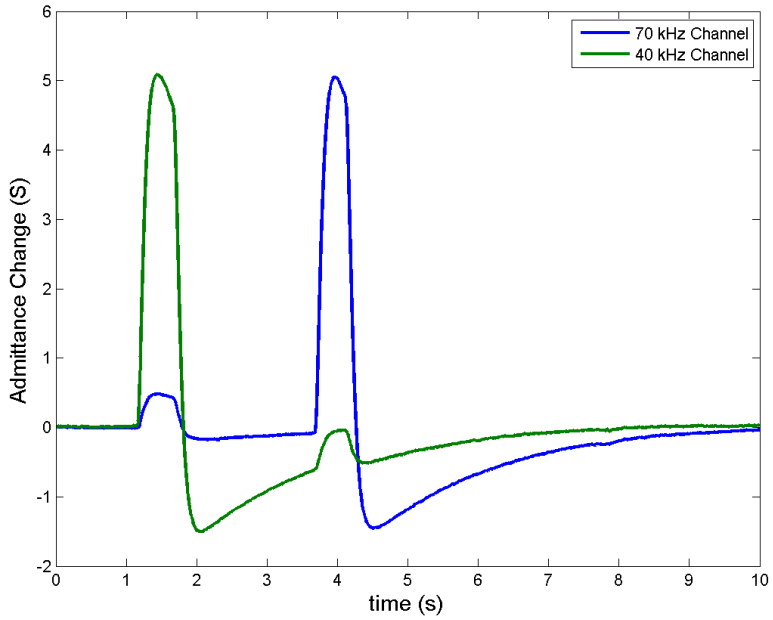

Figure 5.23. Output of the GULPS system using 40 kHz and 70 kHz frequency pair, when a pulse input is applied to the 70 kHz channel (t = 3.687 s) and the 40 kHz channel (t = 1.164 s)

5.5 Isolated Power Supplies

It was hypothesized that electrically isolating the two channels would remove the channel-coupling resistance, and remove the modulation of the signal. With the current, single supply design, the exit node from the subject for the two channels is the same. It was hypothesised that part of the channels signal was being split to the other channels reference node (Figure 5.24). This means the impedance change being measured could be caused due to the changing cross-sectional area between the two channels.

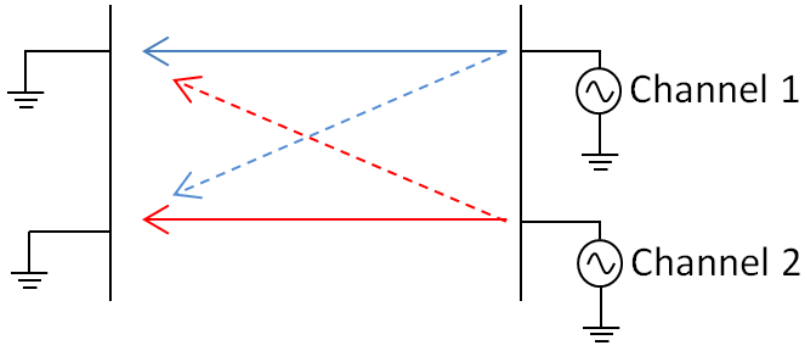

Figure 5.24. Hypothesized current flow through the neck. The solid lines represent the desired current path, the dashed arrows represent a potential current path.

To isolate the channels, an isolated power supply was used for each channel. This required modifications to the instrumentation amplifier (Figure 5.25A) and the constant current modules (Figure 5.25B) because the boards contained both channels, powered by a single voltage supply. For both modules the ground plane was split in half and the positive and negative tracks were cut. This separated the two channels and wires were led from the boards to supply the second power rails. An optocoupler circuit was used to allow the microcontroller to read from the second channel without coupling the power rails. The optocoupler used was the HCNR200 produced by Avago Technologies [80] and the circuit can be seen in Figure 5.26.

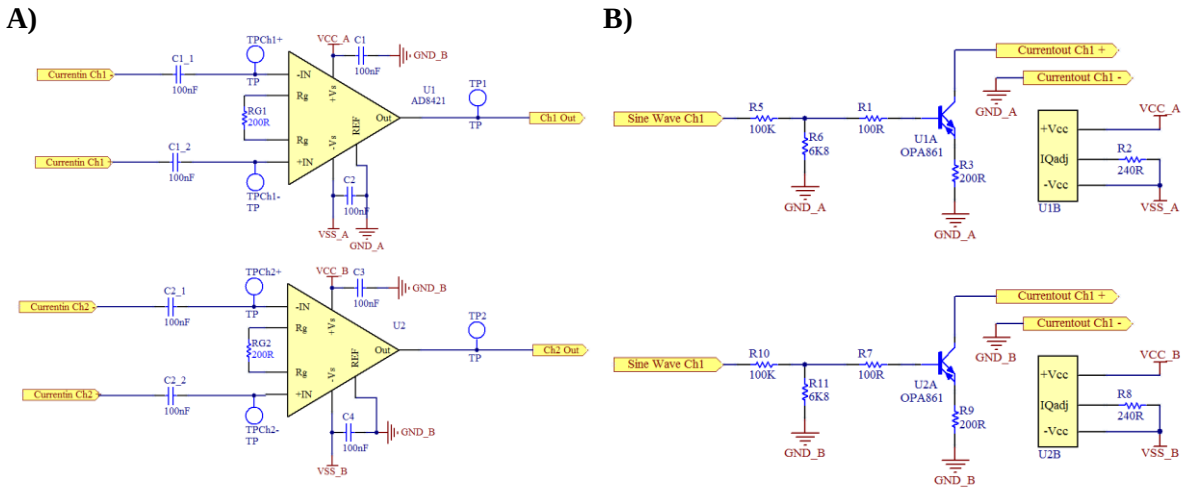

Figure 5.25. The schematics for the A) constant current module and B) the instrumentation amplifier, using isolated power supplies.

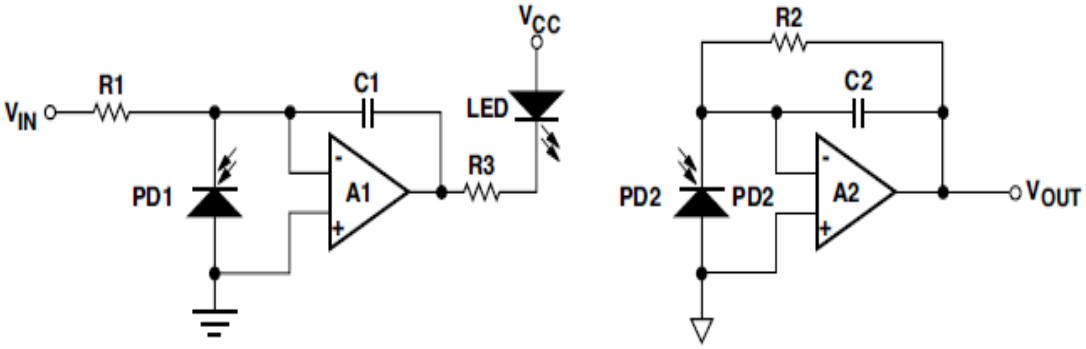

Figure 5.26. The optocoupler circuit diagram [80]. The optocoupler IC consists of the LED, PD1 and PD2

One of the power supplies was isolated from the mains using an isolating transformer. The power supplies were later replaced with battery packs to provide a portable power system. Two sets of four AA batteries (1.5 V per battery) per channel were used, increasing the rails to ±6 V. With the addition of the isolated power supplies, an updated functional block diagram can be seen in Figure 5.27. Using the load in Figure 5.12 and an isolated oscilloscope, the voltage and current waveforms were measured (Figure 5.28). Isolating the two channels has resulted in the voltage and current waveforms no longer being modulated by the other channel.

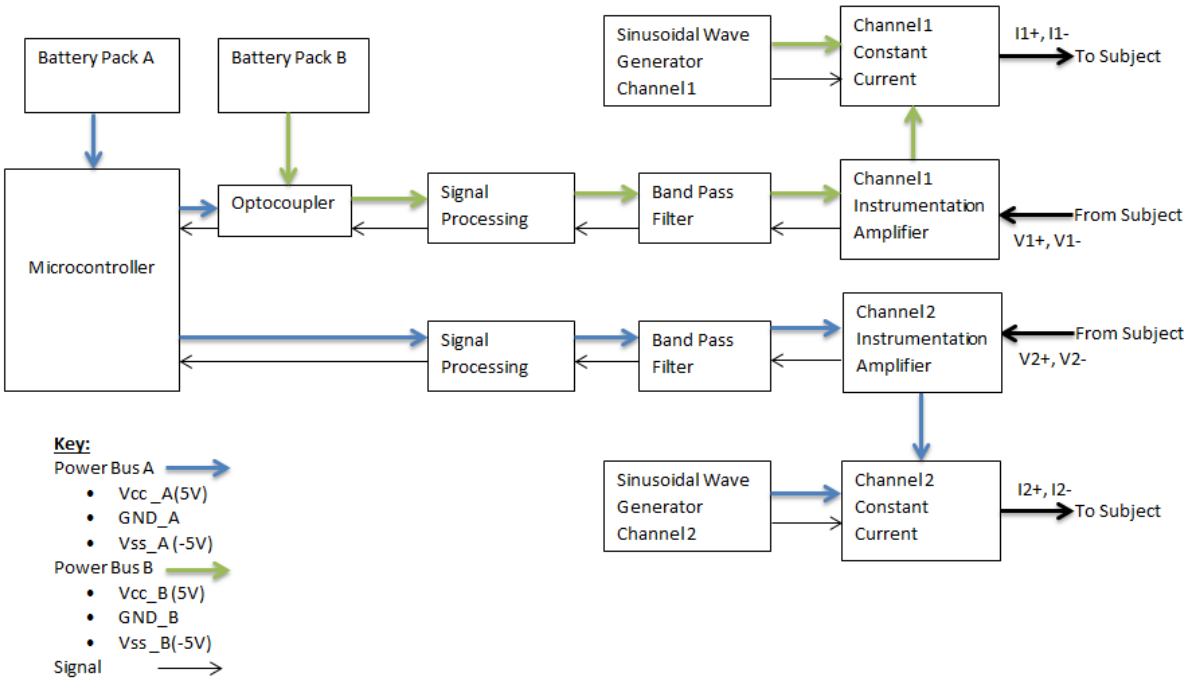

Figure 5.27. Modular block diagram for GULPS using the isolated power supplies. The green arrow represents power bus A and the blue arrow represents power bus B.

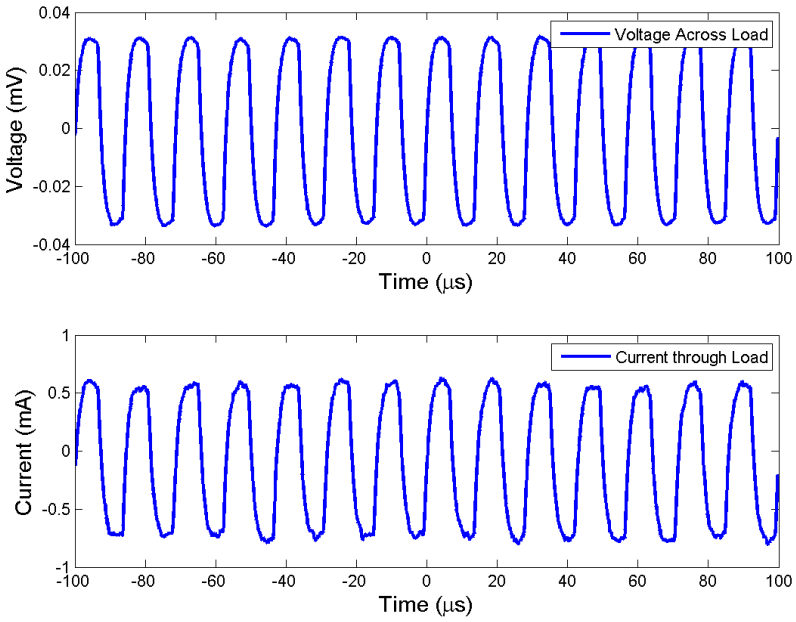

Figure 5.28. Current and voltage of 70 kHz channel through the load resistor with a load of 50Ω and a 67Ω cross-channel coupling resistor.

5.6 Bluetooth Integration

The Bluetooth hardware designed in Section 4.0 was added to the modular GULPS hardware. To integrate the two, the 5 V UART output of the microcontroller needed to be reduced to 3.3 V for the Bluetooth module. A level shifter by Texas Instruments was used to translate the two UART signals. A module for the level shifter was designed and the schematic can be seen in Figure 5.29.

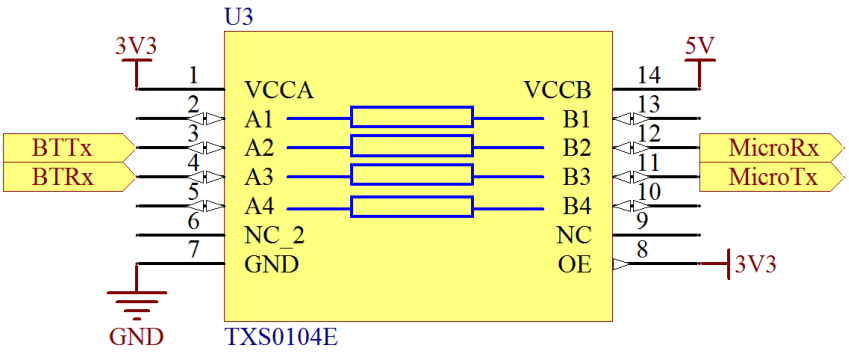

Figure 5.29. Level shifter circuit schematic interfacing between the Bluetooth RN-42 chip and the microcontroller.

5.6.1 Firmware

The firmware used in the microcontroller module of GULPS was modified to remove the rate of transmission's dependency on the speed of the system. To remove this dependency a timer interrupt was used to signal that data needed to be transmitted. To configure the timer, Equation 6 was used [43].

$$Period = PR * prescalar * T_{CY} \quad (6)$$

The *PR* (period register) determines the frequency of the interrupt. The timer prescalar and T_{CY} (time period of the instruction cycle) are fixed values initialized by the software at start-up to 256 and 33.33 ns respectively. To achieve a broadcast rate of 20 ms, the current transmission rate, *PR* was set to 2344. The timer service interrupt and initialization can be seen in (Figure 5.30), and the full embedded software can be seen in Appendix D.

```
// Initialize Timer 1 interrupt service routine
void timer_init() {
    T1CON = 0;              // Clear Timer 1 configuration
    T1CONbits.TCKPS = 3;    // Set timer 1 prescaler (3=1:256)
    PR1 = 2344;             // Set Timer 1 period (max value is 65535)
    _T1IP = 1;              // Set Timer 1 interrupt priority
    _T1IF = 0;              // Clear Timer 1 interrupt flag
    _T1IE = 1;              // Enable Timer 1 interrupt
    T1CONbits.TON = 1;      // Turn on Timer 1
}

// Timer 1 interrupt service routine
void __attribute__((__interrupt__, __auto_psv__)) _T1Interrupt(void)
{
  if (adc_is_new_data())
  {
    adc_data_ch1 = adc_read_ch1();
    adc_data_ch2 = adc_read_ch2();
    adc_set_data_received(0); //turn flag off to indicate data received.
  }

  send_data = 1;
  _T1IF = 0; // Clear Timer 1 interrupt flag

}
```

Figure 5.30. The C code to initialize the Timer interrupt (`timer_init()`) and the Timer interrupt service routine (`_T1Interrupt(void)`).

5.6.2 Android App Verification

The final step to verify the Android App was to compare data recorded by the App with data recorded by an oscilloscope. The resistive load seen in Figure 5.21 was used to generate a step input (with non-isolated power supplies) and the two methods of data recording were compared using MATLAB (Figure 5.31). When comparing the two methods, there was no delay in the data features, although the data recorded by the App did have a dc offset of 91.1 mV for the upper channel and 53.5 mV for the lower channel. This was left unadjusted as it would not affect the temporal feature separation and the peak-to-peak voltage was the same.

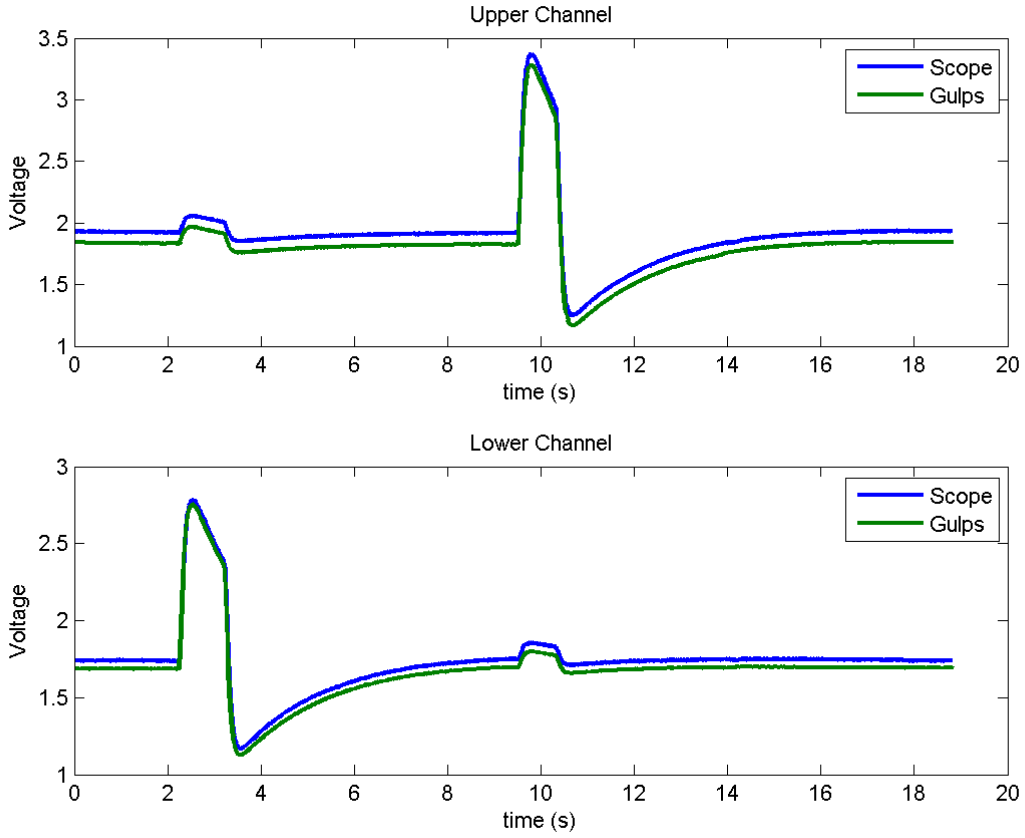

Figure 5.31 Comparing the output of GULPS to go with the measurement of the scope for both channels. This measurement was taken before the isolated power supplies were added.

5.7 Summary

The pre-existing hardware was broken down into a modular design; this allowed the easy replacement of malfunctioning modules and will be used to test the effect of the injection frequency. It was during the individual testing of the constant current module that it was noticed the circuit did not produce a deterministic current and therefore Ohm's law could not be used to calculate the impedance. The current module was redesigned, the first using an operational transconductance amplifier, producing an output which was still modulated; however the resistance of the load could be calculated. Later, to remove the modulation, each channel was electrically isolated, and was powered by separate battery packs. The PCB artwork for the developed modules can be seen in Appendix B. PCB Artwork.

Bluetooth communication was successfully integrated into the existing hardware with the addition of a level shifter. The App was compared to an oscilloscope capture of the same data and it was shown to accurately plot the timing of the data; however there was a DC offset between the App and the oscilloscope.

Chapter 6.0 Human Subject Tests

After testing on a resistive load network for general operation, GULPS was ready to be trialled on subjects. Initially GULPS was trialled on one subject using the injection frequencies listed in Section 5.0. The frequency which provided the clearest features in the output waveform when swallowing was then paired with low resolution pharyngeal manometry to compare waveform characteristics. A subject with a history of pharyngeal mis-sequencing was also evaluated to gauge the changes in the GULPS output for a mis-sequenced swallow. Two hardware changes were also trialled, the electrical isolation of the two channels and a channel subtraction method to measure the effect they had on the output of GULPS. Finally, different signal processing operations were also investigated for possible improvements in visualisation of mis-sequencing.

The original Ethics proposal that was granted to the GULPS study had expired, and an application was accepted by the Health and Disability Ethics Committee to extend this study by another year. This allowed an additional six subjects to be trialled.

6.1 Testing Procedure

Throughout this study the same testing procedure was used. The subject sat upright in a chair and was passed a syringe filled with 10 ml of water, which they would intake and hold in their mouth. A syringe was used because it minimizes head and jaw movement, which changes the impedance. Holding the water in the mouth allows the impedance to return to equilibrium. Once the impedance has returned to equilibrium (approximately 10 s) the subject was told to swallow when they were ready, trying to reduce all movement made by the body and head during the swallow. Ten swallows were performed separated by a minimum of 30 s per swallow.

6.2 Electrodes

Two different types of electrodes were trialled. The first were the Triode electrodes, the same used by Chester. Like Chester, it was found that the signal was hard to obtain and the electrodes required reapplying until the signal was obtained. The Ambu Blue Sensor N [49] (Figure 6.1) was trialled and it was found that these electrodes produced a substantially consistent signal from swallow to swallow.

Figure 6.1. The Blue Sensor N by Ambu [49].

6.2.1 Electrode Performance

During testing it was found that there were several factors related to the electrodes that affected the output signal's amplitude. There was a decrease in the measured change in impedance whenever pressure was applied to the electrodes. It was thought that by applying pressure to the electrodes this was increasing the contact between the skin and the electrode, hence reducing the impedance between the skin and electrodes. In an attempt to isolate which electrodes were affected by the application of

pressure to the electrodes, pressure was applied to the following electrodes and the effects were observed:

- Top channel, current electrodes.
- Bottom channel, current electrodes.
- Top channel, voltage electrodes.
- All electrodes for both channels

When pressure was applied to the electrodes, the measured change in impedance for that channel was decreased (Figure 6.2). This was not dependent on the current or voltage electrodes, as when pressure was applied to the electrodes separately there was a decrease in the change in impedance. When pressure was applied to either the current or voltage electrodes the features present in the waveform became distorted.

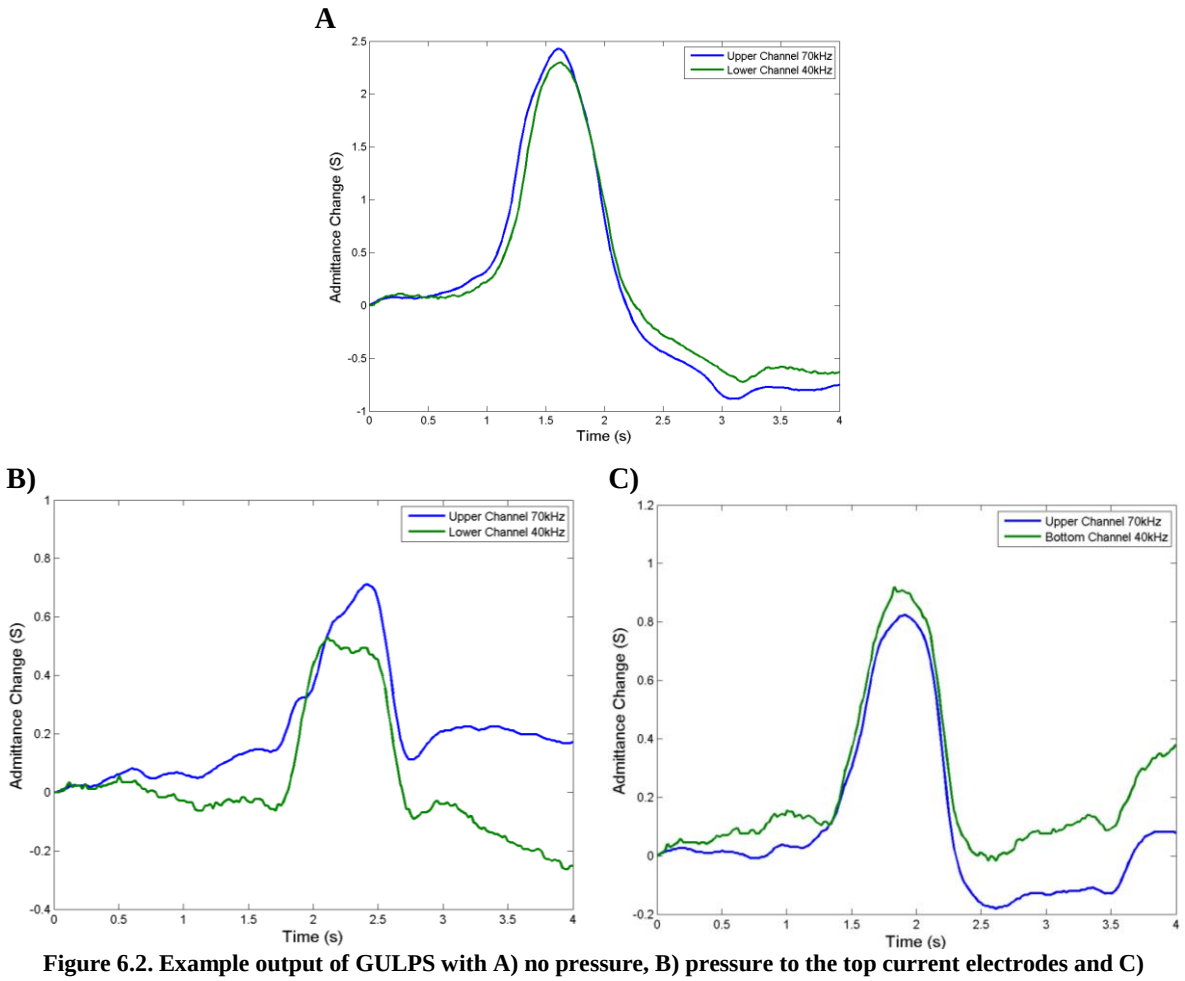

Figure 6.2. Example output of GULPS with A) no pressure, B) pressure to the top current electrodes and C) pressure to all electrodes.

As the adhesive on the electrodes wore out, the pressure holding the electrodes to the skin would decrease with a subsequent decrease in the amplitude of the signal (Figure 6.3). In an attempt to regulate the pressure applied to the electrodes, tape was applied across the electrodes to apply constant pressure (Figure 6.4). However this is not a perfect solution as tape cannot apply even pressure to each electrode. The effect of the contact between skin and electrodes was unexpected as it was thought that the tetra-polar configuration would minimise the effect of the variable skin-to-electrode impedance.

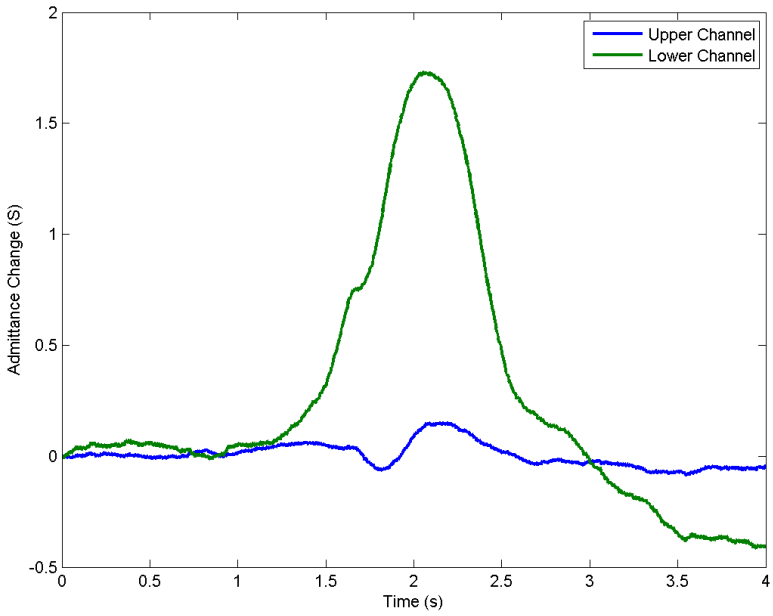

Figure 6.3 The effect of the worn out adhesive can be seen in the drop in the upper channels' amplitude (Subject 1).

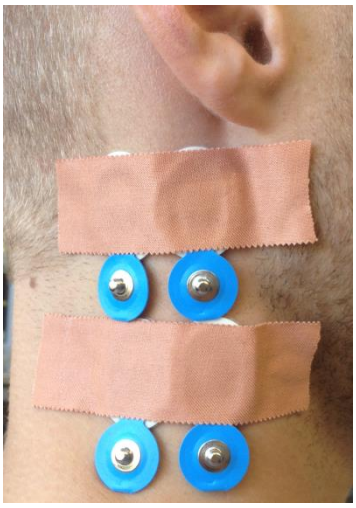

Figure 6.4. The position of the electrodes, applied with tape.

6.3 Electrode Position 1

The first electrode position used to test the new GULPS prototype was outlined by Chester [36] (Figure 6.4, Figure 6.5). This placed the top channel 20 mm below the ear, with the first electrode placed close as possible to the jawline, without placing the electrodes on the jaw (mandible). The bottom channel was placed 40 mm below this. The current electrodes were placed closest to the jaw with the voltage electrodes 20 mm apart, measuring away from the jaw. The frequency used for the top channel was 7 kHz, 70 kHz, 700 kHz and 7 MHz, and for the bottom channel the frequencies were 4 kHz, 40 kHz, 400 kHz and 4 MHz.

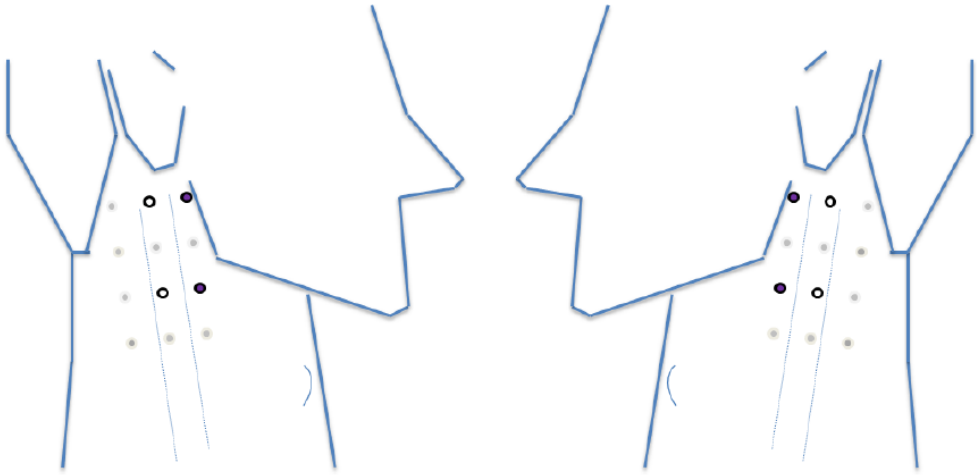

Figure 6.5. Electrode position used by Chester [36]. The signal detection electrodes are the electrodes with a white centre (central) and the current generation electrodes have a purple centre (by the jaw).

6.3.1 Frequency Test

The first test performed measured the effect the injection frequency had on the output of GULPS. The output of the previous GULPS system was unreliable and the features of the waveform when swallowing were inconsistent. The aim of this investigation was to see if a different frequency pair could produce an output that was consistent and had clear features in the output during a swallowing event.

One female subject (Subject 1) was tested over three days; this subject had previously been evaluated using low-resolution pharyngeal manometry and was confirmed as a healthy subject. For all frequencies documented in Chapter 5.0, Hardware Development, it was found that the output of GULPS had the same distinguishable feature, a single main peak for each channel (Figure 6.6). The main peak for each channel appear to be aligned in time, however, post processing performed in MATLAB found that there was a definite time difference between the two peaks. For each frequency pair the number of times the upper channel led the lower channel was recorded. Two pairs had the upper channel lead the lower channel for 100% of the swallows; they were 40 kHz and 70 kHz and 4 MHz and 7 MHz. The 7 MHz frequency still had a small amplitude (see Section 5.4), varying 122 mV during a swallow, and the 4 MHz and 7 MHz frequency-range pair had the most variable time delay between channel-to-channel main peaks over multiple swallows.

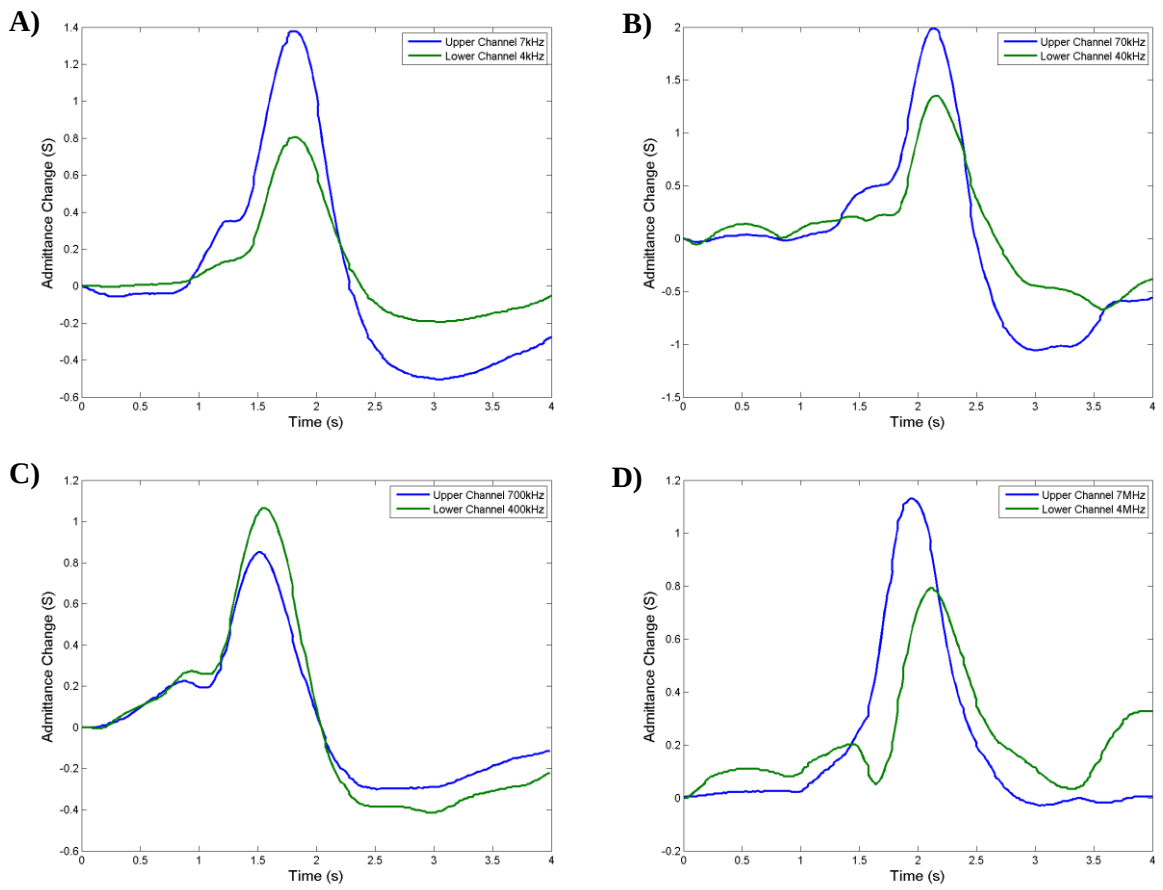

Figure 6.6. Typical output of GULPS (Subject 1) for the injection frequencies A) 4 kHz and 7 kHz (peak separation is 31 ms), B) 40 kHz and 70 kHz (peak separation is 23 ms), C) 400 kHz and 700 kHz (peak separation is 31 ms), and D) 4 MHz and 7 MHz (peak separation is 172 ms).

In a number of swallows, there were two peaks, the first being substantially smaller than the second (Figure 6.7). This peak was not frequency related as it appeared at all frequencies. After questioning, the subject identified this peak as the movement of the tongue to propel the bolus backwards and after experimentation could generate this peak by moving the tongue backwards in preparation of a swallow.

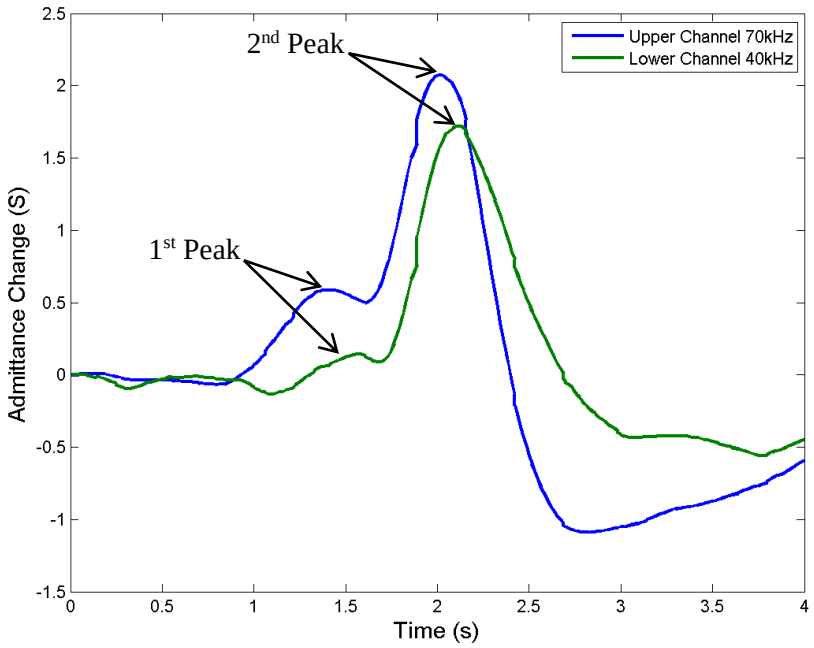

Figure 6.7. Identification of the first and second peaks in the GULPS waveform. Injection frequencies are 70 kHz (Top) and 40 kHz (Bottom).

The average time difference between the upper and lower channel peaks was substantially smaller than seen with pharyngeal manometry for all frequency pairs (Table 6.1). The average time delay between peak pressure generation in the upper and lower pharynx measured by pharyngeal manometry for unimpaired subjects is 201 ms [3]. The frequency pair of 40 kHz and 70 kHz was selected for testing on other subjects as this frequency pair produced an upper channel leading 100% of the time, and with less variation than the other frequency pairs.

Table 6.1. The average separation between the two main peaks (Subject 1) across three days. A positive separation means the upper channel leads the lower channel

Frequency Pair	Average Separation (ms)	Separation Range between Peaks (ms)	Percentage Upper Lead Lower Channel (%)
4 kHz, 7 kHz	50.8	67.83	71.67
40 kHz, 70 kHz	93.93	113.1	100
400 kHz, 700 kHz	62.0	103.2	93.06
4 MHz, 7 MHz	107.5	183.35	100

The output of the new GULPS design is different from the previous design (Figure 6.8), and this change is due to the significant hardware redesign for the constant current module. When comparing outputs for 40 kHz and 70 kHz injection frequencies for both systems, the new GULPS design produces a single peak, whereas the previous GULPS system intermittently produced a double peak, separated by a trough.

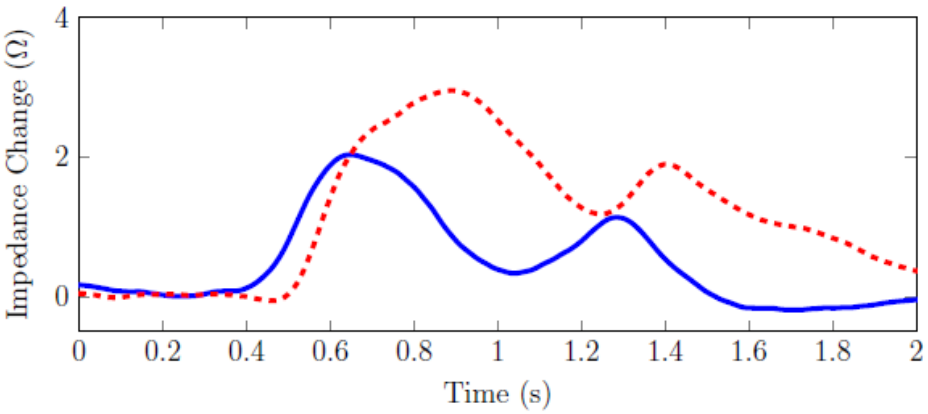

Figure 6.8. The output if the previous GULPS design which uses the injection frequencies of 40 kHz and 70 kHz

6.3.1.1 Frequency Order

The channel frequencies were interchanged, to determine if the temporal separation in the peaks was dependent on frequency. Subject 1 was tested with the 40 kHz channel in the upper position. It was found that the average separation between the two peaks was 93.3 ms. The separation matched the average separation when the 70 kHz channel was in the upper position and the temporal separation measured was not dependent on frequency channel position (upper or lower).

A) **B)**

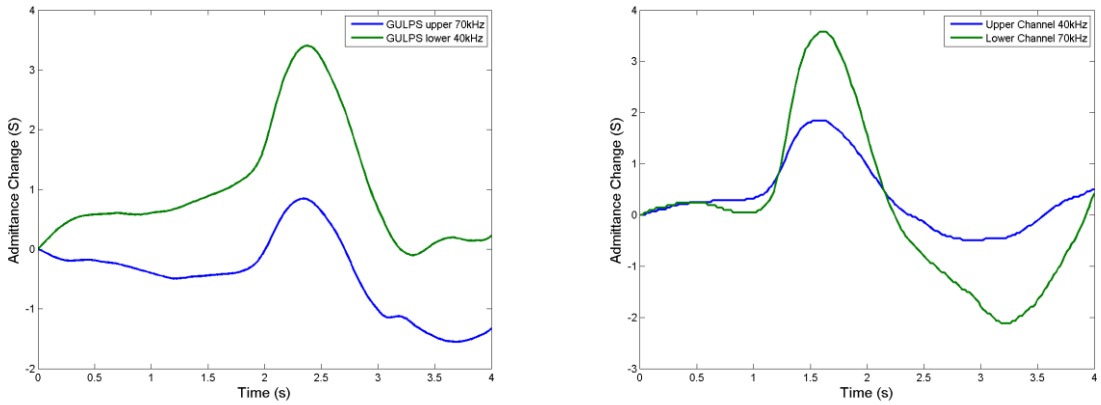

Figure 6.9. The output of GULPS with the upper channel frequency being A) 70 kHz with a separation between peaks of 40 ms and B) 40 kHz with a separation between peaks of 60 ms.

6.3.2 Testing Consistency Across Subjects

After determining that 40 kHz and 70 kHz was the most consistent of the frequency pairs, GULPS was tested on other subjects to see if the same features could be found. GULPS was tested on three healthy male subjects (Subject 2, Subject 3 and Subject 4), where all three had not been subject to previous swallowing testing. All three subjects consistently produced a single main peak in each channel during a swallow; however there was variation in the percentage the upper channel led the lower channel (Table 6.2). Subject 3 had the upper channel leading the lower channel 100% of the swallows (Figure 6.10B), whilst Subject 2's upper channel leads for 92.5% of swallows (Figure 6.10A). The most variable of the subjects was Subject 4 with an upper channel leading percentage of 33.9% (Figure 6.11). The variation between subjects was disconcerting and it suggested that there was a potential that the electrode placement was patient dependent and a different position would need to be used for each patient.

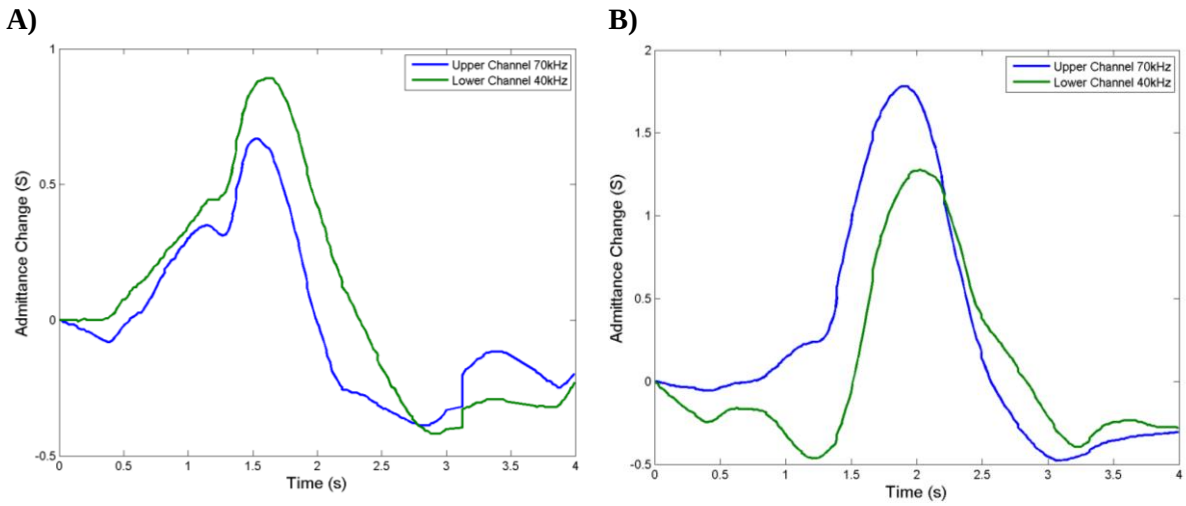

Figure 6.10. The output of GULPS for A) Subject 2 and B) Subject 3.

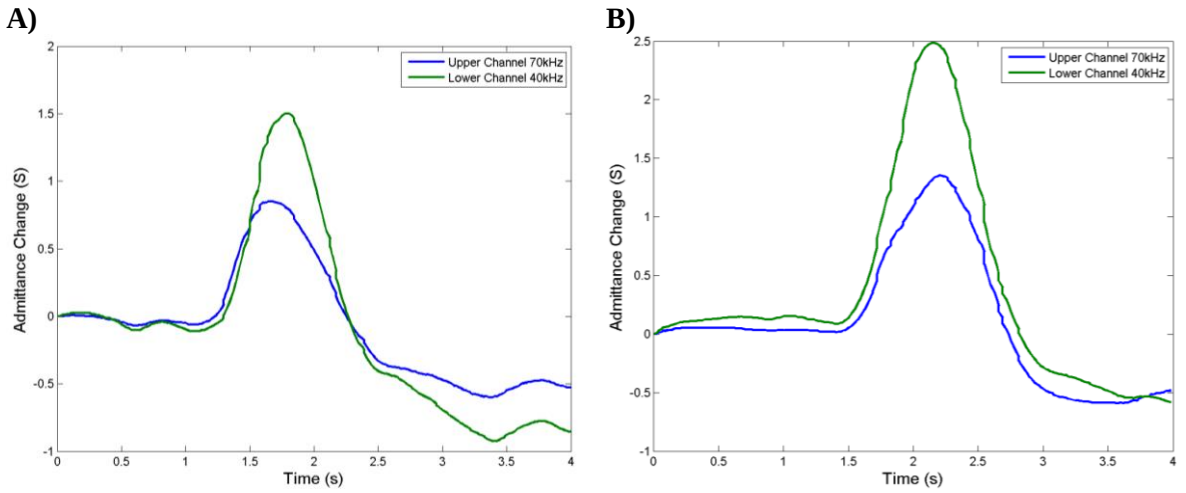

Figure 6.11. Output of GULPS for Subject 4, A) Upper channel leads lower channel by 125.0 ms B) Lower channel leads upper channel by 62.0 ms.

Table 6.2. The details of the GULPS output for Subjects 2, Subject 3 and Subject 4

	Percentage Upper Leads Lower	Average Separation (ms)
Subject 2	92.5%	75.39
Subject 3	100%	71.8
Subject 4	33.9%	-3.83

Initial testing with Subject 2 had the subject facing the display. The peaks produced by GULPS were not as smooth as the first subject and did not produce consistent features (Figure 6.12). When questioned, the subject mentioned they were forcing the swallows, trying to influence the output to match the single peak output. When the subject was orientated away from the display there was a notable difference in the output, with the swallows consistently producing a single main peak for each channel. After this session the subjects were orientated away from the display.

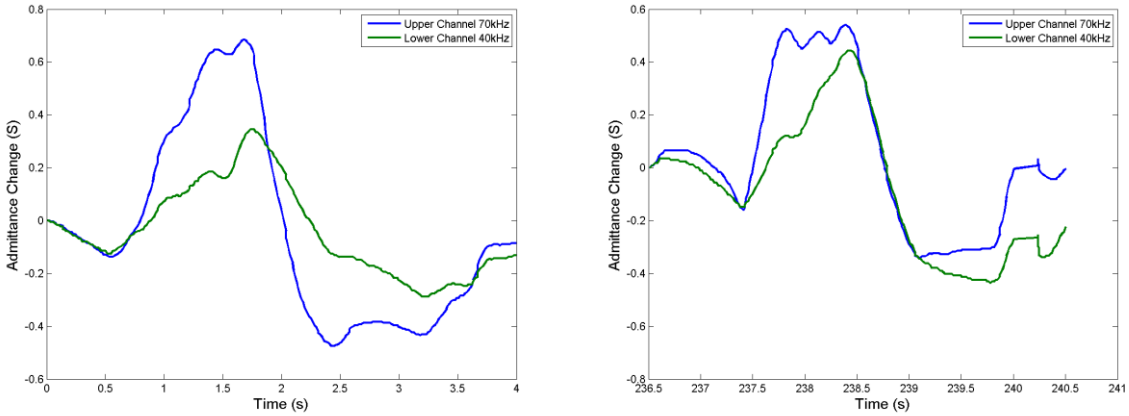

Figure 6.12. Two example waveforms of the output produced when the subject was facing the computer.

6.3.3 Pharyngeal Manometry and GULPS

Low-resolution pharyngeal manometry was used in conjunction with GULPS to determine the relationship between GULPS and the application of pharyngeal pressure. The two were tested on Subject 4. To synchronize the time stamp of GULPS and pharyngeal manometry, the auxiliary output of GULPS was connected to the pharyngeal manometry data acquisition system. There was a concern that the invasive nature of pharyngeal manometry would affect the output of GULPS, which Chester proposed during his studies. However there was little change in the overall wave shape for the new GULPS hardware.

The main peak from each of the GULPS channels lagged behind the main peak from each of the pharyngeal manometry channels (Figure 6.13, Table 6.3). The separation between the peaks for GULPS were consistent with the previous "GULPS only" testing on Subject 4, with the upper channel leading the lower channel for only 40% of the swallows. With the features unaligned, the correlation between the temporal separation between the upper and lower peaks was calculated (Table 6.3). For 10 swallows, it was found that there was a weak and non-significant linear relationship between the two, with r = 0.41 (Figure 6.14).

Subject 1 was also tested with pharyngeal manometry (Mano) and GULPS, but, the amplitude of the lower channel was very low and features could not be determined. After testing, the cause of the decreased amplitude was hypothesized as having poor contact between the electrodes and skin for the bottom channel. The upper channel matched that of Subject 4 and there was a time delay between the peaks of the GULPS and Mano upper channels.

With the features unaligned and a poor linear correlation between pharyngeal manometry and GULPS (r = 0.41 for Subject 4), different electrode positions were trialled to determine if a better correlation between the two feedback methods could be obtained and the consistency of upper channel leading the lower channel could be improved for Subject 4. These position trials are detailed in Section 6.4.

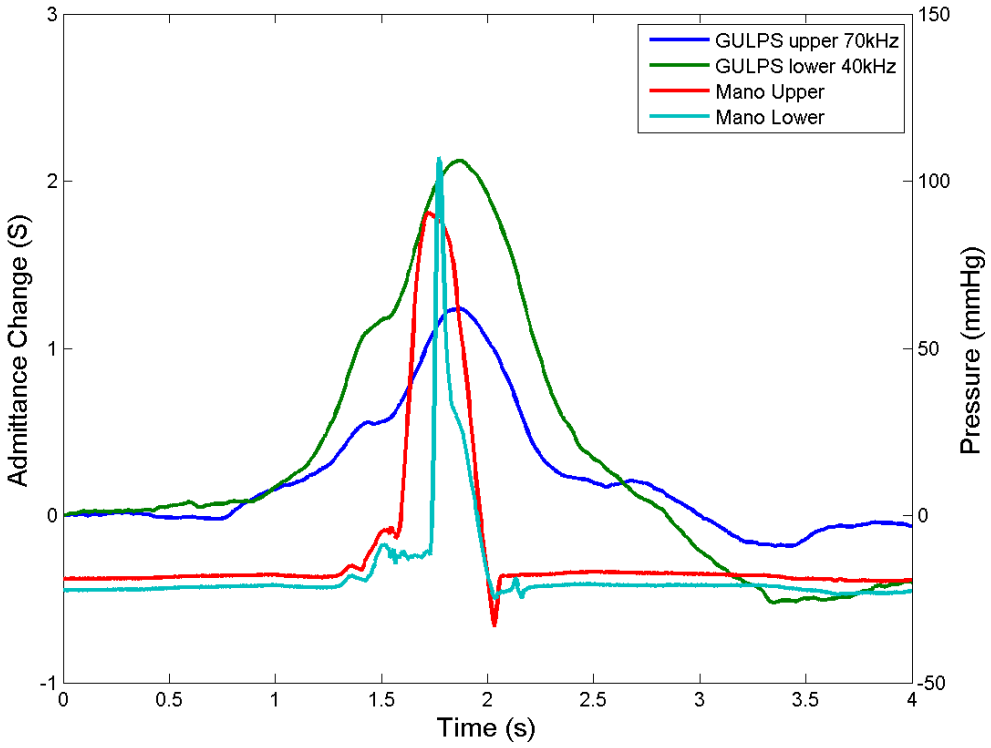

Figure 6.13. The output (Subject 4) of GULPS and manometry using electrode position 1.

Table 6.3. Comparing the output (Subject 4) of GULPS with pharyngeal manometry, N = 10.

	Mean Separation (ms)	Percentage Upper Lead Lower	Vs Manometry		
			Upper Channel Offset (ms)	Lower Channel Offset (ms)	r Value
Manometry	40.88889	100%	-	-	-
GULPS	-1.77778	40%	-145.2	-112.0	0.41

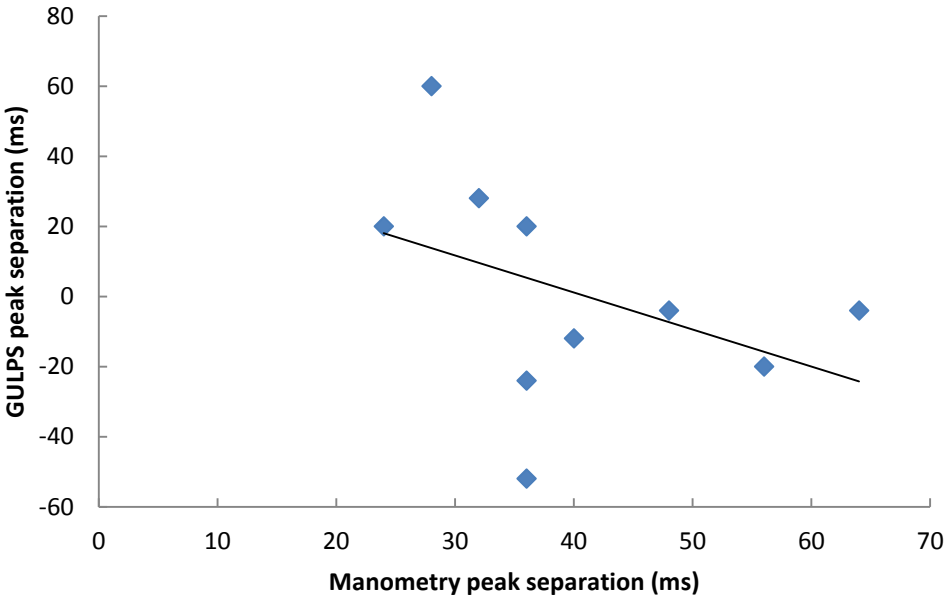

Figure 6.14. Regression plot comparing the temporal separation between peaks of manometry with GULPS (Subject 4). The linear regression model had the equation *y = -1.057x + 43.73*.

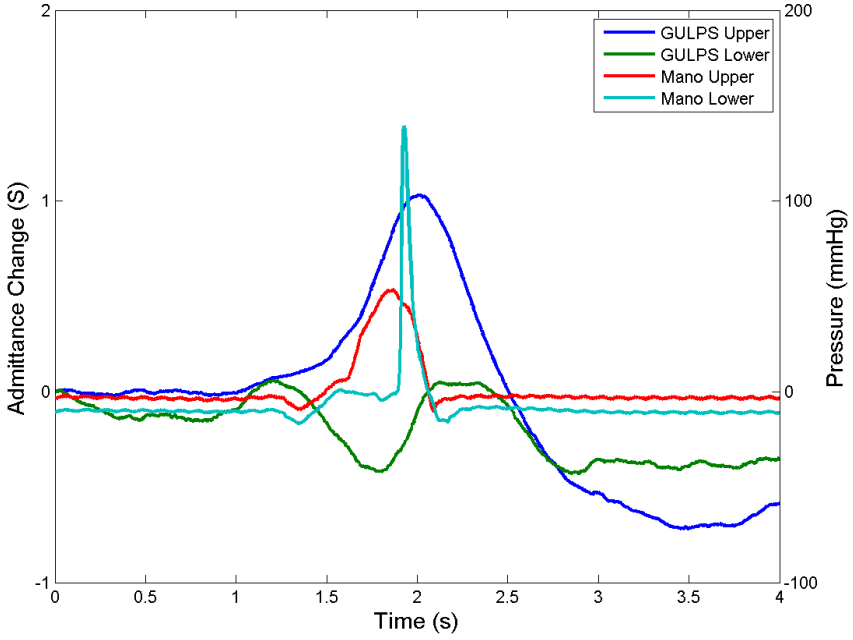

Figure 6.15. The output of GULPS and Manometry for Subject 1.

6.3.4 Computer Software

Initially the software developed by Chester [36] was used to record the data. However, after recording the first day of trials, it was noticed that there was an error on assigning the time stamps of the received data. A common error the software made was to attribute the same time stamp for several received data

points, resulting in artificial linear regions in the recorded data (Figure 6.16). This problem was left untreated; instead the smart device App detailed in Chapter 4. was used to record the sessions.

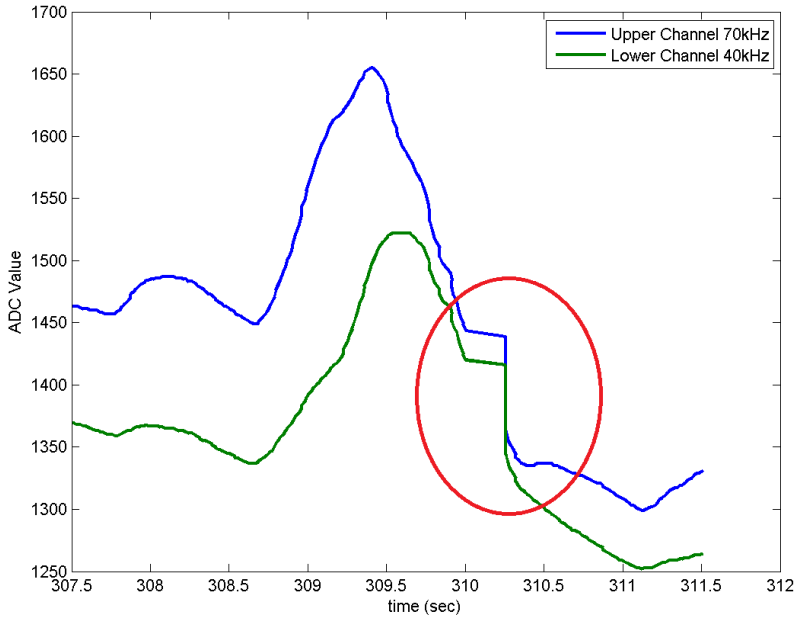

Figure 6.16. The output of the recording software showing the time stamp error, highlighted by the red circle.

6.4 Electrode Position 2

A new position was trialled which placed the upper current electrode at half the distance from the point of the mandible and the inion. The second channel current electrode was placed 30 mm below this electrode and for each channel, the voltage measurement electrodes were placed 20 mm beside the current electrodes moving away from the jaw. This position would approximately place the current electrodes in the middle of the pharynx according to CT scans of the head.

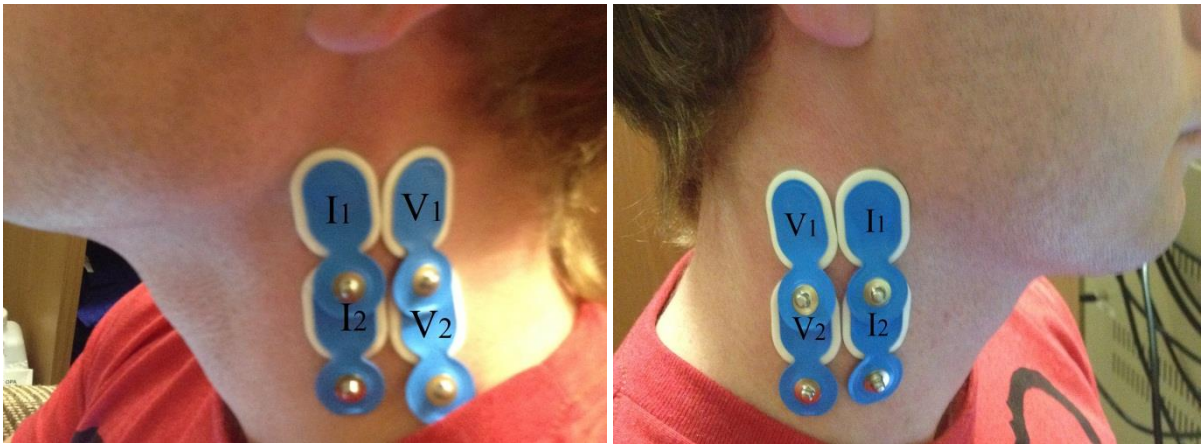

Figure 6.17. The second position of the electrodes, I are the current electrodes for each channel and V are the voltage electrodes.

The main features of the GULPS output were unchanged, but with both channels having a peak that appeared almost simultaneously (Figure 6.18B). Comparing with manometry, the GULPS waveforms had shifted so that they aligned with the middle of the pharyngeal manometry's upper channel. This

position was trialled with manometry two times on the same subject (Subject 4), the first trial (Day 1) produced a time difference between the upper and lower channels in GULPS (Figure 6.18A), although this was not replicated in subsequent tests on this subject (Table 6.4, Table 6.5, Table 6.6). It can also be noted that the time difference in peaks for pharyngeal manometry for this trial was smaller than their average delay.

The correlation between the temporal separations between peaks was calculated, and for both days there was no correlation, (Day 1, r = 0.07, Figure 6.19A, Day 2, r = 0.30, Figure 6.20A). To investigate other feature correlations, the separation of the greatest rate of change of the onset slope of the GULPS output and the temporal separation of manometry main peaks was considered. It was found that this relationship had a high correlation for Day 1 (r = 0.71, Figure 6.19B), but a very poor correlation for Day 2 (r = 0.12, Figure 6.20B).

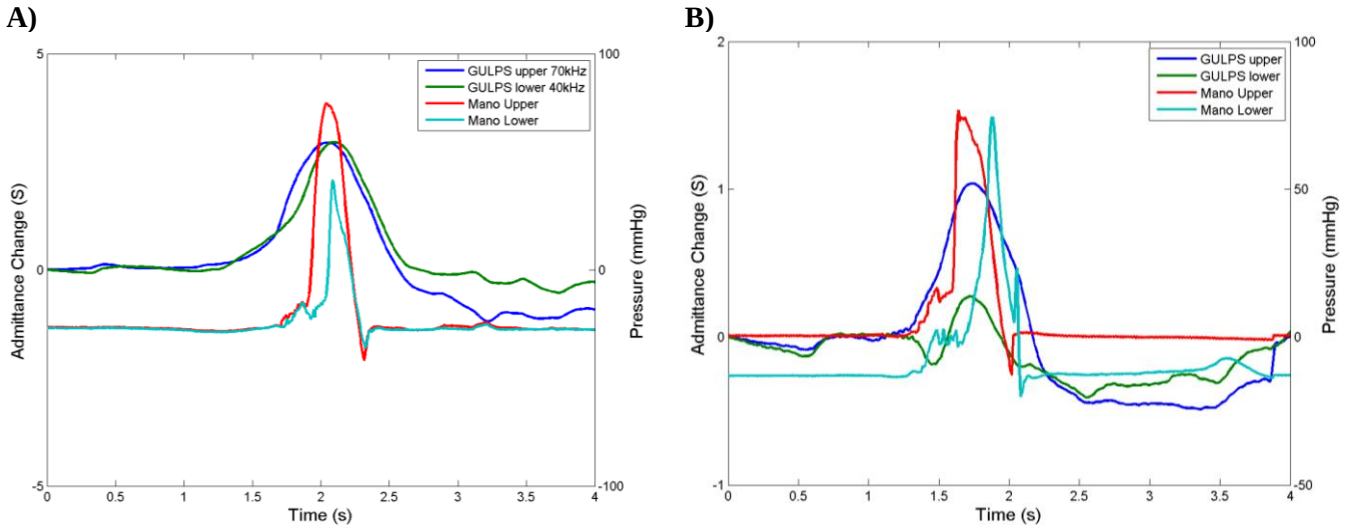

Figure 6.18.The output (Subject 4) of simultaneous GULPS and manometry testing for A) Day 1, B) Day 2.

Table 6.4. Day 1 GULPS and Manometry data (Subject 4) for the second electrode position. During this test an abnormally large time delay was captured and has not been reproducible, N = 11.

	Mean Separation (ms)	Percentage Upper lead Lower	Manometry Linear Regression		
			Slope	Offset	R^2 Value
Manometry	64.36	100%	-	-	-
GULPS	60.36	100%	-0.046	63.32	0.07
GULPS rate of change	174.55	100%	0.62	134.87	0.71

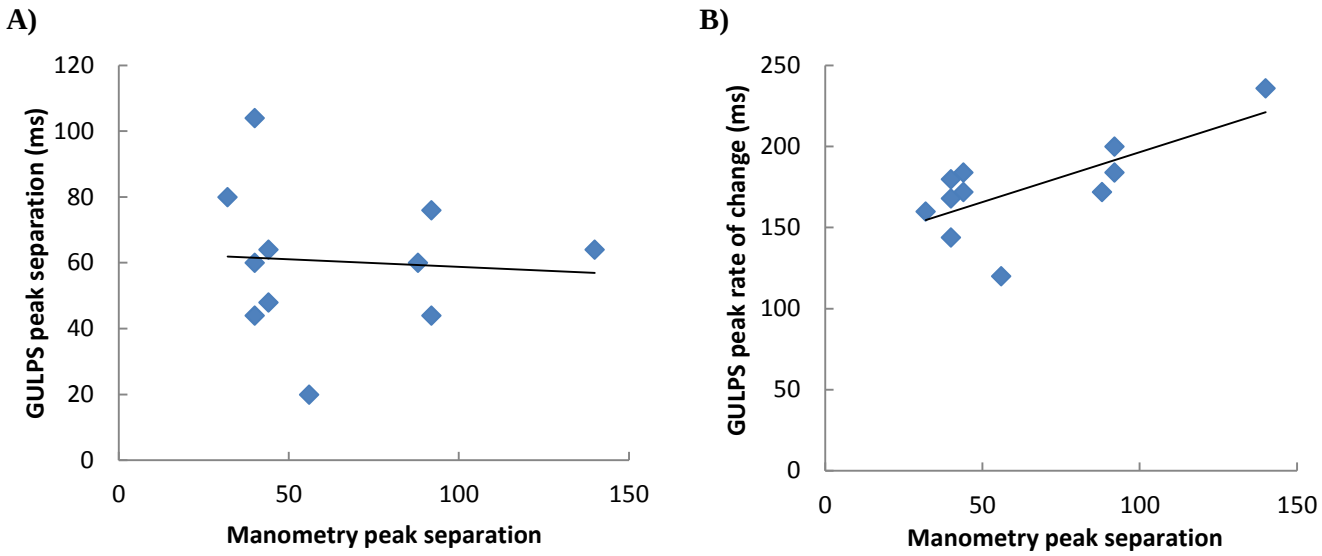

Figure 6.19. Regression plots for day 1 (Subject 4), comparing the temporal separation in peaks between manometry and A) the peaks in GULPS, B) the temporal separation of the greatest rate of change in the GULPS output.

Table 6.5. Day 2. GULPS and Manometry data for the second electrode position. These results match the other tests performed using standalone GULPS, N = 21.

	Mean Separation (ms)	Percentage Upper Lead Lower	Vs Manometry		
			Slope	Offset	r Value
Manometry	209.14	100%	-	-	-
GULPS	-13.90	43.81%	-0.21	29.21	0.30
GULPS rate of change	24.46	37.86%	0.099	0.92	0.12

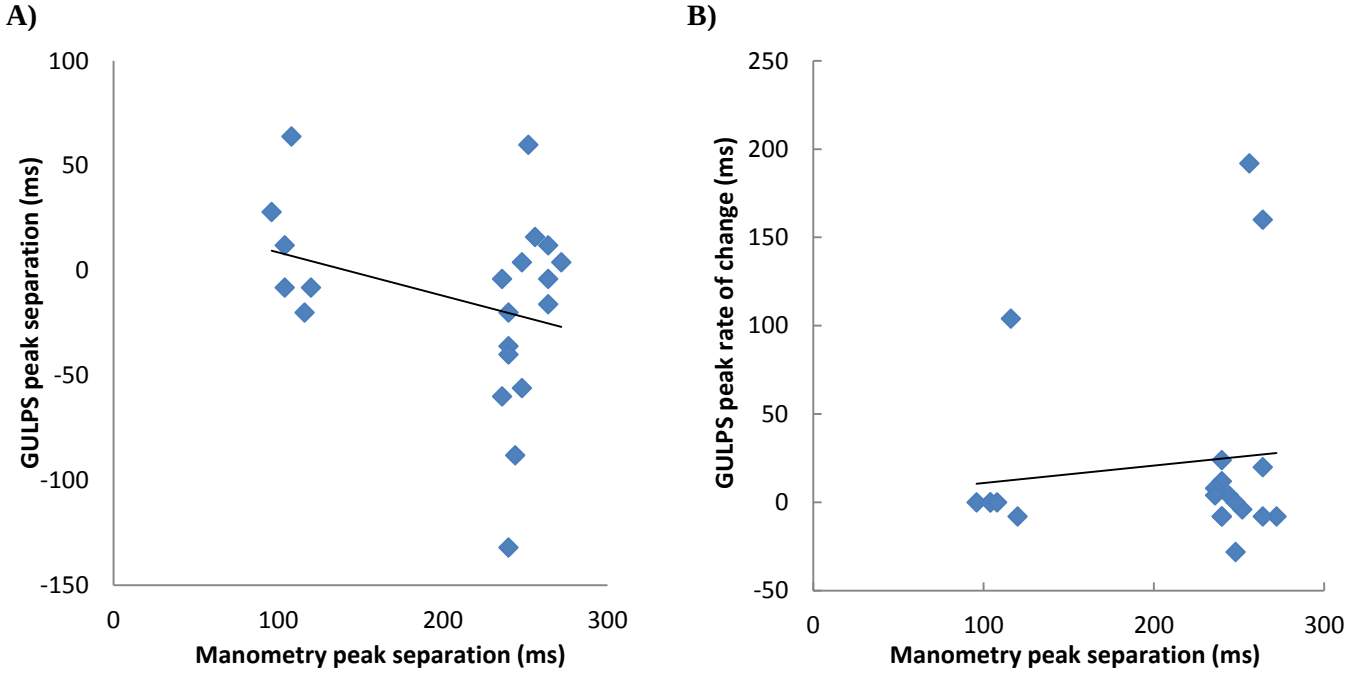

Figure 6.20. Scatter plots for day 2, comparing the temporal separation in manometry to A) the temporal separation in the GULPS peaks and B) the temporal separation between the greatest rate of change in the GULPS output.

GULPS without pharyngeal manometry was also trialled on Subject 4. The trials produced an average separation of 2.5 ms (Table 6.6). The results from Day 1 (Table 6.4) could not be reproduced using this electrode position, and it still remains unclear how the results were obtained in that trial.

Table 6.6. The results using standalone GULPS for electrode position 2 on Subject 4.

	Average Separation (ms)	Percentage Upper lead Lower	Average Separation Range (ms)
Subject 4	2.5	58%	177

A second subject (Subject 5) was trialled using electrode position 2, but only 7 of the 10 swallows for this subject were useable because the output of GULPS exceeded the configured scale on the manometry recording station. For this subject the output of GULPS aligned with the upper channel of pharyngeal manometry, but, out of the 7 swallows only 1 had the upper channel main peak leading (Table 6.7).

Table 6.7. Results for Subject 5, using GULPS and manometry for the second electrode position, N = 7.

	Mean Separation (ms)	Percentage Upper lead Lower	Manometry Linear Regression		
			Slope	Offset	R^2 Value
Manometry	270.29	100%	-	-	-
GULPS	9.14	14.29%	-0.114	0.022	0.5526
GULPS rate of change	34.29	57.17%	0.313	-50.55	0.186

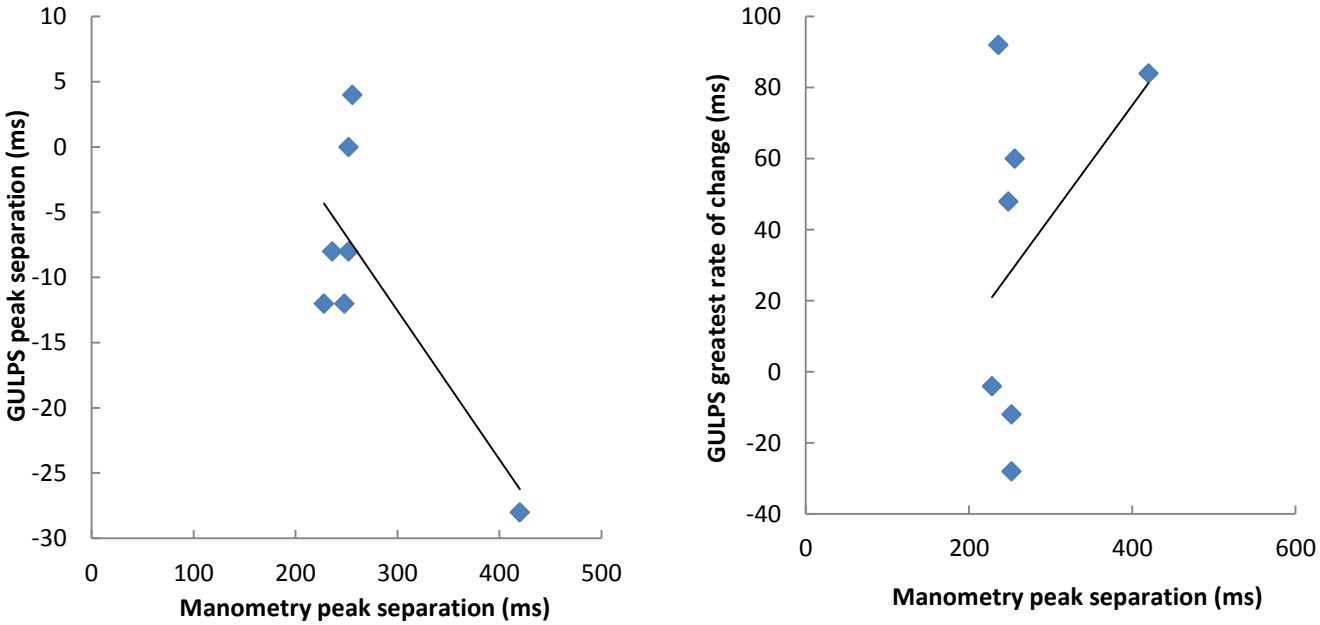

Figure 6.21. Scatter plots for Subject 5 comparing the temporal separation of pharyngeal manometry with A) GULPS peak separation and B) the greatest rate of change of the GULPS output.

Shifting the electrodes to position 2 has resulted in the peaks produced by GULPS to align with the upper channel of pharyngeal manometry, suggesting the change in impedance is occurring during the pharyngeal stage of the swallow. This position did not increase the percentage the upper channel lead

the lower channel for Subject 4 and Subject 5 also had a small percentage of the upper channel leading the lower channel.

6.4.1 Other positions

In an attempt to separate the two GULPS channels, two different electrode positions were trialled on Subject 4. In the first position, the upper electrodes were the same as electrode position 2 (Figure 6.17). The lower channel was moved downwards from their original positioning in electrode position 2 by 20 mm, increasing the gap to 50 mm. By increasing the separation between electrodes it was hypothesized that this would result in an increase in the separation of peaks. It was found that this did not change the output of GULPS with the lower channel still aligned with the upper channel.

The second position trialled during a GULPS and pharyngeal manometry session, shifted both channels upwards to align the top channel with the corner of the subjects jaw, the lower channel was placed vertically in line with the top channel 30 mm below. This position did not vary the shape of the GULPS output, the timing relative to pharyngeal manometry and the separation between peaks remained the same.

By varying the electrode positions, it was found that they did not seem to have an impact on the separation of the main peaks produced by the two channels. Other changes to the system would need to be made to produce a clear linear correlation between manometry and GULPS. The electrode position used for all of the following tests was electrode position 2 (Figure 6.17), due to the output aligning with the upper channel of pharyngeal manometry in this position.

6.5 Pharyngeal Mis-sequencing Trials

A male subject with a history of pharyngeal mis-sequencing was trialled using electrode position 2. For a mis-sequenced swallow there was a substantial change in the GULPS features (Figure 6.22). With GULPS, every swallow the lower channel had a single peak but the upper channel had two distinct peaks. There was also a change in the pharyngeal manometry output; the lower channel had two peaks in the waveform. To calculate the separation between the two channels, the peak with the largest amplitude was used. The average separation between the two channels for pharyngeal manometry was 32.75 ms.

With the new features, correlations using the two upper peaks and the lower channel peak in GULPS were drawn (Table 6.8, Figure 6.23), with the temporal separation with the first peak having a much stronger relationship ($r = 0.70$).

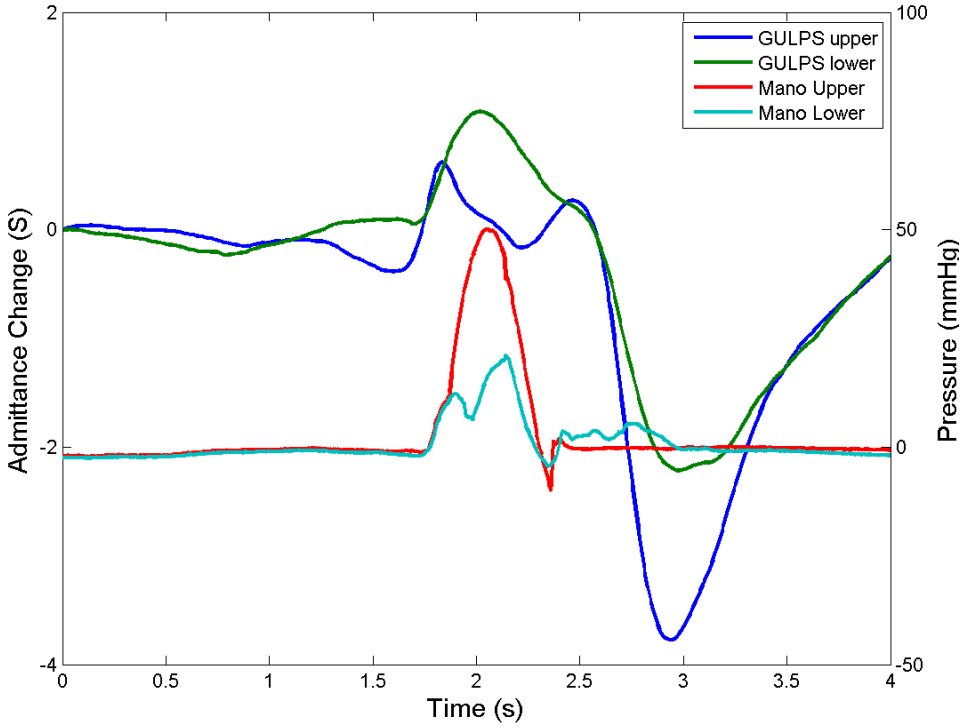

Figure 6.22. Simultaneous GULPS and Manometry for a mis-sequenced swallow.

Table 6.8. Correlation for the features presented in a mis-sequenced swallow, N = 10.

	Mean Peak Separation (ms)	Manometry Linear Regression		
		Slope	Offset	R^2 Value
Pharyngeal Manometry	32.75	-	-	-
1st Peak	216.8	-0.54	238.0	0.487
2nd Peak	369.2	-0.14	-363.9	0.0315

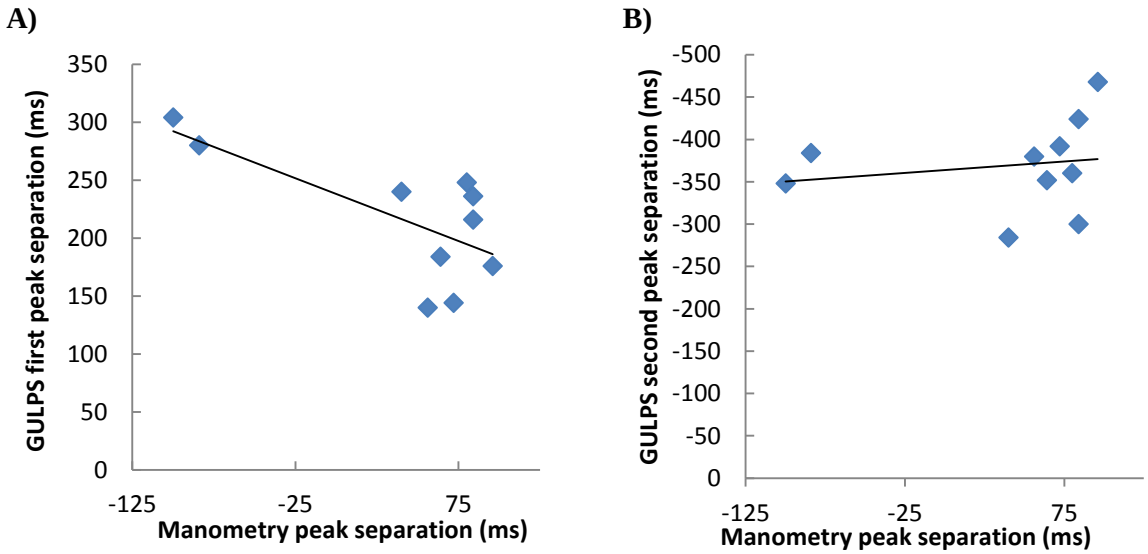

Figure 6.23. Scatter plots of the upper channel of GULPS A) first peak and B) second peak temporal separations against manometry.

6.6 Isolated Voltage Supplies

Outlined in Section 5.5, the two channels of GULPS were electrically isolated, this was to test the hypothesis that the sharing the same reference node was creating cross-over current paths. The cross-over current paths would cause the two channels to measure effectively the same impedance change related to a cross-sectional area between the two channel locations, producing the simultaneous waveform seen. It was hypothesized that isolating the two channels would remove the cross-over paths and the output of GULPS would appear sequential, as the impedance change of each channel would be due to changing cross-sectional area local to that channel's electrode position.

Subject 4 was tested using the isolated system, with electrode position 2 (Figure 6.17). Using a water bolus, it was found that the features of GULPS were almost unchanged from the non-isolated system (Figure 6.24). The waveform was very similar to the shape of the non-isolated GULPS system, and demonstrated that the cross-over current did not seem to substantially influence the impedance measurement.

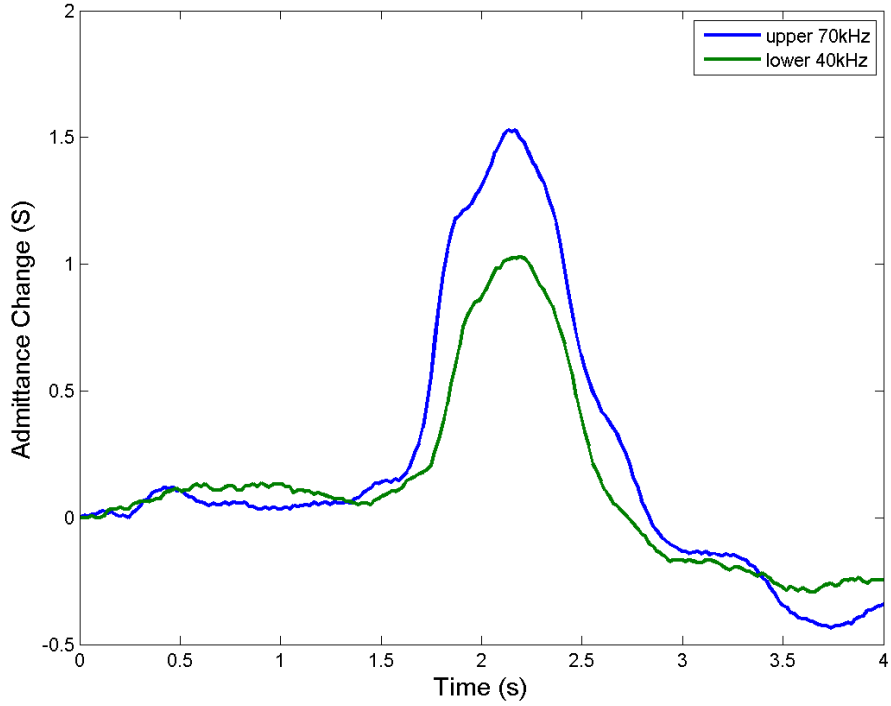

Figure 6.24. The output of GULPS using isolated power supplies

The second type of swallow performed was a dry swallow. A dry swallow is when the subject generates saliva to form the bolus. The waveform shape of the GULPS output using a dry swallow, has a second peak in both channels. When using the non-isolated system the upper channel displayed this peak, however it did not occur in every swallow (Figure 6.25A). Using the isolated power supplies, this peak was apparent in every swallow and had twice the amplitude compared to the non-isolated system (Figure 6.25B). The first peak was identified as being caused by movement of the tongue when generating a saliva bolus. Though this peak does not relate to the pharyngeal stage of swallowing, the temporal separation was investigated. The average separation for the first peak was 270.22 ms (Table 6.9), however this separation was inconsistent and had a range of 864.3 ms. The trough had a smaller separation of 7.37 ms (Table 6.9) and this too had a wide range of 242.0 ms. The two features were not

compared to pharyngeal manometry due to the variation in the feature separation and the first peak not being related to the pharyngeal stage of swallowing.

Table 6.9. The results using a dry swallow and the isolated GULPS system, on Subject 4. N = 20

Feature	Mean Separation (ms)	Percentage Upper Lead	Separation Range (ms)
1st Peak	270.22	84.21%	864.3
2nd Peak	-100.5	9.52%	140.7
Trough	7.37	85.71%	242.0

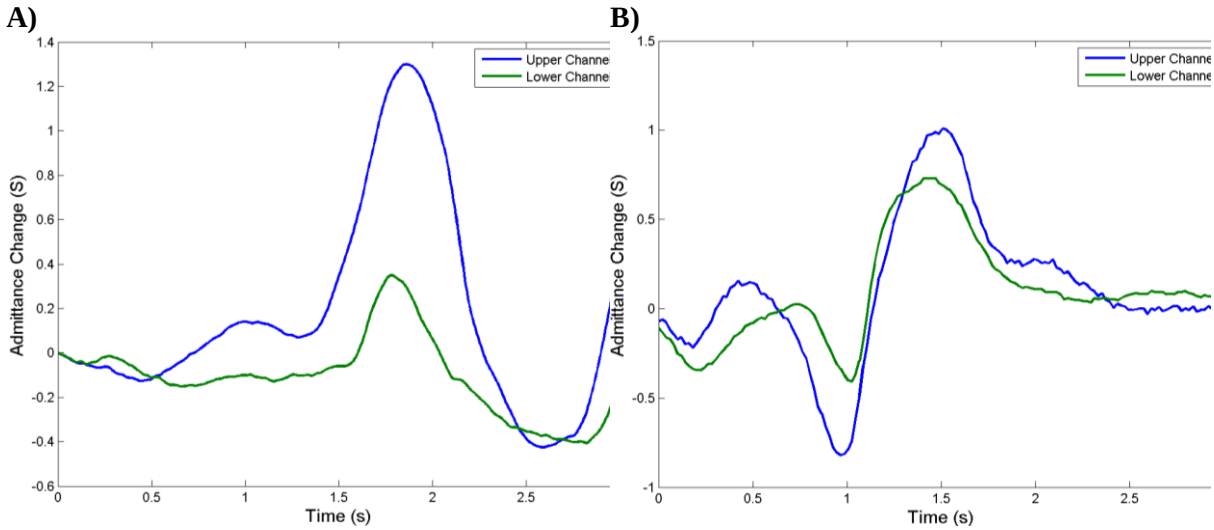

Figure 6.25. The output of a dry swallow for Subject 4 with A) non-isolated supplies, where the swallow occurs at t = 1.75 s and B) isolated supplies where the swallow occurs at t = 1.5 s.

6.7 Subtraction Method

The aim of the subtraction method was to remove the impedance change due to cross-sectional area between the two channel positions from the output. This would leave an impedance change caused by the cross-sectional area local to that injection location. This was performed by measuring the change in impedance due to both frequencies at both upper and lower channel locations. This resulted in the measurement of two changes in impedance for the each channel location, one related to the local frequency and one related to the paired frequency. The measured output for each channel location was the change in impedance related to the local frequency minus the change in impedance due to the paired frequency. This method required an additional bandpass filter module and signal conditioning module for each channel (Figure 6.26). The output current of the constant current converter for the 40 kHz channel was adjusted to match the output current of the 70 kHz channel. It was desired for the amplitude of the two channels to be matched so the output would not be biased by one channel. The output of the four signal conditioning modules were measured by an oscilloscope and then the subtraction was performed in MATLAB [81].

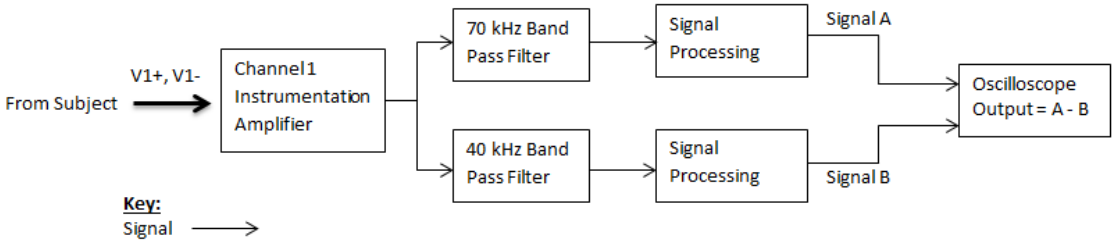

Figure 6.26. Block diagram of the hardware for the subtraction method for the 70 kHz channel.

Subject 4 was tested over two days using the subtraction method. There was a substantial difference in the shape of the output waveform (Figure 6.27) compared to standard GULPS, however the output was only consistent within a session and varied between the two days. Due to the changing features between each day, no attempt was made at a correlation between the subtraction method and pharyngeal manometry. One repeating feature that is visible in the output is the presence of the subject's pulse, clearly seen in the lower channel in Figure 6.27A and Figure 6.27B, which is not visible in the GULPS output.

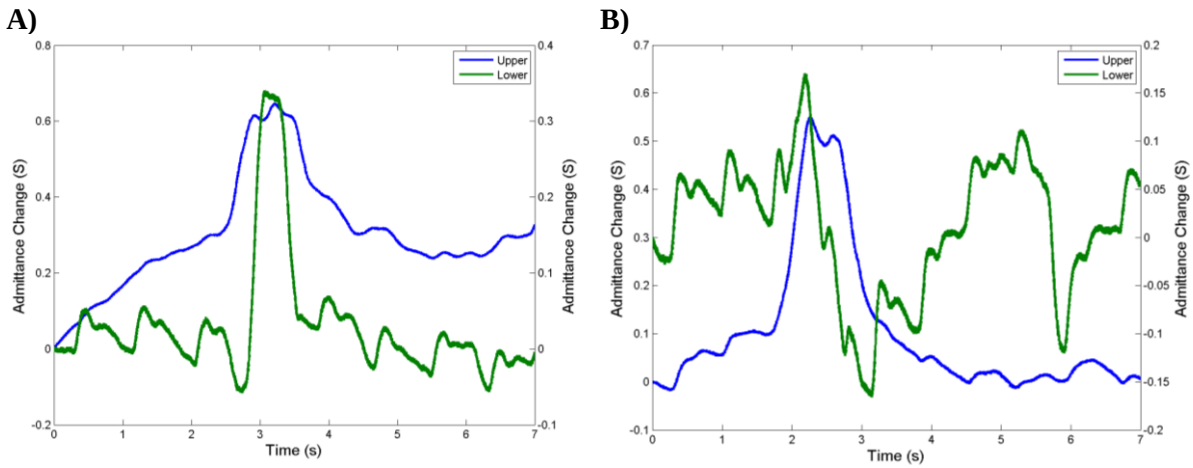

Figure 6.27. The output using the subtraction method on Subject 4 for A) Day 1, where the swallow occurs at t = 3 s and B) Day 2, where the swallow occurs at t= 2.25 s.

The difference in the shape of the waveform between the two days is potentially due to the effect the electrode contact has on the output waveform. This method requires the amplitude of the two signals to be matched to remove the impedance of the paired channel from the output. If one channel has greater amplitude due to an uneven electrode contact then there could be a visible difference in the output.

6.8 Summary

GULPS was trialled on several subjects and was found that each channel produced a single peak, however there was inconsistent temporal separation of the channels. GULPS was tested concurrently with manometry and the electrode position was adjusted to align the peak of GULPS with the upper channel of manometry. Different electrode positions were trialled however it was found that they did not affect the temporal difference between the GULPS peaks but did affect the relationship between the output of GULPS and the output of manometry.

Two other hardware designs were tested, isolated power supplies and subtraction of the paired frequency from each channel. The isolated frequencies did not substantially change the features of the GULPS waveform and the subtraction method, while showing potential, did not provide a consistent output.

Chapter 7.0 Discussion and Final Remarks

The new development for the GULPS system has improved the consistency of the output features. GULPS now produces two peaks, one for each channel, which occur consistently for every swallow. This is an important improvement from the previous design which could only produce features for 22% of the swallows, with a liquid bolus. This improvement in consistency is due to the change in the constant current module, switching from a basic opamp based design to an OTA IC. Changing the electrodes from the Triode dry electrodes to the Ambu Blue sensor N wet electrodes also improved the consistency of the output.

Using a modular system, the effect of the injection frequency on the output could be determined. The features present in the output of GULPS did not change substantially between frequencies; but there was a decrease in amplitude for the higher frequencies, with the 7 MHz frequency being the smallest in amplitude and required an additional amplification stage for the change of impedance to be visible in the output. Two frequency pairs produced time differences between the peaks of every swallow: the 40 kHz and 70 kHz frequency pair and the 4 MHz and 7 MHz pair, however the 4 MHz and 7 MHz pair was less consistent with the widest range in the separation of peaks. Therefore 40 kHz and 70 kHz was chosen to continue further investigation into the relationship between the GULPS output and the pharyngeal manometry.

Pharyngeal manometry and GULPS were simultaneously trialled on a healthy subject to define the relationship between the GULPS output and the pharyngeal pressure during swallowing. Using the first electrode position there was a delay between the pharyngeal manometry output and GULPS, with the GULPS output lagging the manometry output. A second electrode position was trialled, which aligned the two channels of GULPS with the centre of the upper channel of pharyngeal manometry. However, in all but one trial the features of GULPS were close to being temporally aligned. Two more electrode positions were trialled but gave no increase in the separation between the two main peaks.

GULPS was trialled on a patient with dysphagia due to pharyngeal mis-sequencing, and was found to have substantially different impedance waveforms to those of healthy subjects. This distinct difference between a mis-sequenced swallow and a healthy swallow confirms that GULPS has potential as a swallowing rehabilitation biofeedback device, by providing visual feedback on the variation in electrical impedance of the neck at multiple points during a swallow. However, to actually be used as a clinical and/or rehabilitation tool, the impedance variation must first be definitively associated with some known physiological changes that occur during a swallow.

Bluetooth communication was successfully added to the GULPS hardware, and the developed Android App successfully plotted and recorded the data. This was used for the majority of the data capture for this project after discovering a fault in the previously developed computer software.

7.1 Discussion

The goal of this project was to develop a non-invasive, portable tool to evaluate swallowing behaviour for use in a clinical and home environment. With the current system there is no clear relationship between the change in impedance and the closure of the pharyngeal lumen. Therefore in its current state, the project goal remains incomplete and further work needs to be performed before this goal can be meet.

7.1.1 Pharyngeal Movement

Careful consideration of the physiology behind swallowing may suggest that the simultaneous upper and lower channel change in impedance observed could be due to the vertical movement of the pharynx during swallowing. During a swallow, the pharynx simultaneously shortens and rises to reduce the distance the bolus needs to travel (Figure 7.1) [3]. The approximate distance the pharynx rises during a swallow is 10 mm and shortens by 15 mm [82].

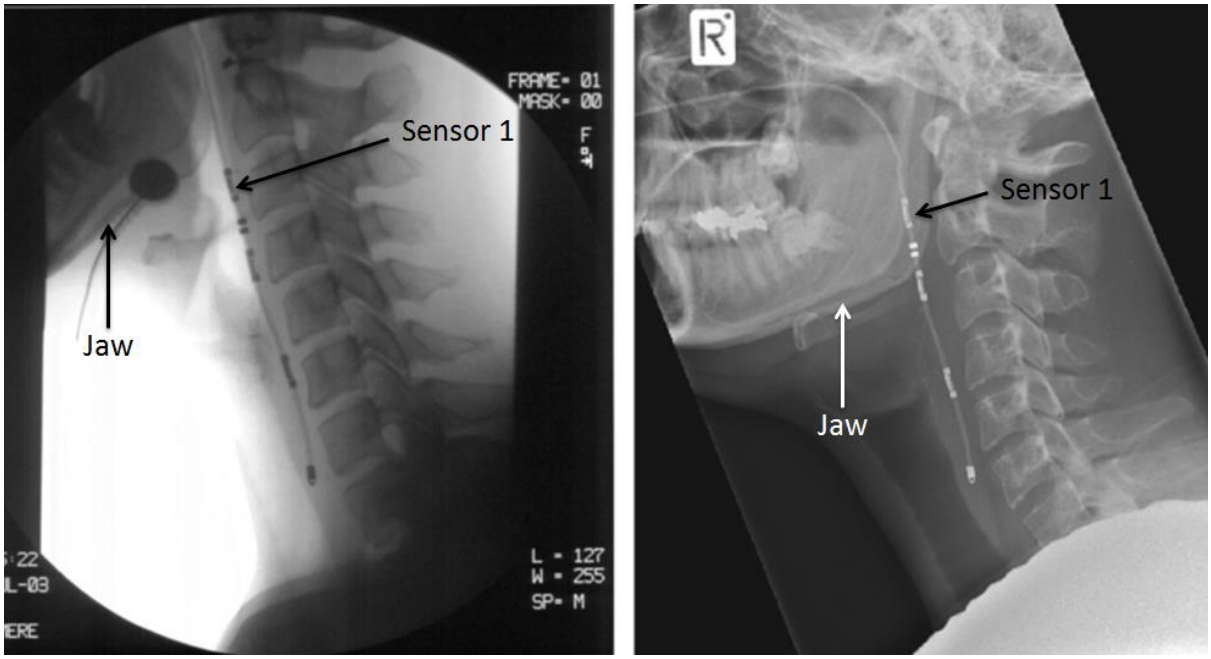

Figure 7.1 Simultaneous videofluoroscopy and Pharyngeal Manometry revealing the movement of the pharynx during a swallowing event. A) at rest B) during swallowing [3].

During a swallow, the hyoid bone and the larynx move vertically upwards and forwards to rest under the base of the tongue (Section 2.1.3 Pharyngeal Phase). The vertical movement will place the hyoid bone and the larynx in the horizontal, cross-sectional plane of the electrodes. This will increase the cross-sectional area and reduce the impedance. The movement of organs such as the oesophagus, respiratory tract, pharynx and epiglottis causing the change of the impedance has been stated by several sources [34, 83]. Schultheiss *et al.* [84] used videofluoroscopy to test the hypothesis that the impedance change was due to the movement of the organs. Schultheiss found a significant correlation ($R^2 = 0.813$) between the change in impedance and the movement of the hyoid and larynx towards the second and fourth cervical vertebra.

Pharyngeal manometry is not affected by the shortening and movement of the pharynx because the length of the pharynx shortens will still contain the top two sensors on pharyngeal manometry catheter [82] and will measure the pharyngeal pressure applied. When the pharynx constricts as it moves upwards, the catheter moves with it.

To measure closure of the pharyngeal lumen with impedance, first the impedance change related to the movement of the pharynx and other organs must be removed from the output. This was attempted with the subtraction method (Section 6.7). The subtraction method produced a different waveform shape from the GULPS waveform and has potentially removed the effect of the pharynx movement. Further investigation into this method to produce a consistent waveform output, could provide an impedance change related to the closure of the pharyngeal lumen.

7.1.2 Literature Comparison

The admittance plot produced by GULPS has similar features to the impedance plot produced by Kusuhara *et al.* [34] (Figure 7.2), and noting the inverting function employed by GULPS which gives a rising waveform for reducing impedance). This verifies the modification of the constant current module, and further development of the base hardware is no longer a priority and full attention can be given to identifying the physiological cause of the change in impedance and how to relate the change to the pharyngeal sequence.

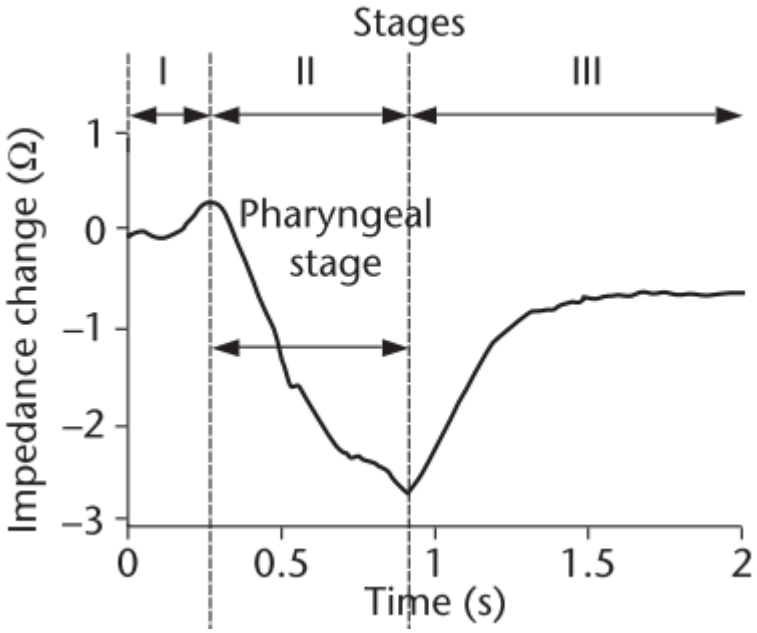

Figure 7.2. The impedance change measured by Kusuhara *et al.* [34].

7.1.3 Impedance Measurement of Swallowing Disorders

Yamamoto *et al.* [83] performed single channel impedance measurement on a subject with a swallowing disorder (Figure 7.3). The impedance waveforms produced by Yamamoto have multiple peaks and they concluded five features of the waveform:

1. The waveforms become multiphase, with repeating the up and down changes,
2. The IPG will not become consistent
3. The time from the signal to the start becomes long,
4. The total duration of swallowing becomes long
5. The IPG change corresponding to the laryngeal rise is not clear.

In all of the GULPS waveforms for a mis-sequenced swallow there were two distinct peaks. Little comparison between the two can be drawn due to the unknown nature of subject presented by Yamamoto. However the multi-peak waveform presented in the two cases presents that swallowing disorders do have an effect on the impedance waveform and further investigation should be carried out into the physiological causes of the multiple peaks.

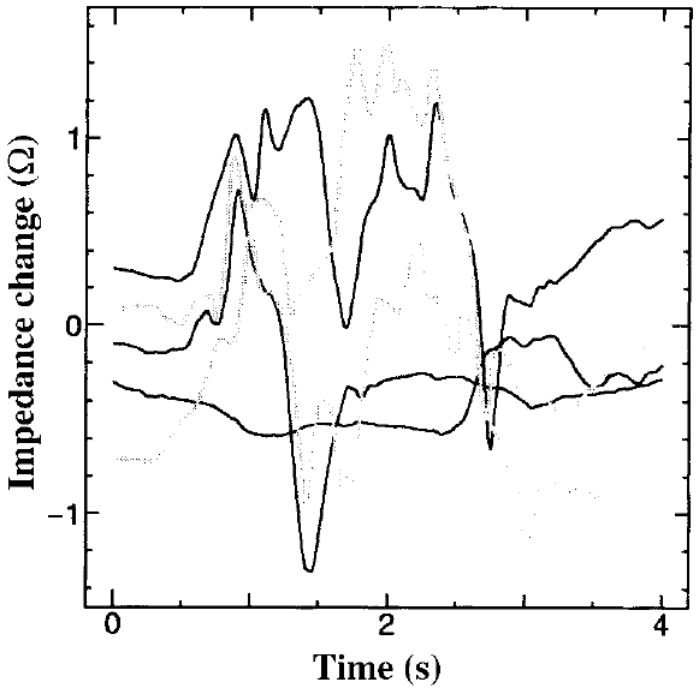

Figure 7.3. Impedance waveform of a subject with swallowing disorders [83].

7.1.4 Electrodes

During testing it was noticed that the output amplitude was related to the pressure applied to the electrodes (See Section 6.2 Electrodes). Even with the addition of tape the pressure was variable and this influenced the output. It is hypothesized that the pressure on the electrodes is affecting the skin-to-electrode resistance. By using the tetrapolar configuration, variation in the skin-to-electrode resistance should not affect the impedance measured, and this was shown by using the resistor network load in Section 5.4. Using the resistive network load, the resistance between the current and voltage electrodes could be dynamically changed and with no change in measured change in impedance. This requires further investigation into minimizing the effect the pressure has on the measured impedance and develop a method to provide consistent contact between the electrodes and skin.

7.2 Further Research

While there is a definite visible difference between a healthy swallow and an unhealthy swallow using GULPS, as indicated above, investigation can still be performed into the cause of the simultaneous peaks, and to find a linear relationship between the output of GULPS and pharyngeal manometry. Improvements can be made to the hardware and to the software, both to the embedded Android App and computer software, which are discussed below

7.2.1 Hardware

The GULPS hardware can be further developed, with several design limitations were mentioned in Chapter 5.0, Hardware Development. The design changes listed will improve the systems portability and increase the output signal range. The new modular GULPS hardware system will allow easy modification of the hardware and reduce development time by only requiring printing PCB's for the new hardware modules. The design limitations mentioned in Chapter 5.0 are relisted and further developed in the following section.

7.2.1.1 Sinusoidal Wave Generator

The output of the sinusoidal wave generator is not a pure sinusoid, due to the presence of odd and especially third and fifth harmonics in the output (Figure 5.4). Increasing the order of the bandpass filter that follows the square wave generator would remove the harmonics and create a pure sinusoidal wave. Another method would involve using a digitally generated wave. There are two methods of digital sinusoidal wave generation [85], programmable read-only memory (PROM), which involves storing all, or part of the sinusoidal wave, and sequentially stepping through the stored values. The second method is to use a direct digital synthesizer (DDS) IC. Both methods would require a digital-to-analogue converter (DAC) to convert the digital information to an analogue signal. The effect of using a pure sinusoidal wave will have on the output is undetermined and an initial investigation can be performed using signal generators.

7.2.1.2 Power Module

A power supply module was not designed for the modular system and currently operates on a dual output lab power supply. With the addition of a power module to generate the ±5 V rails, the system would be easier to move and use outside the lab in testing environments. The base of the design of this module can be taken from Chester's design [36] and can be seen in Appendix A. Figure A.17.

7.2.1.3 Demodulation Stage

Another design change mention by Chester was the use of a precision full wave rectifier in the demodulation stage, instead of a diode [36]. The diode was changed in the new GULPS system from a Silicon diode to Geranium diode to reduce the amplitude loss across the diode. Using a precision rectifier would reduce the voltage drop across this stage further and the signal would require less amplification in later stages.

7.2.1.4 Wireless Communication

Bluetooth was used for this project due to the short development time it offered, in the speed hardware could be developed and development of the required operation software. Another potential wireless communication method is Wireless Direct, which allows Wi-Fi (Wireless-Fidelity) devices to connect point-to-point. Wireless Direct achieves typical Wi-Fi speed, which can reach 250 Mbps [86]. In comparison, the RN-42 Bluetooth module used in this project has a transfer speed of 3 Mbps [55]. However, Wi-Fi Direct draws uses more power compared to Bluetooth, drawing up to 2000 mW. Wi-Fi Direct is only on a small number of devices, available on 1964 smart phones and 270 tablets [87], compared to Bluetooth which is available on 5134 smart phones and 2552 tablets [88]. Bluetooth also has a larger online developer support compared to Wi-Fi Direct. With the modular design of both the hardware and the Android App software, the integration of Wireless Direct would require minimum changes to the current structure.

7.2.2 Software

The Android App software developed in Section 4.0 can be developed further to increase the functionality and the user performance. It was also discovered that there was an issue in the previously developed software which was left unsolved.

7.2.2.1 Time Stamp

For both the computer software and the Android App, there are imperfections with the time stamp associated with the data recorded. The computer software would intermittently assign the same time stamp to multiple data points, resulting in vertical lines in the plots. The Android App uses an incrementing counter to assign time values to data. An incremental counter makes the assumption that no points have been missed. One method of improving the time stamp problem is to keep track of the

time on the microcontroller and send the time with the measured impedance data. Sending the time with the data would remove the need for the App and computer to keep track of the time. This would be an advantage as the time would not be disrupted by background tasks of the computer or App and a data point would not be assigned the wrong time stamp if a point is missed. If the time stamp is to be sent with the impedance data, an investigation needs to be performed to determine if the impedance and time stamp values can be transmitted within the 20 ms cycle.

7.2.2.2 Android Graphing Software

Further improvement to the performance of the Android graphing module can be carried out as lag is experience infrequently in the App when graphing displays larger than 5 s. The currently used API is AChartEngine, however different graphing packages are available and could be investigated to decrease the lag.

7.2.3 Smart Device Operating System

Currently an App has been developed for the Android operating system, however the hardware has been chosen to easily integrate support for the Apple iOS operating system and no additional hardware is needed to support the Windows 8 OS. One of the advantages of adding smart device communication with GULPS was to allow users to use smart devices they already own to connect to GULPS. Whilst Android has the largest share of the market [50], support for the remaining OS's would accommodate the majority of subjects, and remove the need for subjects or hospitals to buy specialized smart devices to communicate with GULPS.

7.2.4 Pharyngeal Impedance Modelling

Another topic of research is to develop a dynamic computational model of the structure and the electrical properties of the throat. Using this model, the cause of the impedance change can be visualized and the electrode placement can be trialled to find a placement which would output a change in impedance that reflects the pharyngeal sequence.

7.3 Conclusion

This aim of this project was to continue development of an impedance based swallowing biofeedback tool. The biofeedback tool, GULPS, required development further due to inconsistent output. Development was continued with the addition of Bluetooth communication and an Android Application to plot and record the data sent from the GULPS device. The development of the impedance measurement hardware was also continued with the previous design being split into functional modules with individual PCB's made for each module.

The constant current module was identified as producing a non-deterministic current and was redesigned. Using the redesigned module, the output of GULPS matches the literature and the features produced are consistent across different patients and on different days. The features produced by GULPS did not differ with injection frequency and the original frequency (40 kHz and 70 kHz) was used throughout the remaining development

The cause of the impedance features is hypothesized to be the movement of the larynx, hyoid bone and the shortening and vertical movement of the pharynx. One method that was unsuccessfully trialled but can be further developed is the subtraction method, which produced varying results across different days.

With GULPS now producing a consistent output that matches the literature, an investigation can now be performed into the cause of the change in impedance measured during a swallow. Previous research

into bioimpedance change during swallowing suggests that the cause is due to the movement of the larynx and hyoid. If this hypothesis is correct, the impedance change caused by the movement needs to be taken into account before the output of GULPS can be related to pharyngeal lumen closure.

Appendix A. Previous GULPS Hardware

A.1 40 kHz Channel

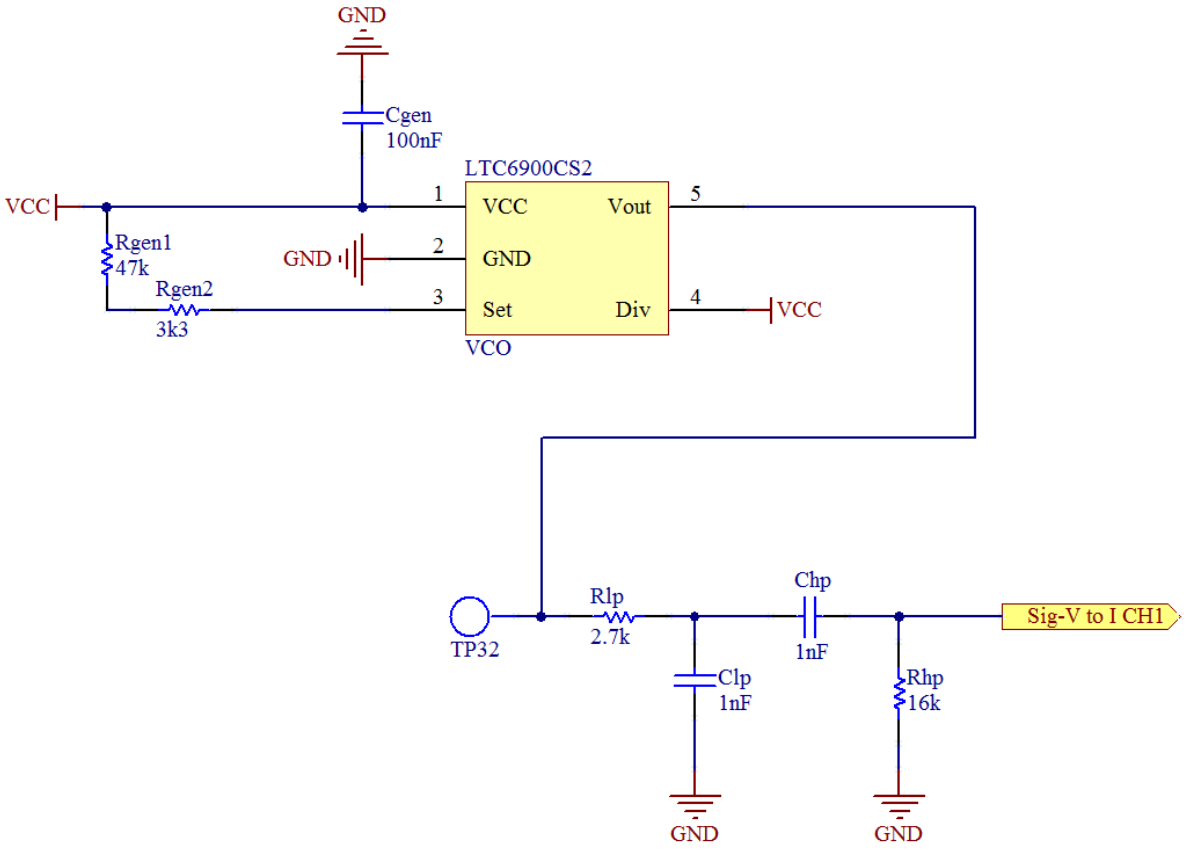

Figure A.1. Circuit diagram of the 40 kHz sinusoidal wave generator.

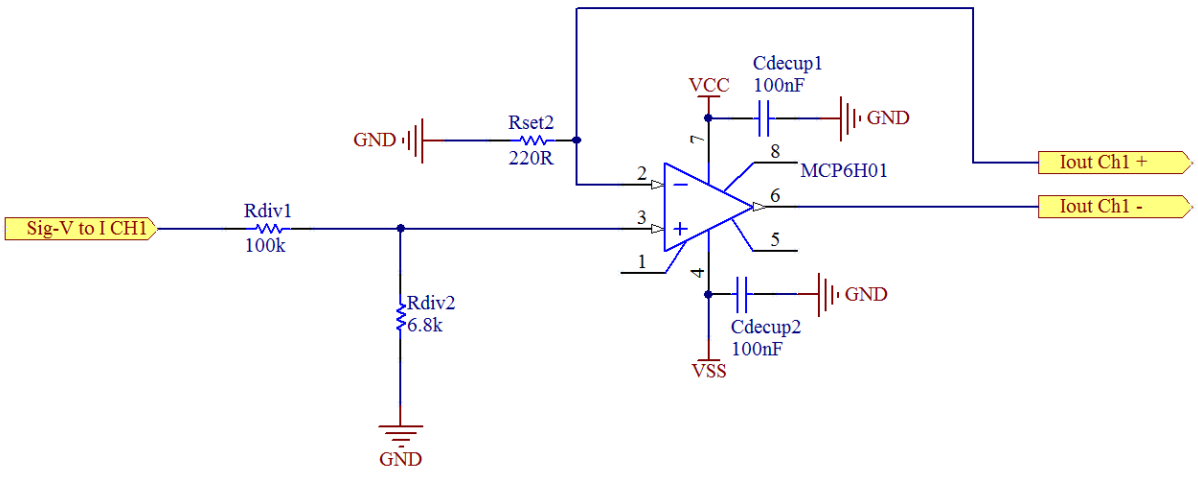

Figure A.2. Circuit diagram of the 40 kHz constant current module.

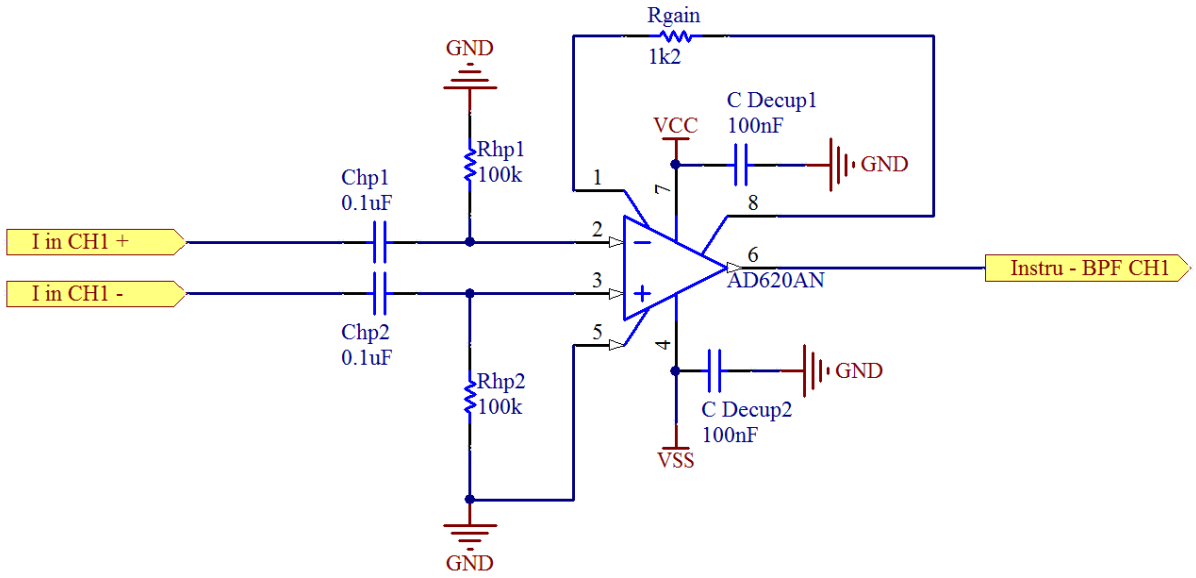

Figure A.3. Circuit diagram of the instrumentation amplifier used in the 40 kHz channel.

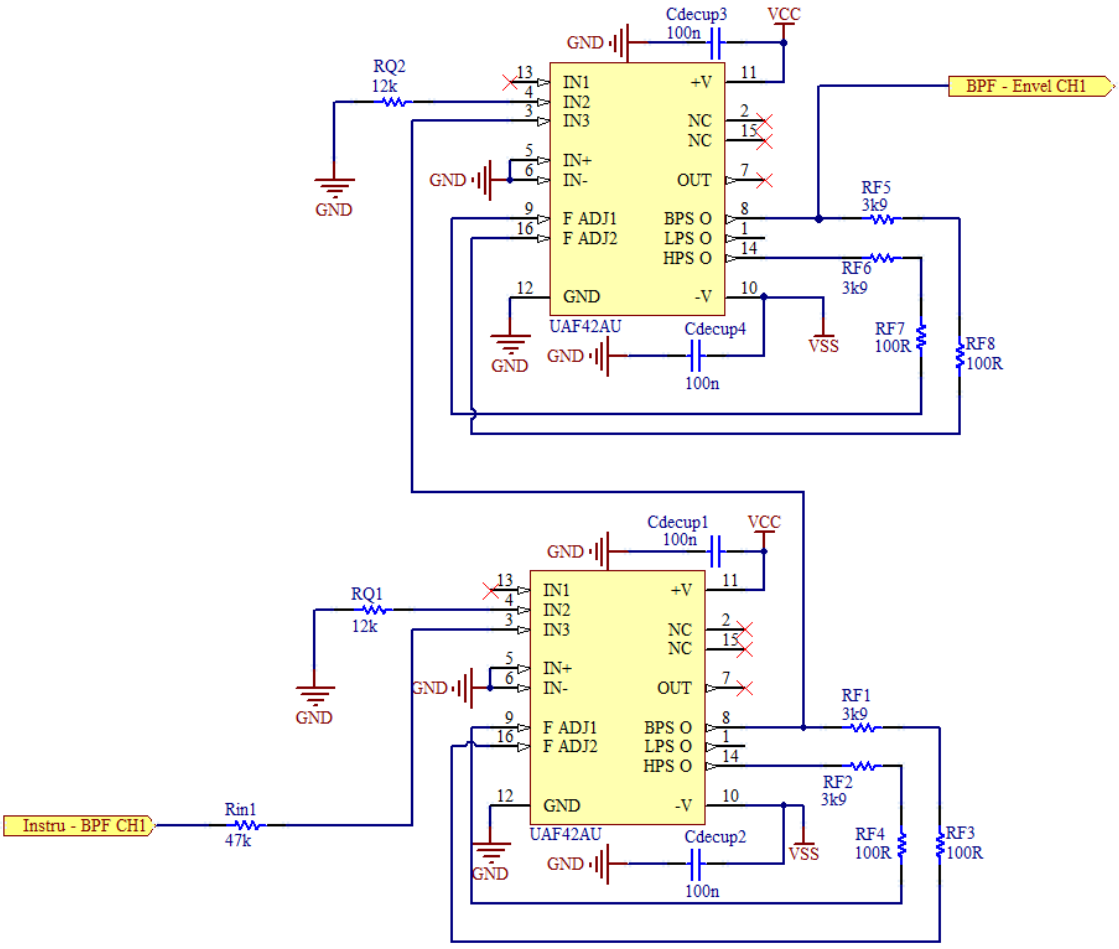

Figure A.4. Bandpass filter centred at 40 kHz.

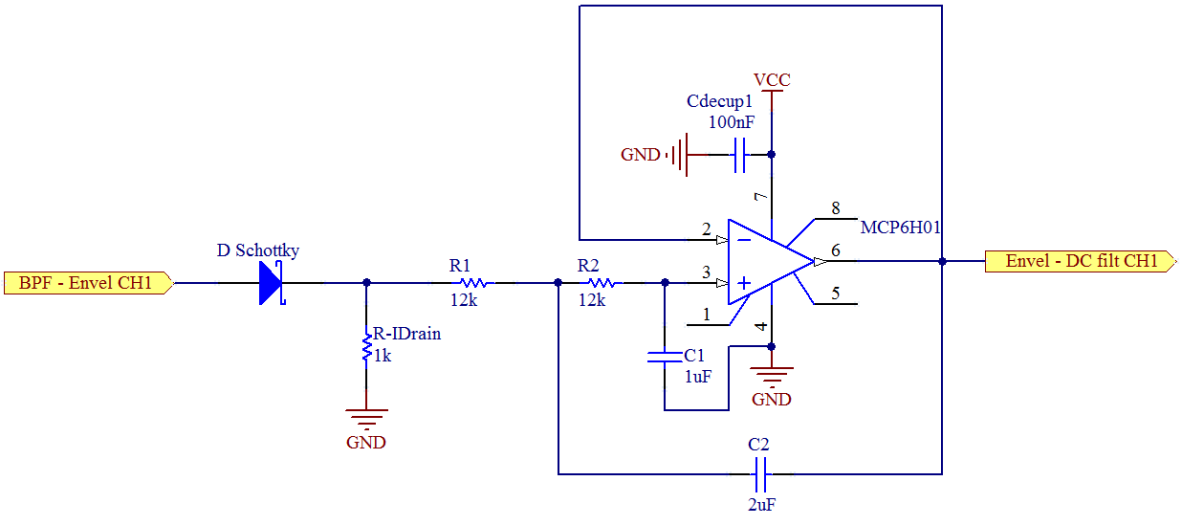

Figure A.5. The demodulator circuit used in the previous prototype for the 40 kHz channel.

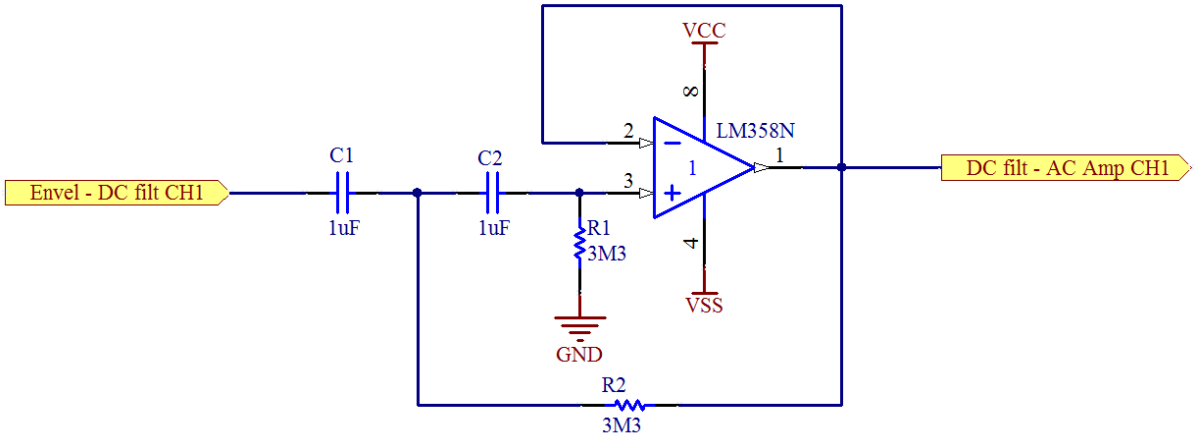

Figure A.6. The DC filtering module circuit diagram in the 40 kHz channel.

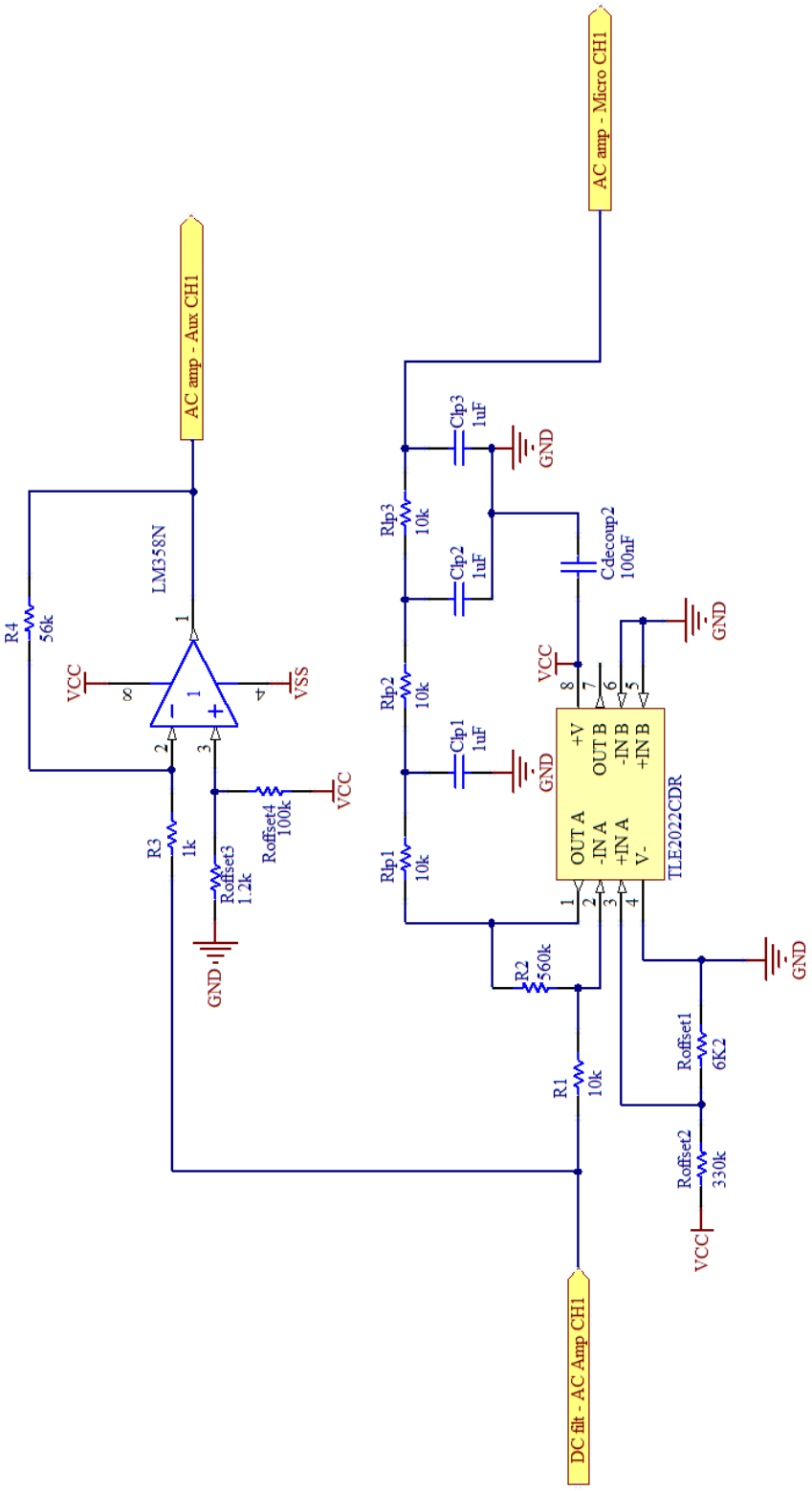

Figure A.7. Circuit diagram of the AC amplifier module for the 40 kHz channel.

A.2 70 kHz Channel

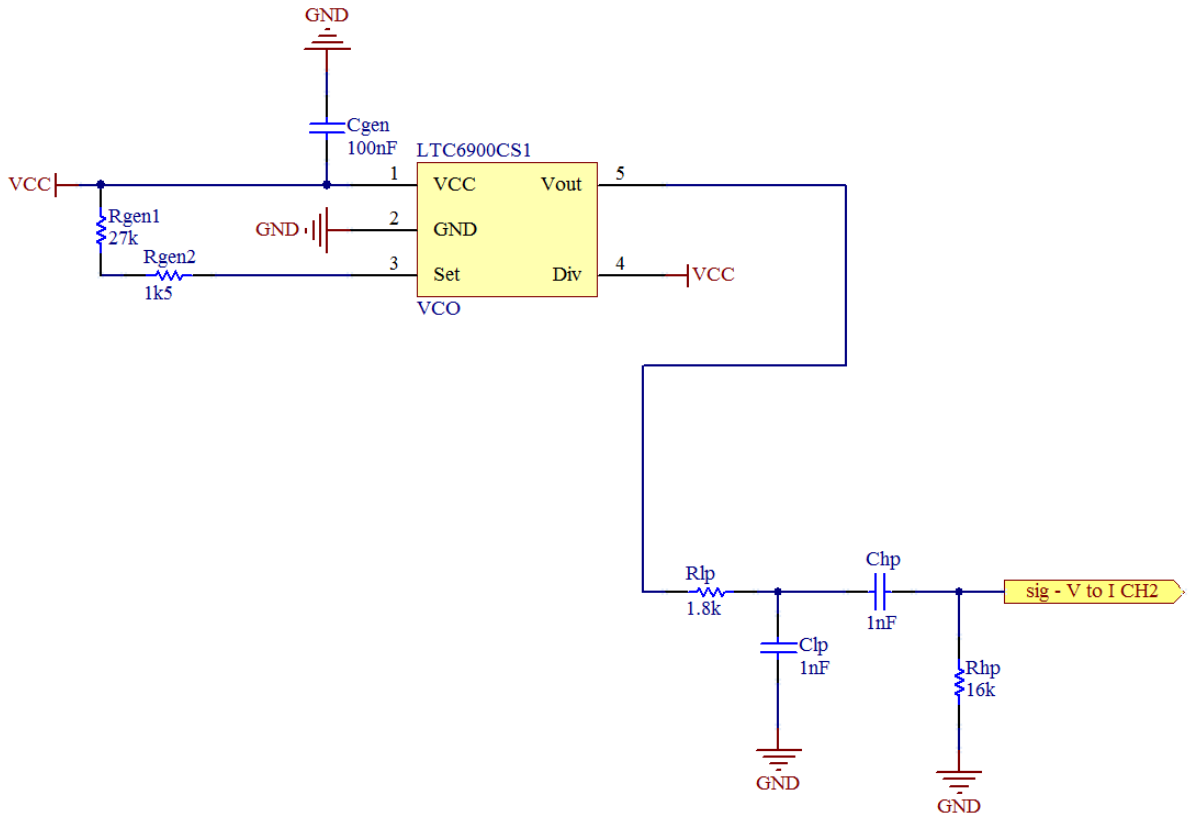

Figure A.8. The 70 kHz sinusoidal waveform generator circuit diagram.

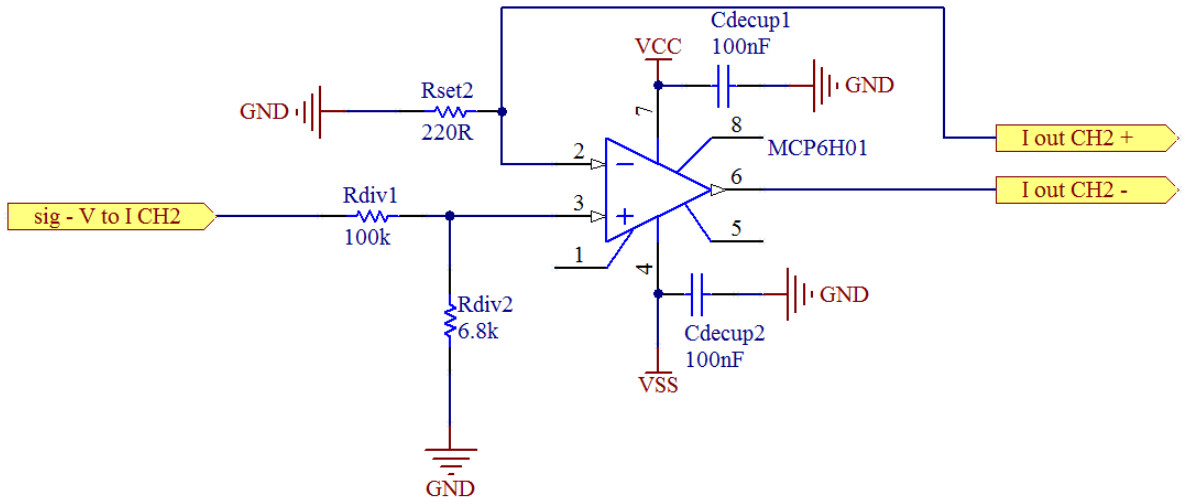

Figure A.9. The circuit diagram for the constant current module in the 70 kHz channel.

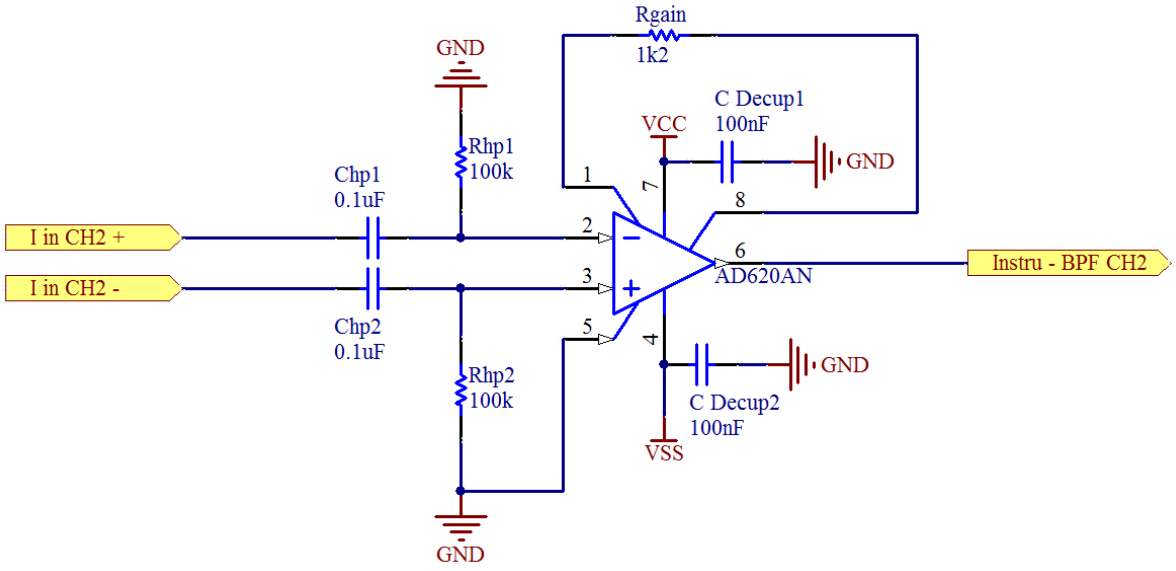

Figure A.10. The circuit diagram of the instrumentation amplifier for the 70 kHz channel.

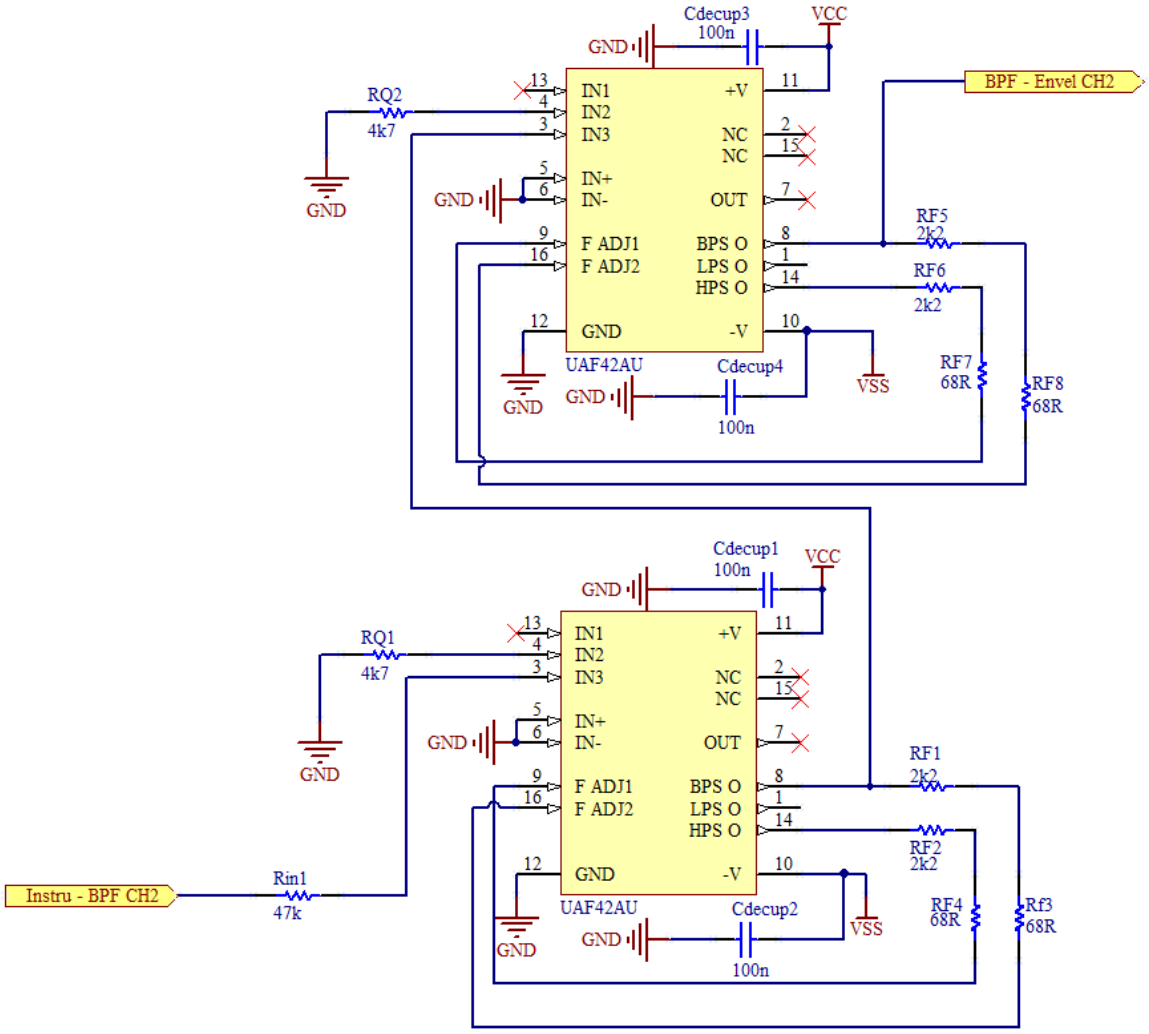

Figure A.11. The circuit diagram of the bandpass filter centred at 70 kHz.

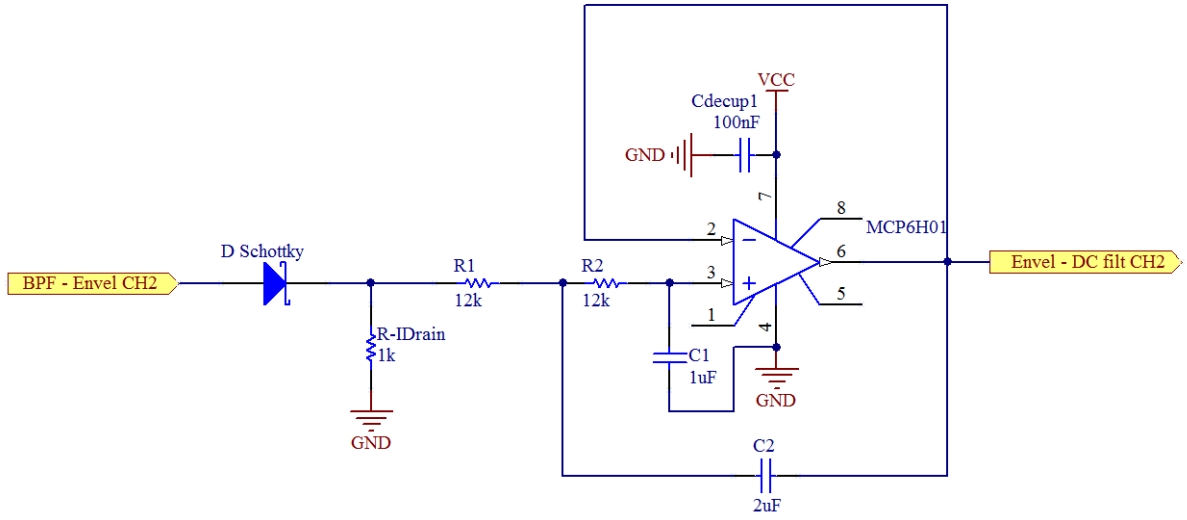

Figure A.12. The demodulator circuit diagram for the 70 kHz channel.

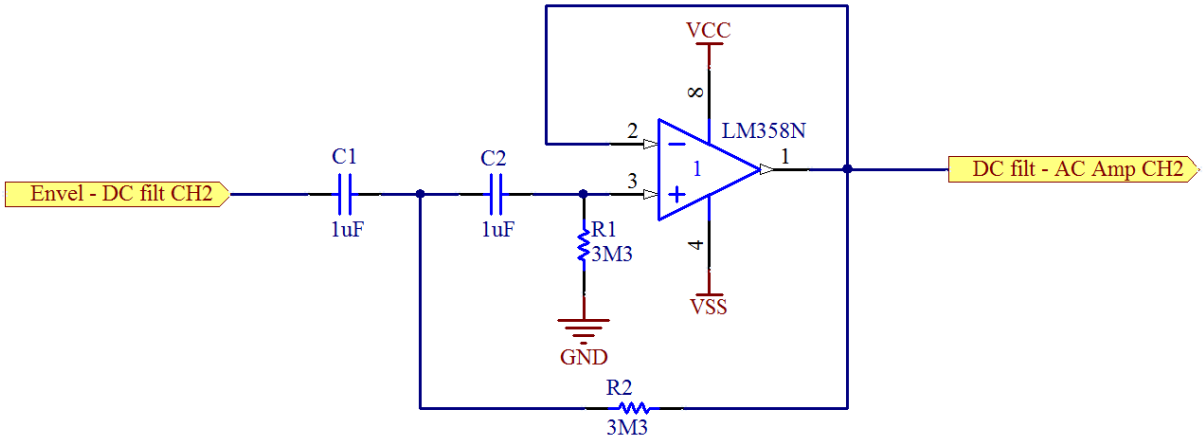

Figure A.13. The circuit diagram for the DC filter in the 70 kHz channel.

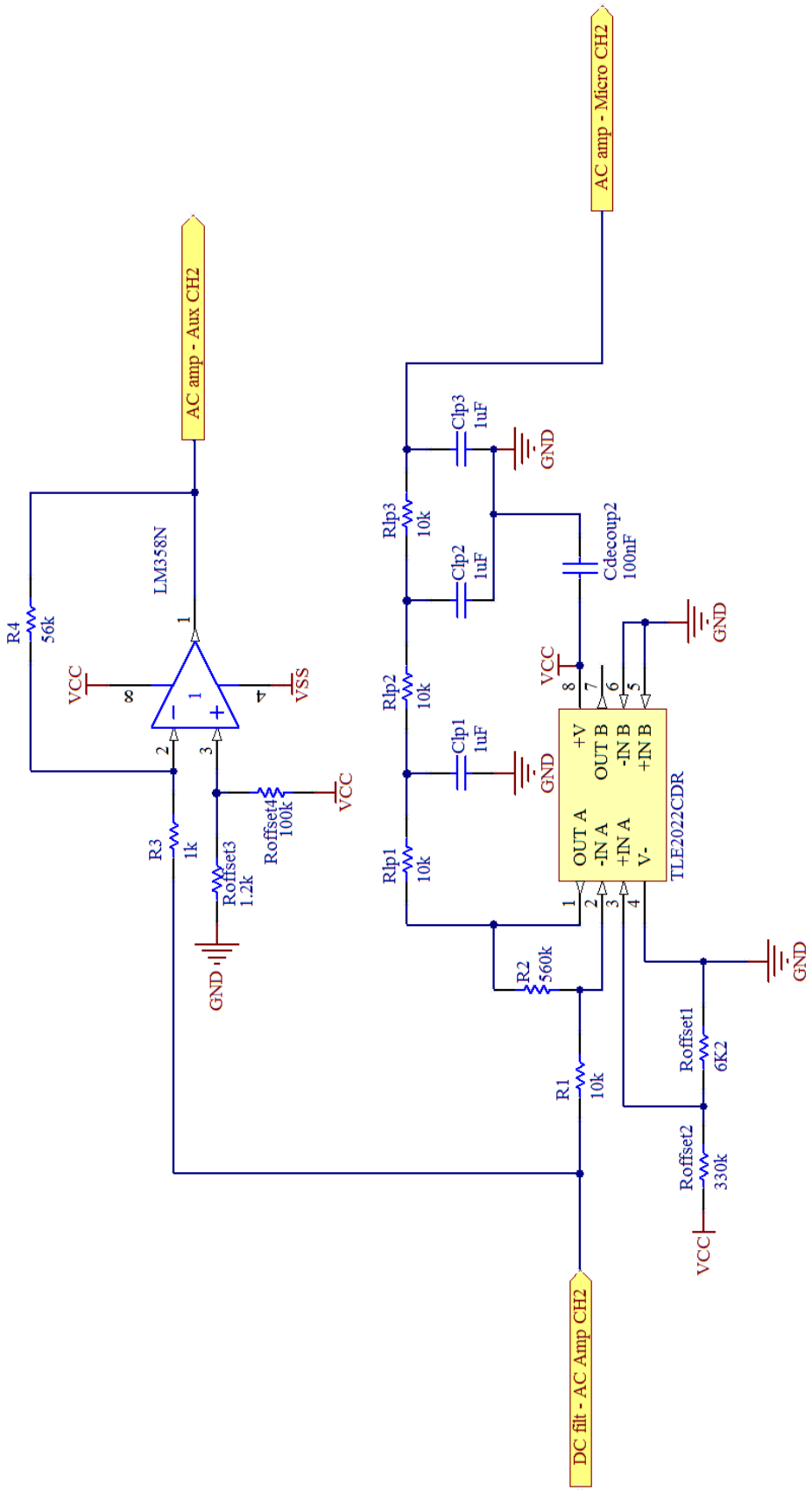

Figure A.14. The circuit diagram of the AC amplifier module for the 70 kHz channel.

A.3 Universal Sections

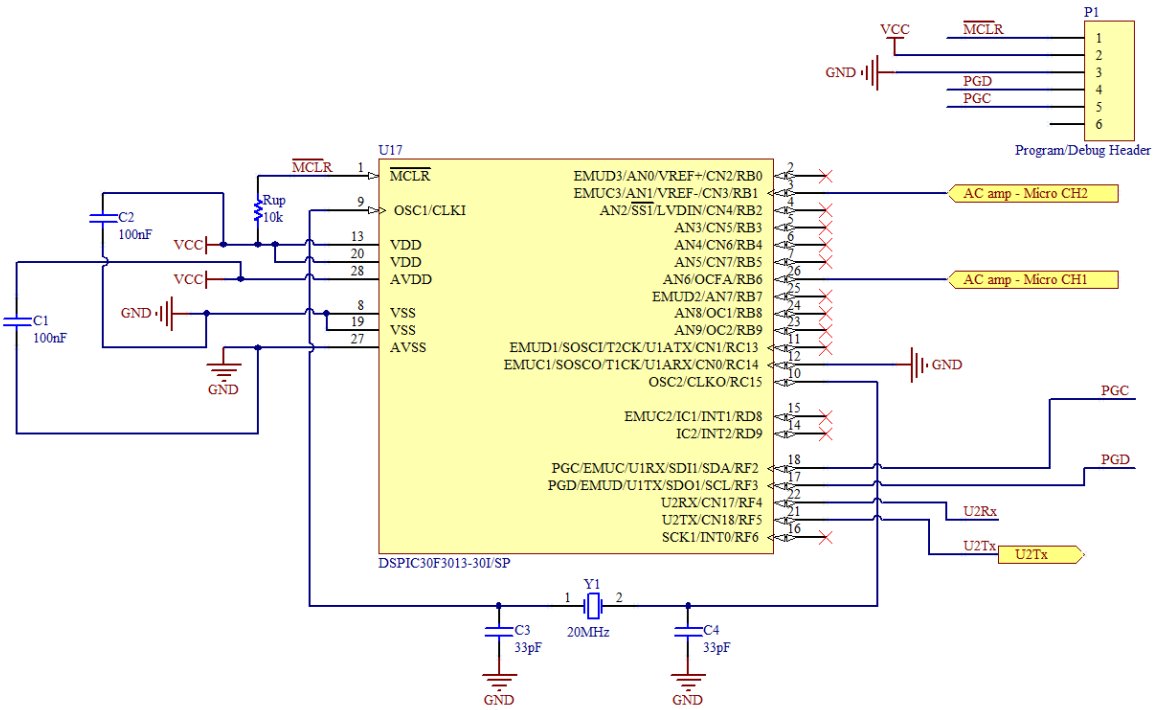

Figure A.15. The circuit diagram of the microcontroller.

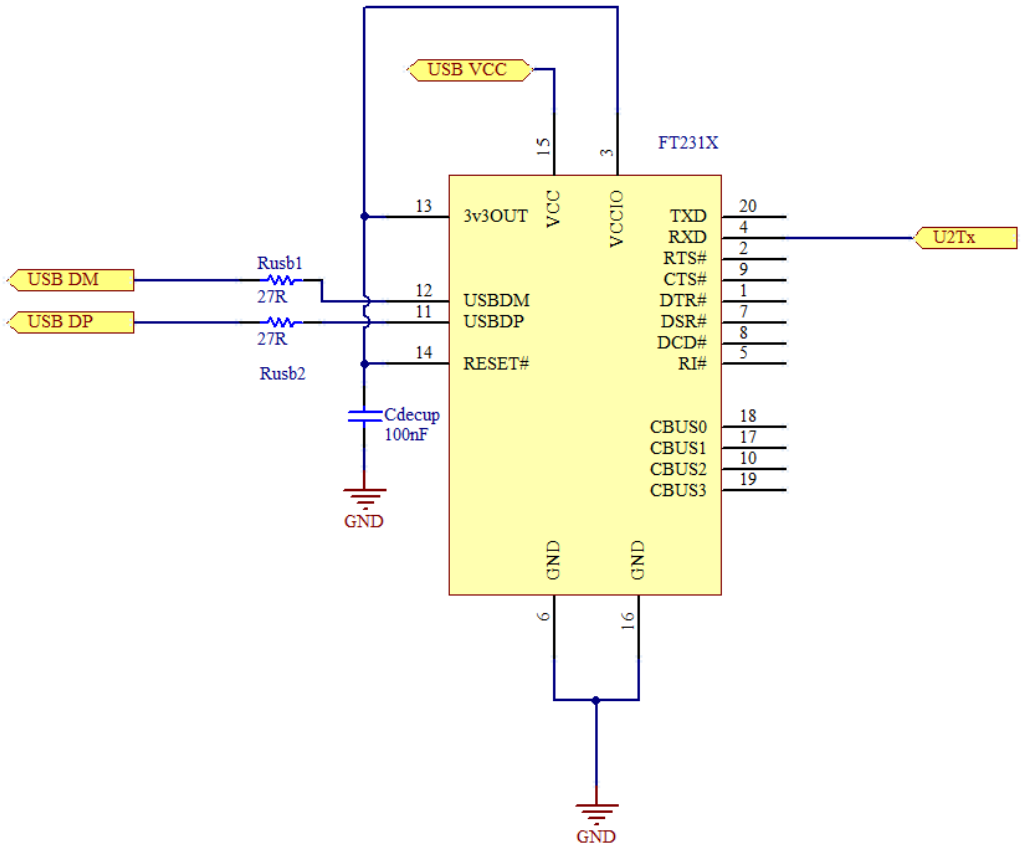

Figure A.16. The circuit diagram of the serial to USB converter.

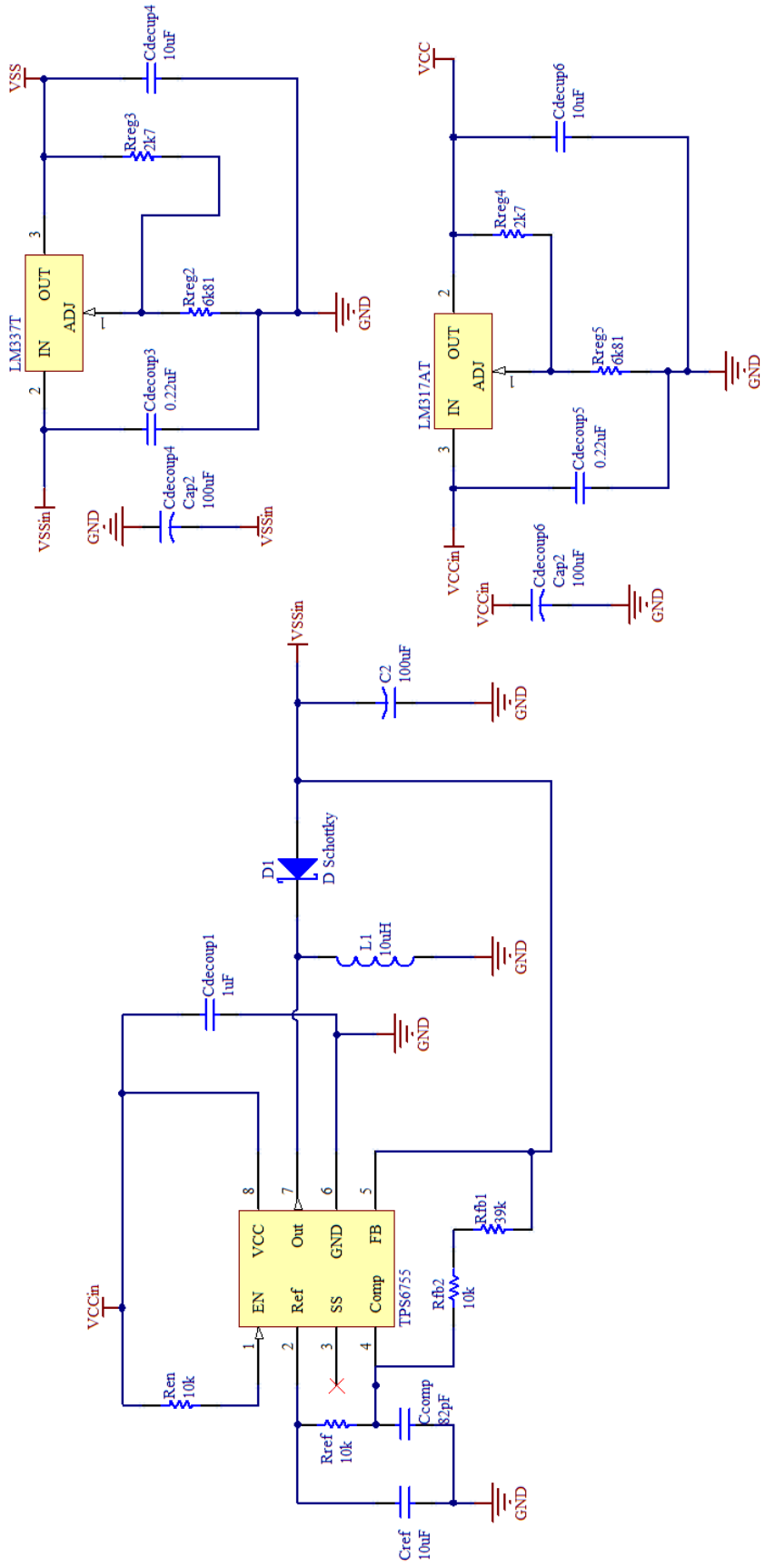

Figure A.17. The circuit diagram of the power module.

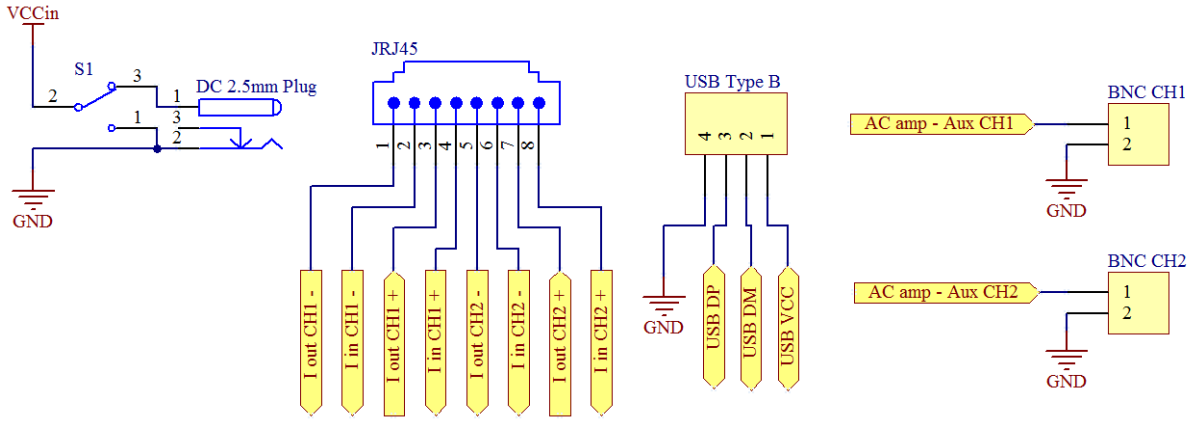

Figure A.18. The headers in the GULPS prototype.

Appendix B. PCB Artwork

B.1 Sinusoidal Wave Generator

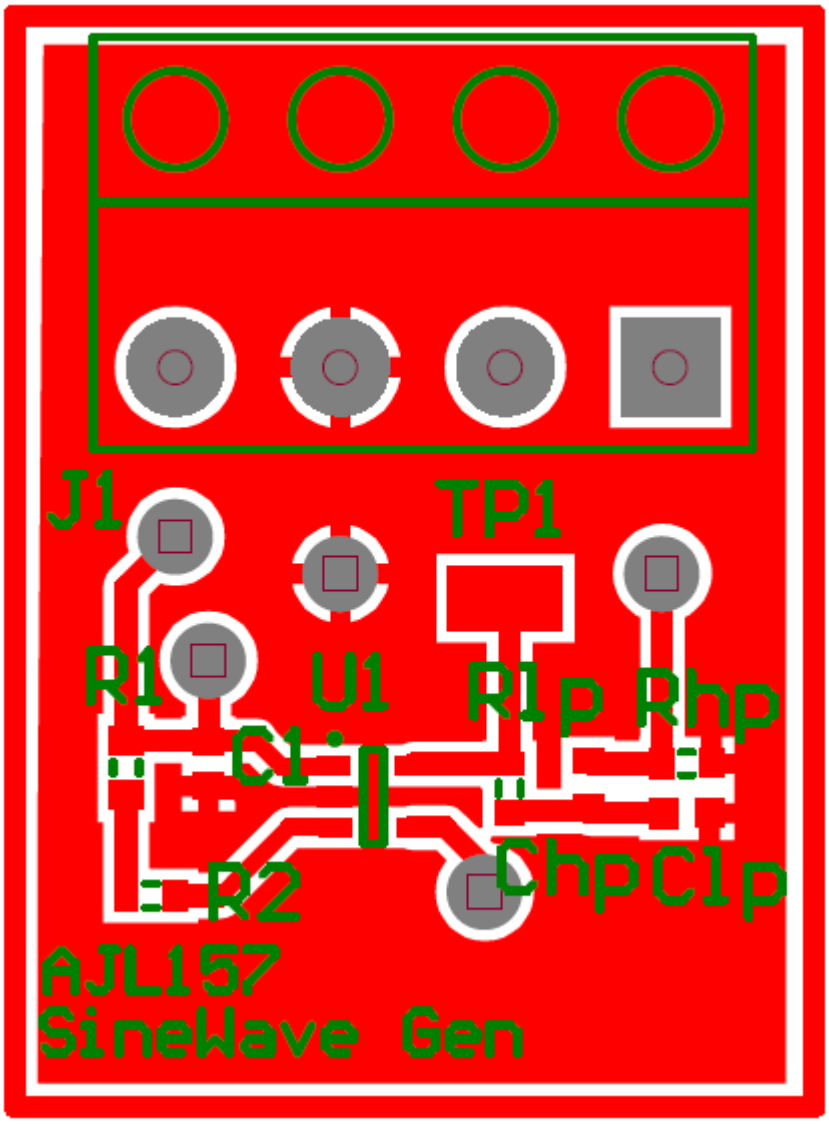

Figure B.1. The PCB artwork for the sinusoidal wave generator.

B.2 Constant Current Module Version 1

A) B)

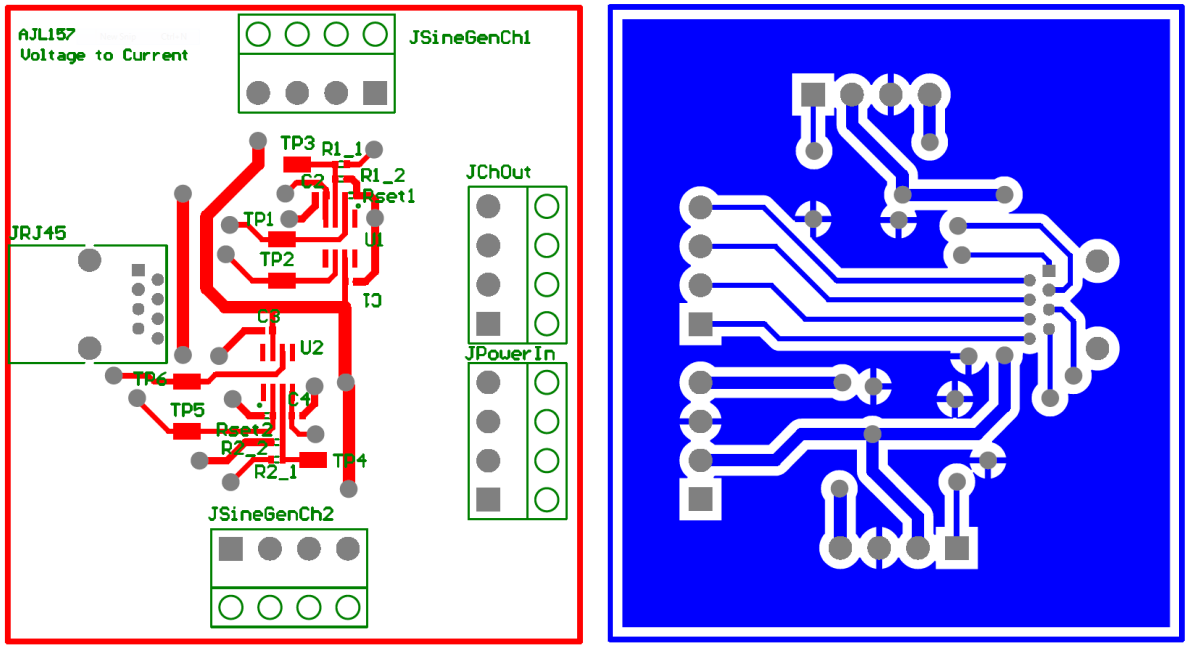

Figure B.2. Constant current module PCB artwork, for the opamp based design. A) Top B) Bottom side of the PCB

B.3 Constant Current Module Version 2

A) B)

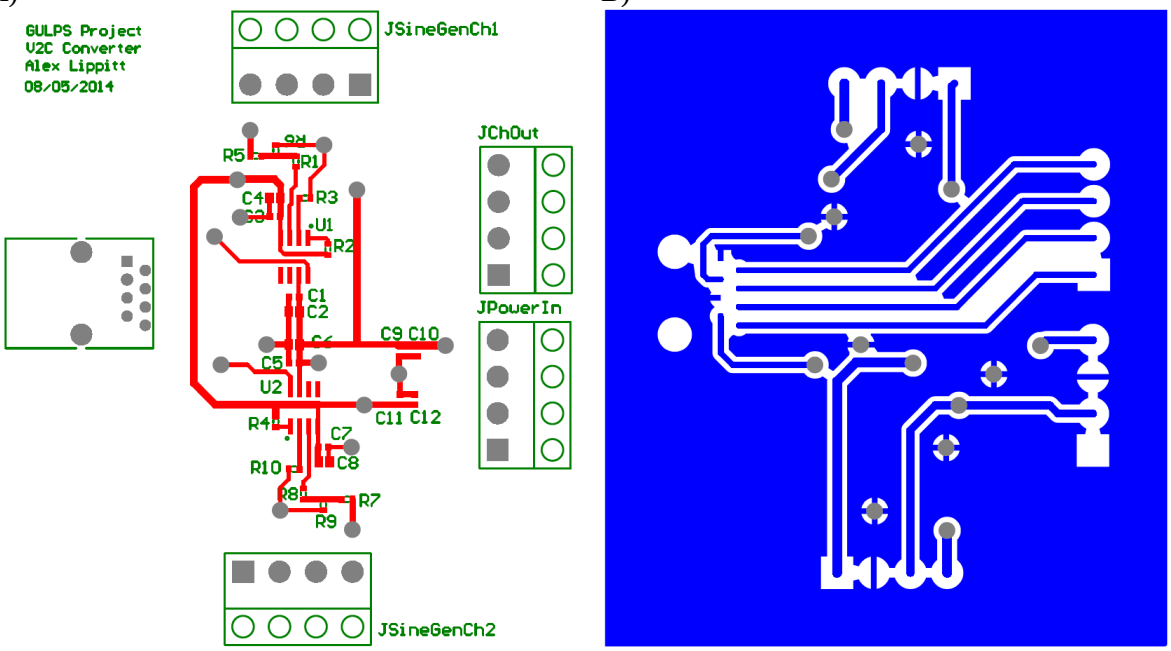

Figure B.3. The PCB artwork for the constant current module, using the OTA. A) Top B) Bottom side of the PCB

B.4 Instrumentation Amplifier

A)

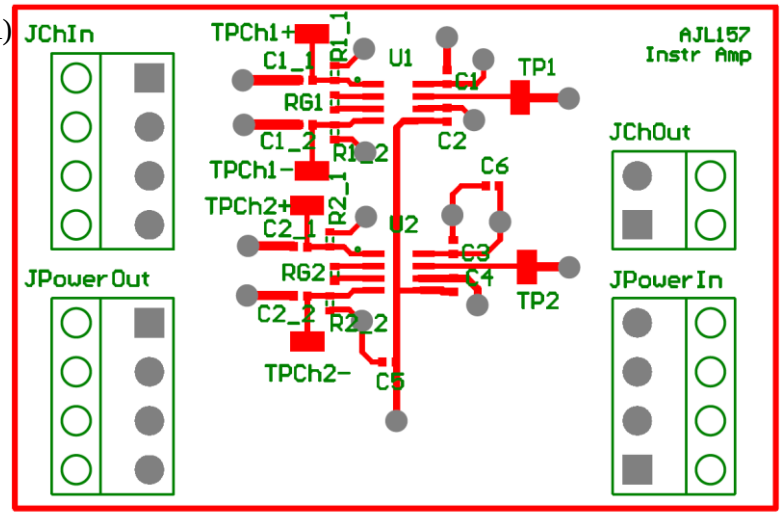

B)

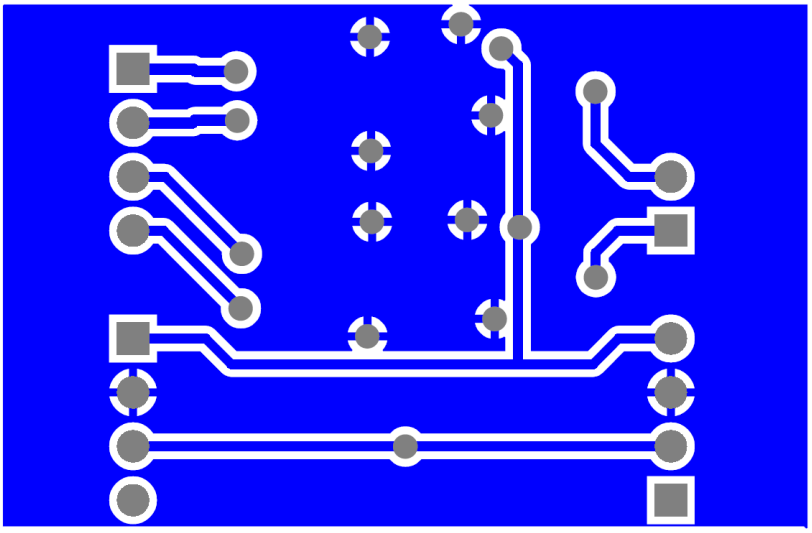

Figure B.4. PCB artwork for the instrumentation amplifier for the A) Top B) Bottom side of the board.

B.5 Bandpass Filter – Low Frequency

A)

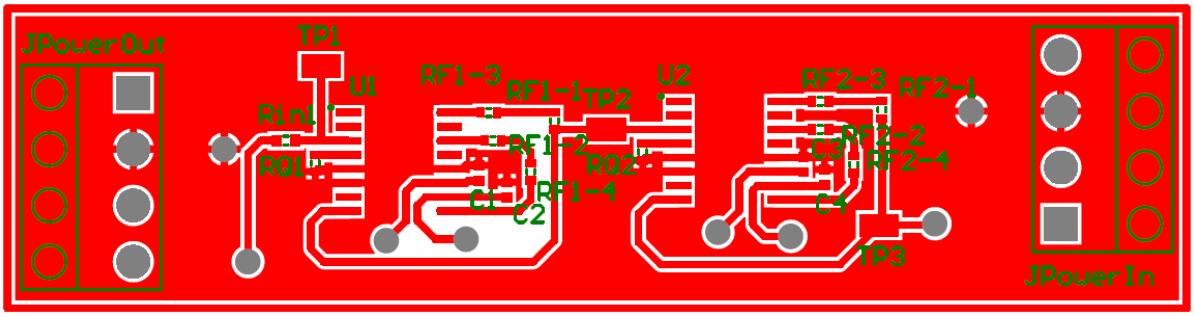

B)

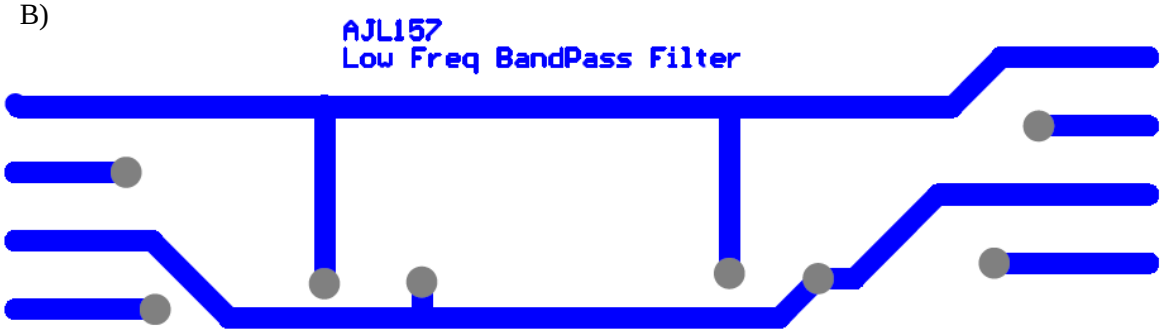

Figure B.5. Low frequency bandpass filter PCB artwork for the A) Top and B) Bottom side of the board.

B.6 Bandpass Filter – High Frequency

A)

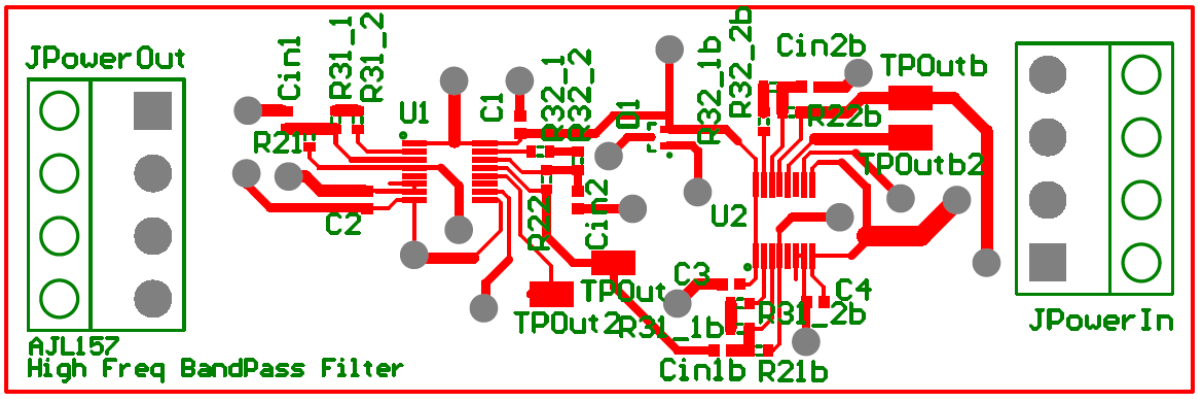

B)

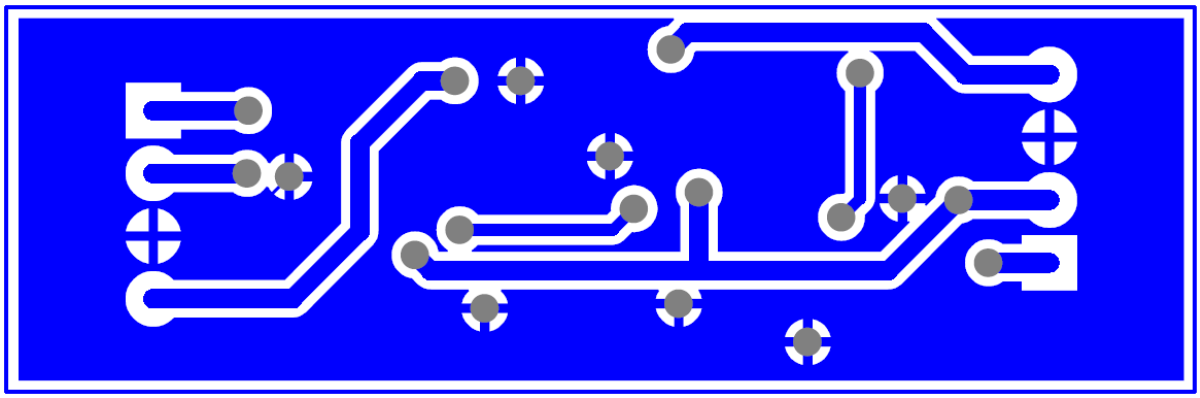

Figure B.6. PCB artwork for the high frequency bandpass filter. A) Top side and B) Bottom side of the PCB

B.7 Signal Conditioning Module

A)

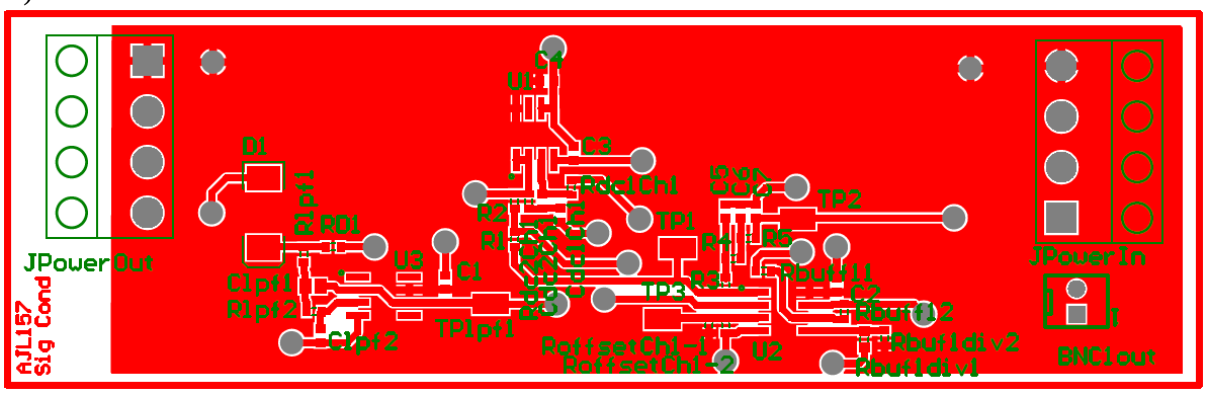

B)

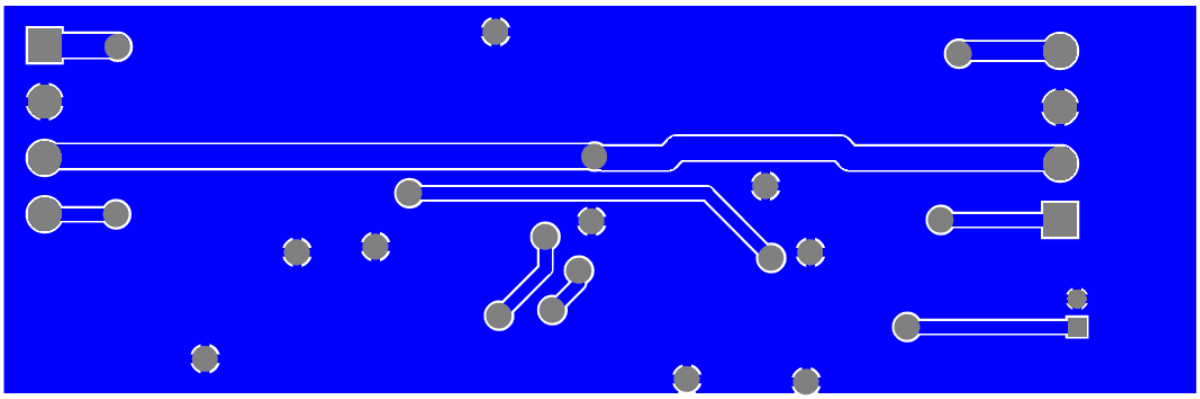

Figure B.7. PCB artwork for the signal conditioning board. A) Top side and B) Bottom side of the board.

B.8 Microcontroller

A)

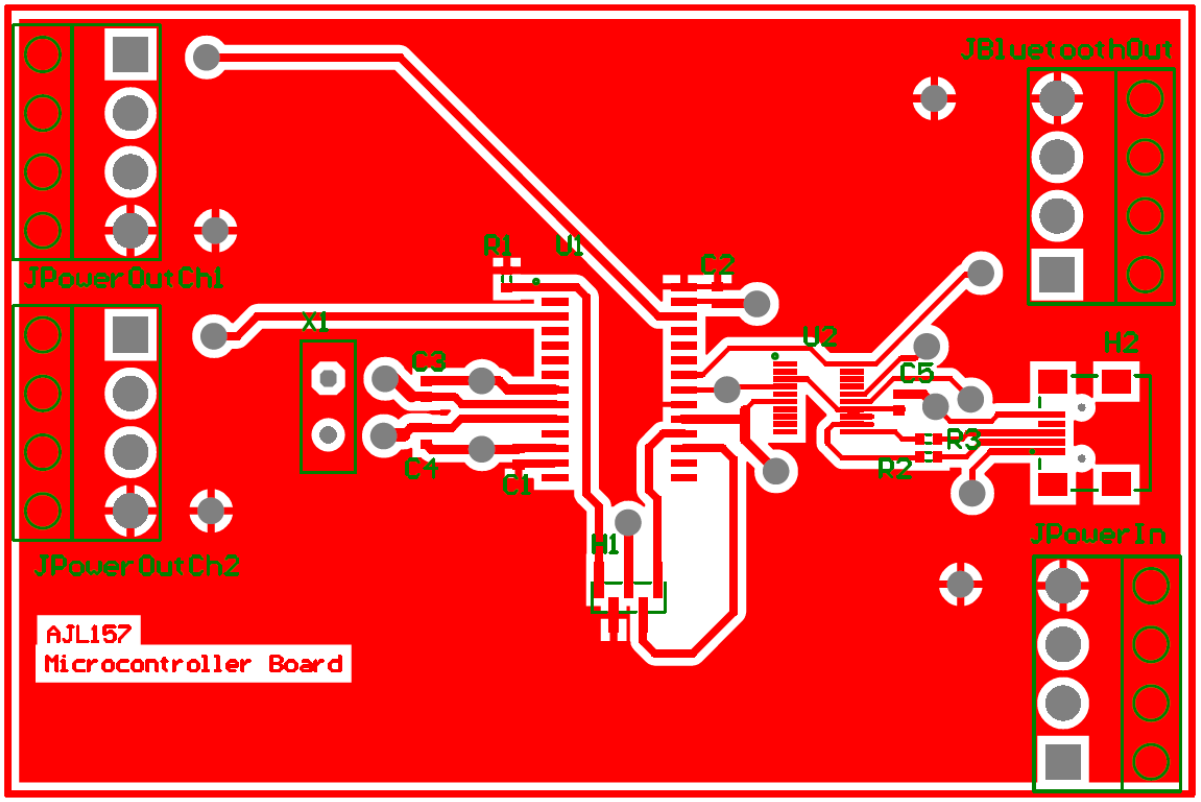

B)

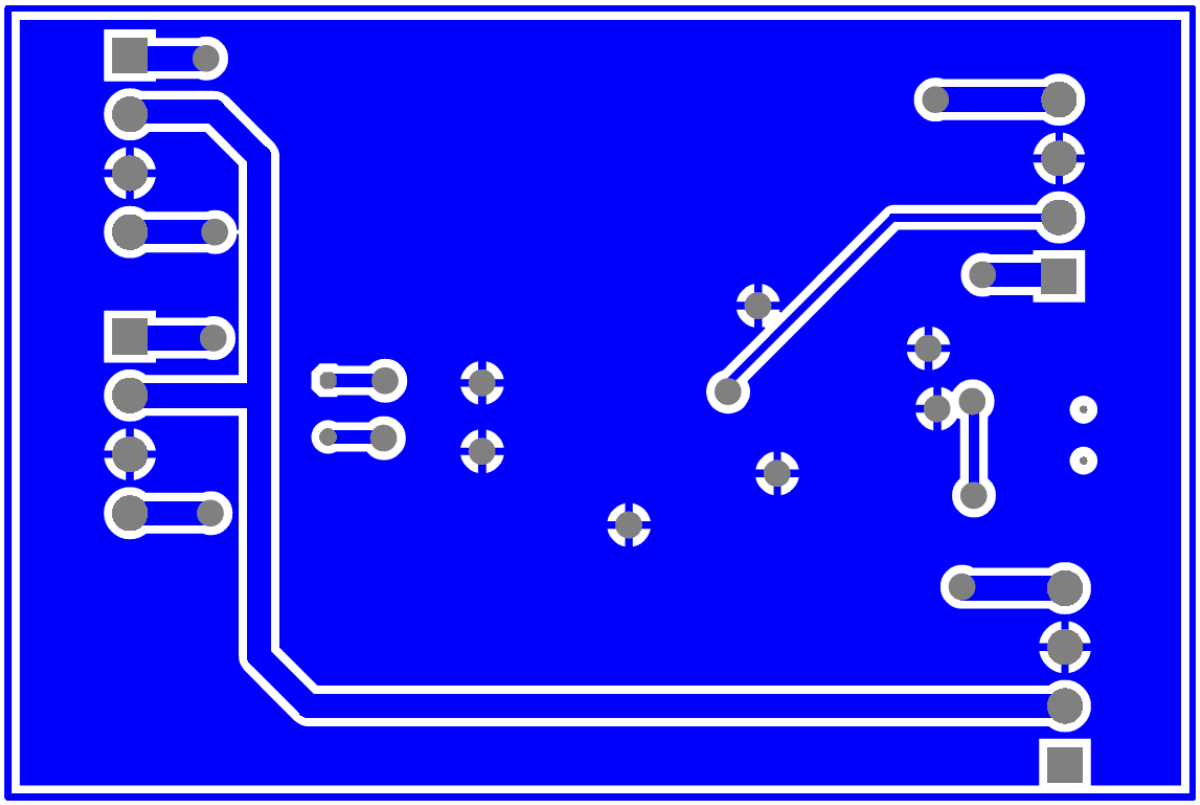

Figure B.8. Microcontroller module PCB artwork, A) is the Top side and B) is the bottom side.

Appendix C. Filter Resistor and Capacitor Values

C.1 Low Frequency Bandpass Filter

Table C.1. The resistor and capacitor values for the UAF42 bandpass filter.

Centre Frequency (kHz)	RF1-1 (kΩ)	RF1-2 (kΩ)	RF2-1 (kΩ)	RF2-2 (kΩ)	RQ (kΩ)
4	39	1	39	1	12
7	22	0.68	22	0.68	4.7
40	3.9	0.1	3.9	0.1	12
70	2.2	0.068	2.2	0.068	4.7

C.2 High Frequency Bandpass Filter

Table C.2. The resistor and capacitor values for LT1568 bandpass filter.

Centre Frequency (kHz)	C_{IN} (pF)	R1-1 (Ω)	R1-2 (Ω)	R2 (Ω)
400	35	2200	160	3300
700	16	1200	10	2400
4000	18	200	10	390
7000	22	110	12	200

Appendix D. Embedded Software Code

```
/* Filename: main.c
   Original Author: Chris Chester
   Original Date: 20/09/2012

   Modified By: Alex Lippitt
   Modified Date: 19/06/2014

   Changes Made: Uses a timer to schedule the ADC sampling and sending

   Description: The main code designed to be operated with a PIC micro
   to work with the bioimpedance circuit.

   Notes: ADC data retrieval, and UART transmit with one channel takes
   184us to complete and with two channels 458us to complete.
*/
#define FCY 500000UL
#include <libpic30.h>
#include <p30f3013.h>
#include <stdlib.h>
#include <stdio.h>

#include "debug_led.h"
#include "uart_bisskit.h"
#include "adc.h"

#define SYNC_BYTE 0xFF

#define BORV_SET 0x30 //Brown out voltage

#define ADC_MAX 0xFD

#define HIGH_BIT_SHIFT 8

#define TRANSFER_DELAY 100

//Channel 1 data
volatile uint16_t adc_data_ch1 = 0;
uint8_t high_byte_ch1 = 0;
uint8_t low_byte_ch1 = 0;

// Channel 2 data
volatile uint16_t adc_data_ch2 = 0;
uint8_t high_byte_ch2 = 0;
uint8_t low_byte_ch2 = 0;

uint16_t timer_count_1 = 0;

// Initial Microcontroller Configuration
_FOSC(CSW_FSCM_OFF & HS3_PLL16); //Use Internal Fast RC oscillator
_FWDT(WDT_ON & WDTPSA_512 & WDTPSB_16);
_FBORPOR(PBOR_ON & BORV_SET & PWRT_64 & MCLR_EN);
_FGS(CODE_PROT_OFF);

// Function prototype for timer 1 ISR
void __attribute__((__interrupt__, __auto_psv__)) _T1Interrupt(void);
```

```
void timer_init();

volatile int send_data = 0;


uint8_t low_milli = 0;
uint8_t high_milli = 0;
uint8_t low_sec = 0;
uint8_t high_sec = 0;

int main (void){
 //To allow for micro to be set-up before UART connection is attempted
  __delay_ms(10000);

 // Initialise UART, ADC and Timer
  uart_init();
  adc_init();
  timer_init();

  while(1){

    if(send_data >= 1) {

      // Check to make sure the data value isn't the same as sync bit
      if(adc_data_ch1 == SYNC_BYTE) {
        adc_data_ch1 = ADC_MAX;
      }
      low_byte_ch1 = adc_data_ch1;
      high_byte_ch1 = adc_data_ch1 >> HIGH_BIT_SHIFT;

      // Check to make sure the data value isn't the same as sync bit
      if(adc_data_ch2 == SYNC_BYTE) {
        adc_data_ch2 = ADC_MAX;
      }
      low_byte_ch2 = adc_data_ch2;
      high_byte_ch2 = adc_data_ch2 >> HIGH_BIT_SHIFT;

      //Send Data
      uart_send(SYNC_BYTE);

      // Channel 1 data
      __delay_ms(TRANSFER_DELAY);
      uart_send(low_byte_ch1);
      __delay_ms(TRANSFER_DELAY);
      uart_send(high_byte_ch1);

      // Channel 2 data
      __delay_ms(TRANSFER_DELAY);
      uart_send(low_byte_ch2);
      __delay_ms(TRANSFER_DELAY);
      uart_send(high_byte_ch2);

      send_data = 0;  // Clear Flag

    }
  }
}
```

```
void timer_init() {
    // Configure Timer 1.
    // PR1 and TCKPS are set to call interrupt every 500ms.
    // Period = PR1 * prescaler * Tcy
    T1CON = 0;            // Clear Timer 1 configuration
    T1CONbits.TCKPS = 3;  // Set timer 1 prescaler
    PR1 = 2090;           // Set Timer 1 period (max value is 65535)
    _T1IP = 1;            // Set Timer 1 interrupt priority
    _T1IF = 0;            // Clear Timer 1 interrupt flag
    _T1IE = 1;            // Enable Timer 1 interrupt
    T1CONbits.TON = 1;    // Turn on Timer 1

}

// Timer 1 interrupt service routine
void __attribute__((__interrupt__, __auto_psv__)) _T1Interrupt(void)
{
    if (time == 0) {
        time ++;
    }else {
        time = 0;
    }
    if (adc_is_new_data())
    {
      adc_data_ch1 = adc_read_ch1();
      adc_data_ch2 = adc_read_ch2();
      adc_set_data_received(0); // Flag off to indicate data received.
  }

    send_data = 1;
    // Clear Timer 1 interrupt flag
    _T1IF = 0;

}
```

References

[1] J. Reeves, "EMG-biofeedback reduction of tension headache," *Biofeedback and Self-regulation,* vol. 1, pp. 217-225, 1976/06/01 1976.

[2] L. A. Geddes and L. E. Baker, *Principles of applied biomedical instrumentation*: Wiley, 1989.

[3] S. K. Daniels and M.-L. Huckabee, *Dysphagia Following Stroke*. San Diego: Plural Publishing Inc, 2008.

[4] N. A. Leopold and M. C. Kagel, "Dysphagia—ingestion or deglutition?: A proposed paradigm," *Dysphagia,* vol. 12, pp. 202-206, 1997/08/01 1997.

[5] R. Leonard and K. A. Kendall, *Dysphagia Assessment and Treatment Planning: A Team Approach*: Plural Publishing, Incorporated, 2013.

[6] R. Shaker, *Principles of deglutition : a multidisciplinary text for swallowing and its disorders*. New York: Springer, 2013.

[7] J. A. Logemann, *Evaluation and treatment of swallowing disorders*. Austin, Texas: PRO-ED, 1995.

[8] K. Matsuo and J. B. Palmer, "Anatomy and physiology of feeding and swallowing: normal and abnormal," *Physical medicine and rehabilitation clinics of North America,* vol. 19, pp. 691-707, 2008.

[9] R. L. Braddom, *Physical medicine and rehabilitation*: Elsevier Health Sciences, 2010.

[10] M. Broniatowski, *et al.*, "Current evaluation and treatment of patients with swallowing disorders," *Otolaryngology--head and neck surgery : official journal of American Academy of Otolaryngology-Head and Neck Surgery,* vol. 120, pp. 464-73, 1999.

[11] R. W. Doty and J. F. Bosma, "An electromyographic analysis of reflex deglutition," *Journal of Neurophysiology,* vol. 19, pp. 44-60, 1956.

[12] M. R. Spieker. (2000, Evaluating dysphagia. *American Family Physician 61(12),* 3639-48. Available: http://www.aafp.org/afp/2000/0615/p3639.html

[13] D. W. Buchholz, "Dysphagia associated with neurological disorders," *Acta oto-rhino-laryngologica Belgica,* vol. 48, pp. 143-55, 1994.

[14] M.-L. Huckabee, *et al.*, "Pharyngeal mis-sequencing in dysphagia: Characteristics, rehabilitative response, and etiological speculation," *Journal of the Neurological Sciences,* vol. 343, pp. 153-158, 2014.

[15] S. L. Wolf, "Chapter 22 - Biofeedback," in *The Physiological Basis of Rehabilitation Medicine (Second Edition)*, J. A. Downey, *et al.*, Eds., ed: Butterworth-Heinemann, 1994, pp. 563-572.

[16] P. Macrae, *et al.*, "Pharyngeal pressures during swallowing within and across three sessions: Within-subject variance and order effects," *Dysphagia,* vol. 26, pp. 385-391, 2011/12/01 2011.

[17] M. Rugiu, "Role of videofluoroscopy in evaluation of neurologic dysphagia," *Acta otorhinolaryngologica Italica,* vol. 27, pp. 306-316, 2007.

[18] R. Leonard and K. Kendall, *Dysphagia assessment and treatment planning : a team approach*. San Diego: Singular Pub. Group, 1997.

[19] A. L. Perlman, *et al.*, "Electromyographic activity from human laryngeal, pharyngeal, and submental muscles during swallowing," *Journal of Applied Physiology,* vol. 86, pp. 1663-1669, 1999-05-01 00:00:00 1999.

[20] M. A. Crary and M. E. Groher, "Basic Concepts of Surface Electromyographic Biofeedback in the Treatment of DysphagiaA Tutorial," *American Journal of Speech-Language Pathology,* vol. 9, pp. 116-125, 2000.

[21] H. David, "Brief introduction to bioimpedance," in *Electrical Impedance Tomography*, ed: Taylor & Francis, 2004.

[22] A. Ivorra, *et al.*, "Bioimpedance dispersion width as a parameter to monitor living tissues," *Physiological measurement,* vol. 26, pp. S165-73, 2005.

[23] H. P. Schwan, "Electrical properties of tissue and cell suspensions," *Advances in biological and medical physics,* vol. 5, pp. 147-209, 1957.

[24] R. Pethig, "Dielectric Properties of Biological Materials: Biophysical and Medical Applications," *Electrical Insulation, IEEE Transactions on,* vol. EI-19, pp. 453-474, 1984.

[25] H. P. Schwan and K. R. Foster, "RF-field interactions with biological systems: Electrical properties and biophysical mechanisms," *Proceedings of the IEEE,* vol. 68, pp. 104-113, 1980.

[26] H. P. Schwan, "Electrical properties of tissues and cell suspensions: mechanisms and models," in *Engineering in Medicine and Biology Society. Engineering Advances: New Opportunities for Biomedical Engineers. Proceedings of the Annual International Conference of the IEEE*, Baltimore, MD, 1994, pp. A70-A71

[27] S. Grimnes and Ø. G. Martinsen, "Alpha-dispersion in human tissue," *Journal of Physics: Conference Series,* vol. 224, 2010.

[28] M. Dittmar, "Reliability and variability of bioimpedance measures in normal adults: effects of age, gender, and body mass," *American Journal of Physical Anthropology,* vol. 122, pp. 361-70, 2003.

[29] R. Y. Sung, *et al.*, "Measurement of body fat using leg to leg bioimpedance," *Archives of disease in childhood,* vol. 85, pp. 263-7, 2001.

[30] J.-L. Damez and S. Clerjon, "Meat quality assessment using biophysical methods related to meat structure," *Meat Science,* vol. 80, pp. 132-149, 2008.

[31] S. Zhang, *et al.*, "Multi-frequency EIT hardware system based on DSP," in *IEEE Engineering in Medicine and Biology Society Annual Conference*, New York, NY, 2006, pp. 6677-6680.

[32] R. H. Bayford, "Bioimpedance tomography (Electrical Impedance Tomography)," *Annual Review of Biomedical Engineering,* vol. 8, pp. 63-91, 2006.

[33] W. Lionheart, *et al.*, "The reconstruction problem," in *Electrical Impedance Tomography*, ed: Taylor & Francis, 2004.

[34] T. Kusuhara, *et al.*, "Impedance pharyngography to assess swallowing function," *Journal of International Medical Research,* vol. 32, pp. 608-616, 2004.

[35] T. A. Hughes, *et al.*, "An analysis of studies comparing electrical impedance tomography with x-ray videofluoroscopy in the assessment of swallowing," *Physiological measurement*, vol. 15, pp. A199-209, 1994.

[36] C. Chester, "Electrical-Impedance Biofeedback Instrument for Swallowing Rehabilation," Masters in Engineering, Electrical and Electronic Engineering, University of Canterbury 2014.

[37] *LTC6900: Low Power, 1kHz to 20MHz Resistor Set SOT-23 Oscillator*, Linear Technology Coporation, 2002, Datasheet. [Online]. Available: www.linear.com/product/LTC6900

[38] *AD620: Low Cost Low Power Instrumentation Amplifier,* Analog Devices, 2011, Datasheet. [Online]. Available: www.analog.com/static/imported-files/data_sheets/AD620.pdf

[39] *UAF42: Universal Active Filter*, Texas Instruments, 2010, Datasheet. [Online]. Available: http://www.ti.com/product/UAF42

[40] *MCP6H01/2/4: 1.2 MHz, 16V Op Amps*, Microchip Technology Inc., 2011, Datasheet. [Online]. Available: www.microchip.com/downloads/en/DeviceDoc/22243D.pdf

[41] *LM158, LM258, LM358, LM2904: Dual Operational Amplifiers*, Texas Instruments, 2013, Datasheet. [Online]. Available: http://www.ti.com/product/lm358

[42] *TLE202x: Excalibur High Speed Low-Power Precision Operational Amplifiers*, Texas Instruments, 2010, Datasheet. [Online]. Available: http://www.ti.com/product/tle2022

[43] *dsPIC30F2011/2012/3012/3013: High Performance, 16-bit Digital Signal Controllers*, Microchip Technology Inc., 2010, Datasheet. [Online]. Available: www.microchip.com/downloads/en/DeviceDoc/70139G.pdf

[44] *FT231X: USB to Full Handshake UART IC*, Future Technology Devices International Ltd., 2013, Datasheet. [Online]. Available: http://www.ftdichip.com/Products/ICs/FT231X.html

[45] H. P. Schwan and C. D. Ferris, "Four-Electrode Null Techniques for Impedance Measurement with High Resolution," *Review of Scientific Instruments,* vol. 39, pp. 481-485, 1968.

[46] Sten's Corportation. "Tripletrode Electrodes" [Online]. Available: http://stens-biofeedback.com/products/tripletrode-electrodes

[47] ConvaTec. "Stomahesive Wafer" [Online]. Available: http://www.convatec.co.nz/products/ostomy/other-products/stomahesive-wafer/p-b91cba9a-efd4-4dd4-833c-8d7a858f7ef9/1_0043/

[48] Myotronics. "Norotrode 20 Bipolar SEMG Electrodes" [Online]. Available: https://myotronics.worldsecuresystems.com/norotrodes

[49] Ambu. "Blue Sensor N" [Online]. Available: http://www.ambu.com/corp/products/patient_monitoring_and_diagnostics/product/ambu%C2%AE_bluesensor_n-prod844.aspx

[50] J. Rivera and R. v. d. Meulen, "Market Share Analysis: Mobile Phones, Worldwide, 4Q13 and 2013.," Gartner, www.gartner.com 03/03/2014 2014.

[51] Bluetooth SIG. (2013, 19/02/2014). *Welcome to Bluetooth Technology 101*. Available: http://www.bluetooth.com/Pages/Fast-Facts.aspx

[52] Bluetooth SIG. (21/02/2014). *Bluetooth Basics*. Available: http://www.bluetooth.com/Pages/Basics.aspx

[53] BluetoothSIG. (21/02/2014). *Bluetooth Basics*. Available: http://www.bluetooth.com/Pages/Basics.aspx

[54] RovingNetworks. (2013, 13/11/2014). *RN42/RN42N Class 2 Bluetooth Module*. Available: http://www.microchip.com/wwwproducts/Devices.aspx?dDocName=en558330

[55] Roving Networks. (2013, 13/11/2014). *RN42/RN42N Class 2 Bluetooth Module*. Available: http://www.microchip.com/wwwproducts/Devices.aspx?dDocName=en558330

[56] Roving Networks. (19/02/2014). *Bluetooth Modules that Simply Work with iPhone, Ipad and iPod Devices*. Available: http://www.microchip.com/pagehandler/en-us/technology/bluetooth/technology/apple_ios.html

[57] Texas Instruments. (17/07/2014). *Stellaris® LM4F120 LaunchPad Evaluation Kit* Available: http://www.ti.com/tool/EK-LM4F120XL

[58] Android. (18/02/2014). *Starting an Activity*. Available: http://developer.android.com/training/basics/activity-lifecycle/starting.html

[59] Android. (21/02/2014). *Fragments*. Available: http://developer.android.com/guide/components/fragments.html

[60] Android. (13/02/2014). *Service*. Available: http://developer.android.com/reference/android/app/Service.html

[61] Android. (13/02/2014). *Bluetooth*. Available: http://developer.android.com/guide/topics/connectivity/bluetooth.html

[62] Android. (13/02/2014). *BluetoothSocket Class*. Available: http://developer.android.com/reference/android/bluetooth/BluetoothSocket.html

[63] Android. (13/02/2014). *BluetoothAdapter Class*. Available: http://developer.android.com/reference/android/bluetooth/BluetoothAdapter.html

[64] Dropbox Inc. *DropBox*. Available: https://www.dropbox.com/

[65] Dropbox Inc. (11/02/2014). *Dropbox Platform developer guide*. Available: https://www.dropbox.com/developers/reference/devguide

[66] Dropbox Inc. (12/02/2014). *Sync API for Android Documentation*. Available: https://www.dropbox.com/developers/sync/docs/android

[67] 4ViewSoft. (22/10/2014). *AChartEngine*. Available: http://www.achartengine.org/

[68] AppTornadoGmbH. (2013, 17/06/2013). *AppBrain - AChartEngine*. Available: http://www.appbrain.com/stats/libraries/details/achartengine/achartengine

[69] AppTornadoGmbH. (2013, 17/06/2013). *AppBrain - AndroidPlot*. Available: http://www.appbrain.com/stats/libraries/details/androidplot

[70] Android. (18/02/2014). *Handling Runtime Changes*. Available: http://developer.android.com/guide/topics/resources/runtime-changes.html

[71] Android. (16/09/2014). *Profiling with Traceview and dmtracedump*. Available: http://developer.android.com/tools/debugging/debugging-tracing.html#traceviewLayout

[72] Oracle. (04/05/2014). *Class File*. Available: http://docs.oracle.com/javase/7/docs/api/java/io/File.html

[73] Oracle. (03/05/2014). *Class FileOutputStream*. Available: http://docs.oracle.com/javase/7/docs/api/java/io/FileOutputStream.html

[74] C. Chester, "Electrical-Impedance Biofeedback Instrument for Swallowing Rehabilitation," Masters in Engineering, Electrical and Electronic Engineering, University of Canterbury 2014.

[75] Linear Technology. *LT1568 Filter Design Guide*. Available: www.linear.com/docs/9597

[76] *OPA140, OPA2140, OPA4140: High-Precision, Low-Noise, Rail-to-Rail Output, 11MHz JFET Op Amp*, Texas Instruments, 2010, Datasheet. [Online]. Available: http://www.ti.com/product/opa140

[77] *AD8421: 3 nV/√Hz, Low Power Instrumentation Amplifier*, Analog Devices, 2012, Datasheet. [Online]. Available: http://www.analog.com/en/specialty-amplifiers/instrumentation-amplifiers/ad8421/products/product.html

[78] DesignSoft. (2014, 27/11/2014). *TINA*. Available: http://www.tina.com/

[79] *OPA861: Wide Bandwidth Operational Transconductance Amplifier (OTA)*, Texas Instruments, 2013, Datasheet. [Online]. Available: http://www.ti.com/product/opa861

[80] *HCNR200 and HCNR201 High-Linearity Analog Optocouplers*, Avago Technologies, 2014, Datasheet. [Online]. Available: http://www.avagotech.com/pages/en/optocouplers_plastic/plastic_high_linearity_analog_optocoupler/hcnr200/

[81] MathWorks. (01/12/2014). *MATLAB: The language of technical computing*. Available: http://au.mathworks.com/products/matlab/

[82] J. B. Palmer, *et al.*, "Motions of the posterior pharyngeal wall in human swallowing: A quantitative videofluorographic study," *Archives of Physical Medicine and Rehabilitation*, vol. 81, pp. 1520-1526, 11// 2000.

[83] Y. Yamamoto, *et al.*, "Neck electrical impedance for measurement of swallowing," *Electrical Engineering in Japan*, vol. 130, pp. 35-44, 2000.

[84] C. Schultheiss, *et al.*, "Evaluation of an EMG bioimpedance measurement system for recording and analysing the pharyngeal phase of swallowing," *European Archives of Oto-Rhino-Laryngology*, vol. 270, pp. 2149-2156, 2013/07/01 2013.

[85] J. S. Gary, "EIT instrumentation," in *Electrical Impedance Tomography*, ed: Taylor & Francis, 2004.

[86] Wi-Fi Alliance. (2014, 10/10/2014). *Discover Wi-Fi, Wi-Fi Direct*. Available: https://www.wi-fi.org/discover-wi-fi/wi-fi-direct

[87] Wi-Fi Alliance. (2014, 15/12/2014). *Certified Products*. Available: http://www.wi-fi.org/certified-products-advanced-search

[88] Bluetooth SIG. (2014, 15/12/2014). *Competing Technologies*. Available: http://www.bluetooth.com/Pages/Competing-Tech.aspx